Physics and chemistry at surfaces: exploring molecular architectures and their properties

Inauguraldissertation

zur
Erlangung der Würde eines Doktors der Philosophie
vorgelegt der
Philosophisch-Naturwissenschaftlichen Fakultät
der Universität Basel
von

Aneliia Shchyrba

aus Kiew (Ukraine)

Basel, 2014

Genehmigt von der Philosophisch-Naturwissenschaftlichen Fakultät

auf Antrag von:

Prof. Dr. Thomas Jung

Prof. Dr. Catherine Housecroft

Basel, 24.06.14

Prof. Dr. Jörg Schibler

Dekan

“Science is the century-old endeavor to bring together by means of systematic thought the perceptible phenomena of this world into as thoroughgoing an association as possible. To put it boldly, it is the attempt at the posterior reconstruction of existence by the process of conceptualization.”

Albert Einstein

“It doesn't matter how beautiful your theory is, it doesn't matter how smart you are. If it doesn't agree with experiment, it's wrong.”

Richard P. Feynman

“The coming nanometer age can, therefore, also be called the age of interdisciplinarity.”

Heinrich Rohrer

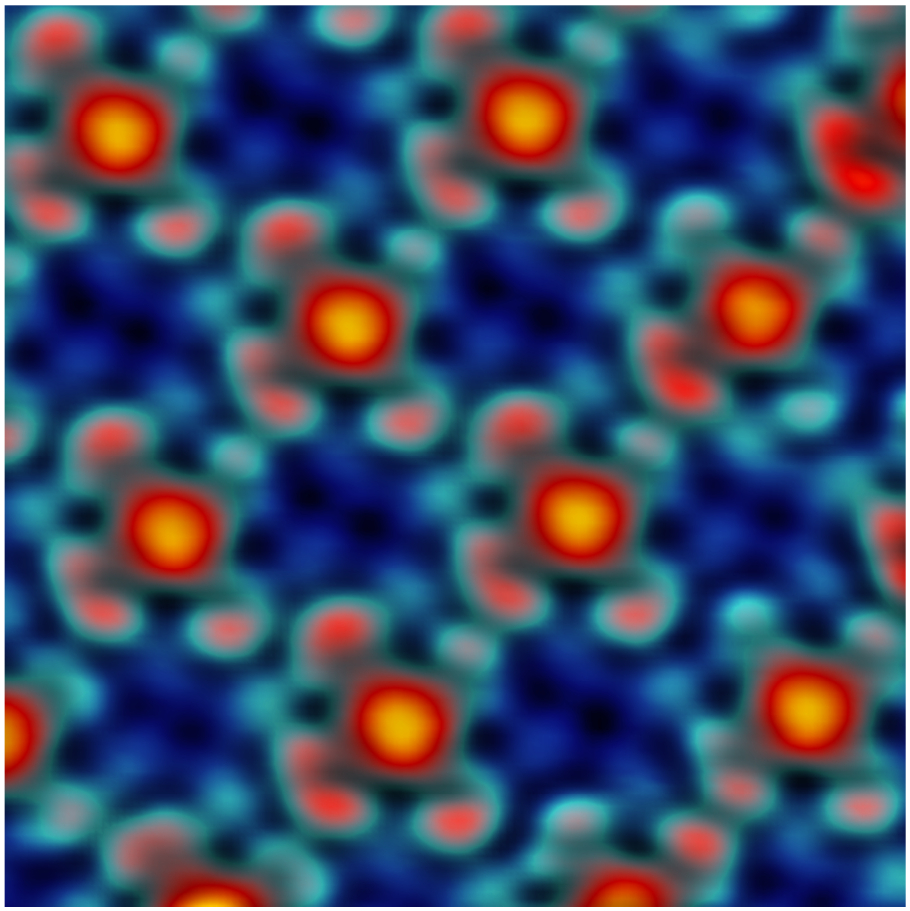

Abstract

In this thesis we combine surface chemistry and surface physics to architecture molecular layers in a bottom-up approach. The formation of self-assembled molecular structures at surfaces on the basis of dipole-dipole interactions, H-bonding, metal coordination and covalent bonding is studied. The molecules of different structure and with specific functional groups are investigated on selected substrates, namely Au(111), Ag(111), Cu(111), Cu(100) or Bi reconstructed Cu(100).

A number of model cases for controlling on-surface architectures and their properties has been found and is reported about in this thesis:

1) Architecture control of a coordination polymer, comprised from chiral and flexible molecular building blocks, by tuning of the intermolecular bonding motif;
2) Chirality transfer in a 1D coordination polymer formed from chiral molecules;
3) Dimensionality (0D, 1D, 2D) control via selection of the transition metal adatom, which modifies a ligand and participates in an on-surface coordination complex;
4) Demonstration of a 2D molecular 'sponge', created on the basis of a borylene derived covalent link with angular flexibility;
5) Investigation of confined 2D electron states in quantum boxes of different size and shape;
6) Self -sorting of bi-molecular system in a 2D array by the coulomb interaction of the surface dipole which depends on band-alignment, charge transfer and the screening in the substrate.

Specifically, we show that chiral and flexible [7]helicene molecules with cyano-groups, covalently attached in symmetric positions, give rise to a 1D arrangement. The intrinsically chiral species imprints its chirality onto the weakly H-bonded assembly, which occurs if molecules are deposited on samples held at low (~90 K) temperatures. This imprint vanishes under the influence of stronger metal-coordination bonds formed after providing metal coordination centers to the H-bonded assembly. The flexibility of the helicene as well as the competition between intermolecular and molecule-surface interactions allow the coordinated chains to assemble in structures with the mirror symmetry apparently being reduced.

The next important issue, addressed in this thesis, is the on-surface modification of the ligand as an approach to control the dimensionality of the resulting on-surface polymer. We present a novel metal-specific reaction of amino- /imino- functionalized perylene derivatives. This precursor is modified upon addition of Co, Fe or Ni at room-temperature into an endo-ligand. In contrast, the presence of Cu adatoms in conjunction with thermal activation leads to the formation of an exo-ligand. Thus the type of metal ligand defines whether a 1D or 2D coordinated polymer can be formed.

We show that borylene-functionalized molecules react upon thermal activation with trimesic acid in a novel on-surface reaction. Moreover, the covalent connection, formed in this reaction, exhibits a high degree of flexibility and allows for the formation of the differently sized pores.

The resulting molecular ‘sponge’, created this way, serves as a template confining the surface state electrons. We investigate the effect of size and shape of the pores on this quantum phenomenon.

Furthermore, we present a new way of creating highly-ordered bimolecular self-sorted chessboard arrays. The bi-component mixture of Mn-phthalocyanine (MnPc) and Cu-phthalocyanine (CuPc) on Bi/Cu(100) self-assembles without participation of any chemical bonding or molecular functionalization but only on the basis of the lateral 2D Coulomb interactions. We resolve charge-transfer channels of two types, directing the supramolecular self-assembly: one oriented perpendicular to the substrate surface, the other oriented in-plane.

These investigations are performed in ultra-high vacuum conditions (UHV) with the use of variable temperature Scanning Tunneling Microscopy / Spectroscopy (STM/STS), X-Ray Photoelectron Spectroscopy (XPS) and synchrotron-based Near Edge X-ray Absorption Fine Structure (NEXAFS) spectroscopy. The experimental results are supported by Density Functional Theory (DFT) calculations, performed by research partners.

List of Publications

The thesis is based on the publications and manuscripts listed below, which are referred in the text by the double square brackets.

[[1]] ***Chirality Transfer in 1D Self-Assemblies: Influence of H-Bonding vs Metal Coordination between Dicyano[7]helicene Enantiomers***, A. Shchyrba, M.-T. Nguyen, C. Wäckerlin, S. Martens, S. Nowakowska, T. Ivas, J. Roose, T. Nijs, S. Boz, M. Schaer, M. Stöhr, C. Pignedoli, C. Thilgen, F. Diederich, D. Passerone and T. A. Jung, *J. Am. Chem. Soc.*, 2013, 135 (41), 15270–15273;

[[2]] ***Controlling the dimensionality of on-surface coordination polymers via endo- or exoligation***, A. Shchyrba, C. Wäckerlin, J. Nowakowski, S. Nowakowska, J. Björk, S. Fatayer, J. Girovsky, T. Nijs, S. Martens, A. Kleibert, M. Stöhr, N. Ballav, T. A. Jung, L. Gade, *J. Am. Chem. Soc.*, 2014, 136 (26), 9355–9363;

[[3]] ***Covalent assembly of a two-dimensional molecular "sponge" on a Cu(111) surface: Confined electronic surface states in open and closed pores***, A. Shchyrba, S. Martens, C. Wäckerlin, M. Matena, T. Ivas, H. Wadepohl, M. Stöhr, T. A. Jung and L. H. Gade, *Chem. Commun.*, 2014, 50, 7628-7631;

[[4]] ***Molecule-specific energy level alignment inducing opposite charge transfer dipoles and formation of a self-sorted bimolecular chess-board on Bi reconstructed Cu(100)***, A. Shchyrba, S. Fatayer, C. Wäckerlin, T. Nijs, S. Nowakowska, T.A. Jung, manuscript in preparation;

Contents

List of abbreviations

General acronyms

- UHV - Ultra-High vacuum
- BE - Binding Energy
- LDOS - Local Density of States

Methods

- XPS - X-Ray Photoelectron Spectroscopy
- STM - Scanning Tunneling Microscopy
- STS - Scanning Tunneling Spectroscopy
- NEXAFS - Near edge X-ray Absorption Fine Structure
- DFT - Density Functional Theory

Chemical compounds

- diCN-Hel - 6,13-dicyano[7]helicene
- DPDI - 4,9-diaminoperylene-quinone-3,10-diimine
- DIBOTAP - *N*,*N*';*N*',*N*'''-diborylene-3,4,9,10-tetraaminoperylene
- TMA - trimesic acid
- MnPc - manganese phthalocyanine
- CuPc - copper phthalocyanine

Introduction

Motivation

Mankind has evolved by the curiosity of man and the never ending search for 'the ultimate truth'. This has affected both the cultural as well as the technological evolution across millennia. Knowledge progresses in cycles of the formulation of hypotheses and their verification/falsification in trials or experiments, a process that has recently impacted the science and the technology on the nanometer scale. Nanoscale science brings along new knowledge about physical and chemical processes as they occur on the scale of individual atoms and molecules. Nanoengineering evolves on this base towards new, as well as more effective or efficient applications. Recent progress in drugs development, telecommunication systems, computers or any other electronic devices, just to name a few, exemplifies how Nanoscience serves society. In particular in the fields of nanodevices and nanoelectronics, there are hopes that the self-assembly of increasingly complex functional patterns, enacted by nature's physic-chemical processes, can surpass current limitation in the controlled top-down fabrication of architecture nanometer sized structures.

In the context of self-organized functional architectures, the two terms "self-assembly" and "self-organization" are important to be considered:

"In essence, we distinguish the two processes on a thermodynamic basis. Although self-organization implies a nonequilibrium process, self-assembly is reserved for spontaneous processes tending toward equilibrium." [1]

This thesis is concerned with the *self-assembly* of molecular modules into molecular architectures and addresses their morphology, as well as their chemical and physical properties. Here, we focus on processes at 2D metal-vacuum interface, i.e. on the self-assembly of functionalized building blocks at atomically clean single-crystal surfaces. Next to the often strong forces at surfaces also physics and chemistry, influencing molecules and being confined to two, one or zero dimensions, varies significantly from the behaviour of the same objects in bulk or solution. Thus, the "nanoscale" offers to researchers the possibility to explore new effects and to realize desired molecular architectures with atomic precision. The development of new self-assembled architectures requires detailed knowledge about the molecule/surface, intermolecular and intramolecular interactions. In our study we employ molecules exhibiting different symmetry, functional groups and physical properties, as well as surfaces of different symmetry and properties. The design strategy includes a use of specific intermolecular interactions: H-bonding or dipole-dipole interactions, as well as the promotion of the on-surface reactions resulting in metal coordination or covalent bonding.

Prior Art

The idea of nanofabrication using a bottom-up approach motivates scientists i) to explore new principles of self-assembly in order to realize highly ordered supramolecular structures, and ii) to investigate their properties with the goal in mind to increase the level of control.

Subsequently, a considerable number of supramolecular structures has been addressed in the scientific literature. [2,3] In most cases at the solid/vacuum interface, the self-assembly relies on the design of building-blocks, i.e. on the functionalization of a molecule which ideally should result in the 'predictable', and thereby controllable assembly following design rules which mostly need to be discovered and investigated still. The architecture of the desired molecular patterns can be based on weak intermolecular interactions (Van-der-Waals, dipole-dipole, H-bond) or on strong intermolecular interactions (metal-coordination or covalent bonds). There is a number of studies reporting on the regular on-surface arrangement based on directional H-bonds between the molecules. [4–6] A broad range of self-assembled structures has been realized via ligands possessing a lone pair and coordinating with appropriate metal-centers. [7–10] More robust 1D and 2D polymers have been shown on the basis of on-surface covalent reactions. [11,12] Furthermore, the consolidation of two different functional groups, inherently embedded in the symmetrical positions of the molecule, has shown to initiate temperature induced reactions, which can be staged in a hierarchical manner. [13,14]

Outline

Nature surrounds us with many interesting features which people try to understand and to describe. Particularly, the overwhelming complexity of biological processes, e.g. in the human body, involves chirality and is crucially affected by the site specific recognition between the molecules as they assemble and operate. [15] One example for the chirality importance is provided by a drug effect in the human body: only the molecules of the 'right' chirality exhibits a beneficial effect, while the other can be attributed to no or even 'harming' effects. [16,17] Thereby the understanding of chirality and the control in molecular assemblies and architectures is of essential importance in pharmaceutical applications but at large not restricted to these.

The mechanisms of chirality propagation and the combined impact of parameters like reduced to 1D dimensionality, intermolecular binding motifs and molecular flexibility were rarely investigated in a systematic way. This motivated a choice of the first system which has been investigated in this thesis, i.e. a chiral molecule, dicyano-functionalized helicene derivative (diCN-Hel) that is shaped like one turn of a screw. The molecule allows to simultaneously study the delicate interplay of three important aspects, namely: the role of functional groups directing self-assembly, the flexibility and the chirality. By the functionalization of the molecule in almost opposite symmetric positions (C-atoms 6 and 13 of the aromatic backbone), linear or close to linear intermolecular connections are facilitated. Indeed, this combination of architectural features leads to the arrangement of molecules in 1D chain-like structures on the substrate surface. Moreover, the cyano-group possesses an electron lone pair, which can participate in a H-bond or, alternatively, in a coordination bond with an eventually present transition metal adatom. The helix of the molecule can be considered as a 'mechanical spring' giving rise to significant molecular flexibility and consequently facilitating adaptation to the underlying substrate, which allows neighbouring molecules to closely interact. Thereby such adaptation mechanisms lead to long-range order in the system after self-assembly. Furthermore, the formation of 1D structures (chains) by metal coordination on noble-metal substrates can promote their arrangement into linear coordination polymers aligned parallel to each other in consequence to the inter-chain repulsion. [18] In the studies reported about here, the Cu(111) substrate releases free Cu-adatoms at elevated temperatures (> 180 K) in amounts, which can be controlled by the temperature. [19] In order to independently verify the bonding motif in H-bonded assemblies and metal coordinated chains, additionally the less reactive Au(111)

substrate has been selected. The Au substrate serves as a rather inert support for the H-bonded structures thereby allowing to control the metal coordination via the deposition of selected transition-metal adatoms. The resulting un-coordinated or coordinated 1D chains are investigated as a model system – the chirality dependent mode of molecular assembly in analogy to Pasteur's experiment, while using scanning tunnelling microscopy to investigate the architectures, neither macroscopic crystal shape nor optical activity. The dependence of this process on the type and strength of the intermolecular interactions is also investigated (Figure 1).

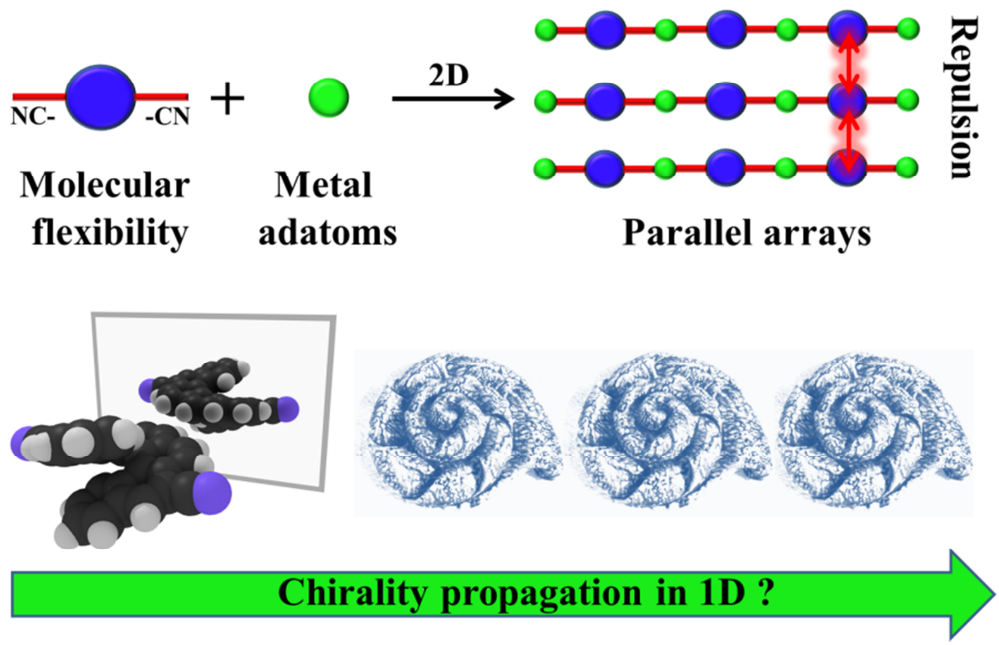

Figure 1 Schematic representation of a hypothetical diCN-Hel metal-coordinated self-assembly on the noble metal substrate. The system can be used to explore the chirality transfer mechanisms at reduced dimension (1D) and to investigate the importance of i) the type and strength of the intermolecular bonding motif, ii) the flexibility of the molecule and iii) the detailed molecular recognition mechanism.

The second molecular system, which has been investigated, is provided by the perylene derivative (DPDI), which has been chosen for its well-defined, planar, molecular structure and for its functionalization with amino- and imino- groups. Earlier studies, performed on DPDI on Cu(111), evidenced the full dehydrogenation of the molecule and subsequent coordination to Cu metal adatoms in a two-step process of hydrogen release (Figure 2a). [20] The first step drives molecule in a singly dehydrogenated (deh-DPDI) state with two imino-nitrogens at each end. The second step includes a potential ring closure and further dehydrogenation driving molecule in a triply dehydrogenated (3deh-DPDI) state, where two azo-bridges are formed. Interestingly, the geometry of the N-ligating atoms, contained in the intermediate and the resulting molecule, would allow it to act as an endo- or as an exo-ligand (Figure 2b). Obtaining endo- or exo- ligating species from the same precursor directly on the surface provides an interesting and powerful approach to control the dimensionality of the coordination polymers.
Understanding of the possible on-surface reactions and their application in the control of the resulting polymers' geometry/dimensionality has straight forward value for controlling polymer

architectures at interfaces as they are e.g. used in organic electronic applications. From this perspective, it would be highly desirable to know if it is possible to dehydrogenate the DPDI precursor only till the first level, in order to obtain the stable quinoidal bis-imino form (deh-DPDI). In case if transformation of DPDI to stable deh-DPDI form is possible, would be advantageous to know whether the molecule can be still converted to its triply-dehydrogenated form by e.g. thermal activation. Studies of amino-related species tending to be modified through reactions with transition metal atoms in solution and subsequent dehydrogenation have been reported in the scientific literature. [21] These motivated our studies of the on-surface coordination of DPDI in presence of different, selected, transition metal adatoms (Co, Fe, Ni, Cu). In similarity to the method used for the CN-coordination studies reported in this thesis, different substrates were used: Cu, which is observed do induce reactions of the DPDI and the more chemically inert Au. Moreover, to study the impact of the surface registry/symmetry we employ the substrates of hexagonal (111) and of square (100) symmetry. In order to assign the chemical state of the molecule after the transformation, we probe the nitrogen contained in the functional groups at the two ends of the molecule by the spectroscopy methods (XPS, NEXAFS). The geometry of the resulting coordination polymer is visualized by STM. Additionally, the experimental assignments of the resulting reaction products and their on-surface geometries are complemented by DFT calculations.

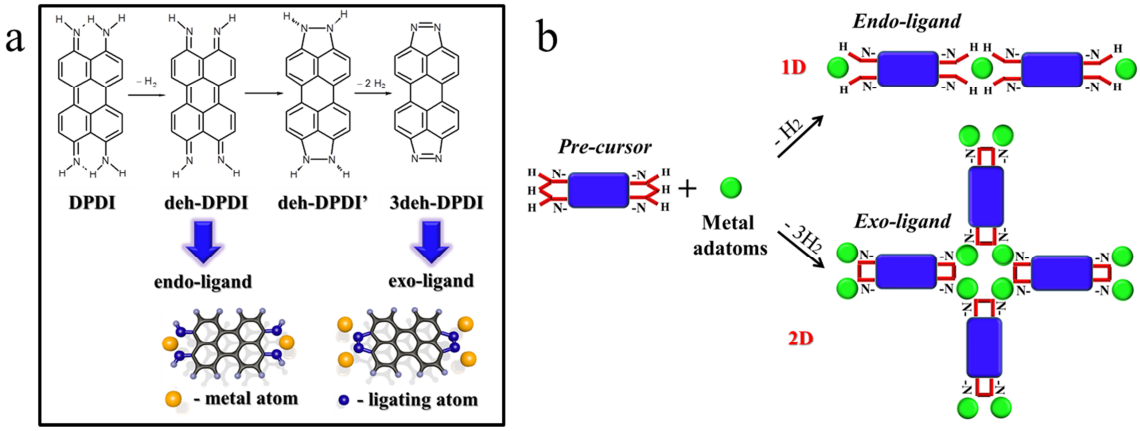

Figure 2 (a) Dehydrogenation route of DPDI via a singly dehydrogenated quinoidal bis-imino form (deh-DPDI) and further dehydrogenation with cyclization resulting in triply dehydrogenated DPDI (3deh-DPDI). [20] (b) Schematic representation of the precursor transformation into endo-/exo-ligand on surfaces depending on the transition metal adatoms supplied. The type of resulting ligand defines a dimensionality of the on-surface coordination-polymer.

On-surface self-assembled molecular architectures require a high degree of stability in view of potential applications. Thereby new covalent polymerization reactions which proceed for molecules adsorbed on surface substrates are highly desired. From this perspective a third system - perylene derivative DIBOTAP, has been selected. Thereby we intended to realize a covalent reaction, which is known to occur in solution [22], on the solvent-free vacuum/solid interface. The reaction involves two components: borylene-functionalized perylene derivative (DIBOTAP) and trimesic acid (TMA), and is expected to form a covalent B-O bond accompanied by the release of H_2. The unique feature of this type of covalent B-O link is its potential flexibility, which lead to the formation of variously-shaped molecular pores. Such

pores provide a unique opportunity to study electron confinement in quantum boxes of different size and shape which are constructed from the barriers of the same molecular backbone (Figure 3).

We employ an element-specific spectroscopic method (XPS) in order to identify the starting materials and the reaction products on the surface substrate. Thereby the evolution of the on-surface covalent reaction can be monitored by assessing the chemical environment of B, N, C and O atoms of the precursors DIBOTAP and TMA being modified by the presence of the reaction. The shape of the resulting polymer is investigated by STM. Also the strength of the surface state confinement inside the molecular pore is probed by STS.

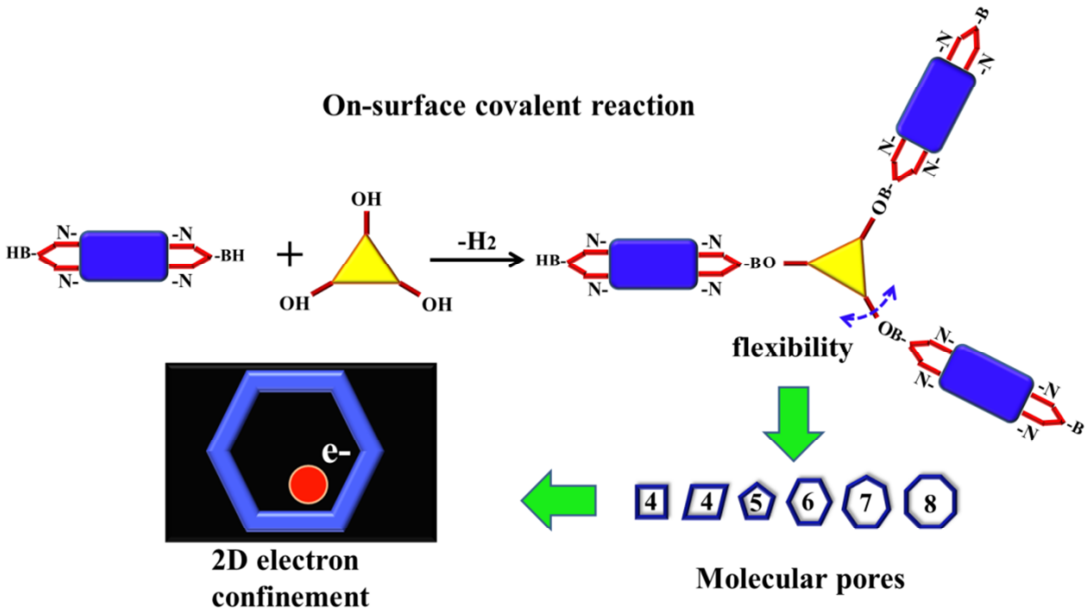

Figure 3 Scheme of the bi-component covalent reaction forming a potentially flexible interconnecting bond between the two components. The covalent reaction can promote the formation of differently sized molecular pores integrated in a 'sponge-like' network, which can be used for systematic investigations of the electron confinement in 2D quantum wells.

Organic nanoelectronics requires a high level of order and precision in the architecture and its manufacturing, which are therefore desirably to be obtained by self-assembly. For this purpose, as has already been described in the earlier paragraphs, many different approaches have been used involving the specially functionalized molecules and their arrangement on the basis of covalent bonds, metal coordination or maximization of H-bonds. The last part of this PhD thesis reports on a radically new mechanism for the self-recognition and self-sorting between the ad-molecules at surfaces: by means of the coulomb interaction between charge-transfer dipoles induced directly on the surface. The proposed scheme of the intermolecular interaction is shown in Figure 4. To date no work had been reported in the literature, which employs this mechanism to order by self-sorting the binary molecular mixtures in a 2D chessboard like lattice.

We have chosen a Bi-reconstructed Cu(100) substrate on the basis of the following considerations: i) this substrate with potentially strong Rashba-type splitting of the electronic states [23,24] has not previously been studied in conjunction with molecular ad-layers; ii) The weak interaction observed between ad-molecules and thick bismuth film [25], which is expected to facilitate a high molecular mobility as a crucial factor for molecular self-assembly; iii) the electron band structure of Bi is classified as a semi-metal and should lead to a higher

Debye length of Bi reconstructed Cu in comparison to bare Cu. The Debye length is a parameter describing the decay of the electric field into a conductive material, thereby is crucial for describing the decay of the coulomb field inside the material and the screening of charge dipoles, which in our case are present at the molecule/surface interface. The model ad-molecules to be investigated on this interface were selected for their distinct of high and low electron affinity [26], i.e. CuPc and MnPc. These respond to doping in the bulk and can undergo reduction or oxidation, as has been reported in literature for molecular thin films. [27] Thereby, deposition of CuPc and MnPc molecules, exhibiting opposite doping characteristics [28,29], may lead to a different charge state of each molecule after adsorption on the surface substrate. In our research we investigate the electronic characteristics of each molecule and corresponding self-assembled patterns for each molecular component and their binary mixture by means of microscopy (STM) and tunneling spectroscopies (dI/dV and I(z)). Scanning tunnelling spectroscopy is capable of local probing, i. e. the transition metal center or benzene ring, accessing the LDOS of *d*- or π- derived orbitals.[30,31] Recording the I(z)-map, i.e. an array of I(z) spectra, over the molecular islands allows to obtain more insight into the spatial variation of the work-function [30,31] on the molecule/surface interface.

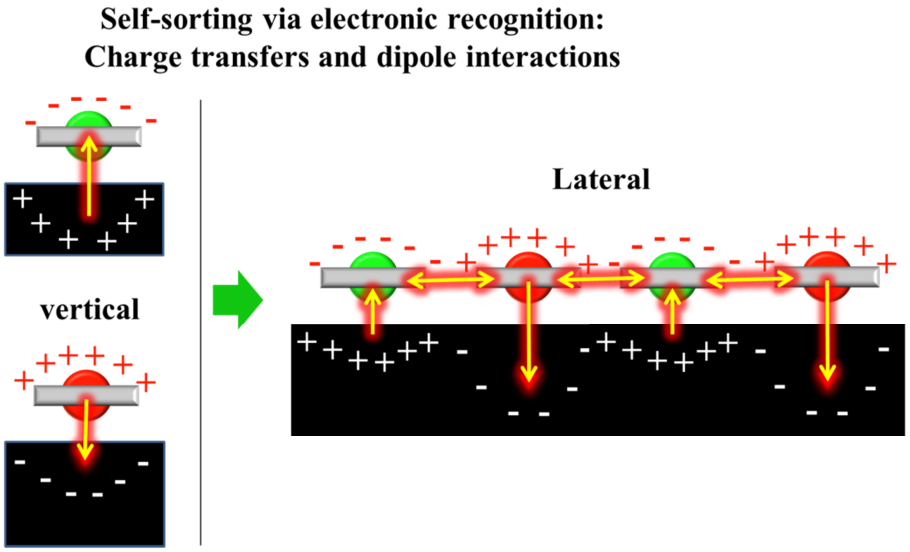

Figure 4 The approach taken for the self-sorting of two different types of ad-molecules (marked by green and red) by their coulomb interaction between charge transfer dipoles. The sketched charge distribution below the molecules indicates how the surface with the limited screening and high Debye length responds to molecular ad-layer. Note that the charge clouds are only provided as a sketch. There are also other factors which need to be considered e.g. HOMO/LUMO alignment which renders the system very complex.

Methods and Concepts

This section gives a short description of the key methods and concepts which are important for the investigation of physical and chemical properties of supramolecular on-surface architectures. The basic approach, which has been taken towards the characterization of nanoscale structures in this thesis, typically includes: a combination of 'local', i.e. probe microscopy and 'non-local', i.e. X-ray absorption and Photoelectron Spectroscopy methods. More specifically, the samples' morphology has been assessed by STM and the electronic properties have been inquired locally by STS, as well as the work function / barrier height above molecule or sample has been assessed by I(z) spectra. For quantitative and qualitative element specific analysis a number of different techniques have been used, i.e. XPS, XAS and NEXAFS. For a more detailed description of the methods than what is briefly reviewed below the reader is referred to the cited articles and textbooks.

X-Ray Photoelectron Spectroscopy (XPS) is an element-specific and surface sensitive technique, which is based on the photoelectric effect. Here the binding energies (BE) of the electronic core-levels of the atoms are probed by analysing their kinetic energy after excitation with monochromatic X-ray light. At first, this allows to obtain information about the elemental composition, as binding energies for the core levels of different elements vary largely. In a more refined analysis also the degree of 'core level shift' can be analysed, which depends on the details of the interaction of the outer lying shell electrons with binding partners. Thereby different oxidation states of the same element can be identified as they depend on the specific atomic environment of the species under study (e.g. C1s BE of CH_4 vs. CH_3F). Thereby, the analysis of the peak positions and their relative intensities gives qualitative and also quantitative information. [32] In comparison to other analytical methods, XPS is generally considered semi-quantitative as often quite significant knowledge has to be taken into account about the sample composition to obtain reasonable stoichiometry by fitting the finite line shape peaks which at time also overlap with other photo-excitation features. The finite line width of laboratory X-ray sources depends on whether a monochromator has been used or on whether synchrotron light is available for the particular experiment.

X-ray absorption spectroscopy (XAS) is based on the excitation of electrons by photons and recording absorption as a function of the photon energy. Thus, the method requires a tunable X-ray source, which can currently only be provided by a synchrotron or a Free Electron Laser.

Near edge X-ray Absorption Fine Structure spectroscopy (NEXAFS) is a technique based on XAS, which determines the position of the core level by determining the X-ray absorption edge corresponding to it. The X-ray absorption near the X-ray peak structure depends critically on different factors like the density of states, transition probabilities (allowed by selection rules), resonances and many-body effects. Also here the oxidation state molecules can be determined [33] via chemical shift of the edge position. By using linear polarized X-ray light in NEXAFS, also the orientation of different absorbers can be analysed.

Scanning Tunneling Microscopy (STM) is a local probe method based on the quantum tunneling effect, where the electron has a non-zero probability to pass through the tiny vacuum

gap between tip and sample. The tunnelling current is defined by the bias voltage between the tip and a sample and their local density of states (LDOS). Scanning can be performed in two modes: the constant height mode or the constant current mode. In the latter case the current is kept constant by a feed-back loop and the height is recorded. Probing the sample at different bias voltages allows to extract information on the LDOS. Thereby the 'electronic morphology' of the surface structures can be assigned with molecular, sub-molecular or even atomic resolution. By applying negative or positive sample voltages occupied and unoccupied states of the sample can be probed. [30,34]

Scanning Tunneling Spectroscopy (STS) is a local probe spectroscopy technique, where a sinusoidal modulation voltage is superimposed to the constant bias voltage. Tunneling current modulation, being in-phase with the applied voltage modulation (by means of lock-in amplifier), is recorded. The resulting dI/dV features in dependence on voltage are directly proportional to the LDOS. [30,34]

Current-distance I(z) measurements allow to determine the relative local work-functions on the surface. From the recorded I(z) map recorded above the surface the relative change in the work-function can be extracted by fitting the I(z) spectra with exponentials. [31]

Molecular Beam Epitaxy (MBE) is a method of the film growth by thermal sublimation. Typically it involves a Knudsen-cell deposition source, where the material is heated to the sublimation temperature and deposited onto the surface. This technique only works for sublimable materials but allows the well-controlled growth of monolayers, multilayers and thin films on well-defined crystalline surfaces and multilayer films. [32]

Results

This thesis is based on four publications concerning on-surface molecular architectures and the investigation of their properties, including the exploration of new physical effects and new on-surface reactions. [[1-4]] This thesis is provided in the ‘cumulative’ format and the following text provides a brief summary of each article as a service for the fast reader. All reports depend on highly functionalized building blocks which are programmed in characteristically different ways towards their integration in macromolecular or supramolecular on-surface architecture. It has been a long term goal of the hosting group to unravel the interdependence of the structure of the building blocks with the architecture and the functional properties of the self-assembly. In this context ground-breaking work has been reported in the context of chiral-molecules linking in chains, of metal coordination chains and networks being programmable by triggering endo- or exo-ligation through the selected metal provided for coordination, by exploring a borylene derived and flexible chemical motif to provide a ‘sponge’ like on-surface polymer and last but not least the selectively different charge transfer of molecules demonstrating an unprecedented mode of binary supramolecular ordering by charge transfer dipoles and their electrostatic, i.e. coulomb interaction.

Chirality Transfer in 1D Self-Assemblies: Influence of H-Bonding vs Metal Coordination between Dicyano[7]helicene Enantiomers

Summary:

Here we present a long-range ordered and tunable chain which is built by on-surface self-assembly, based on the enantiopure 6,13-dicyano[7]helicene building-block. We show that H-bonded 1D chains can be switched to metal-coordinated chains by the addition of Cu adatoms. We study the mechanism of the chirality transfer in a system of reduced dimensionality (i.e. 1D) for the first time. The overall structure of chains changes from short-range ordered chains to highly ordered parallel arrays after Cu-coordination. Moreover, the corresponding chain architecture changes from zig-zag to linear. We found 'zig-zag' chains in mirror symmetry which we attributed to H-bonded arrays. By switching to a stronger bonding motif, however, the mirror symmetry of the chain architecture on the substrate disappears. Furthermore, we found a significant flexibility of the molecules which adapt to the constraints imposed by the strong coordination bond in conjunction with the fixed adatom positions in registry with the substrate. In our analysis of this system we relate intermolecular bonding strength and molecular flexibility, as they affect chiral recognition and chiral separation in an on-surface chain assembly.

The bonding motifs and corresponding supramolecular architectures are investigated via Scanning Tunneling Microscopy (STM), X-Ray Photoelectron Spectroscopy (XPS) and supported by the Density Functional Theory (DFT) calculations.

Paper [[1]] has been published in the Journal of the American Chemical Society in 2013. Contribution of Aneliia Shchyrba: carried out the experimental investigation (STM, XPS), analysed the data, wrote the manuscript.

JACS
JOURNAL OF THE AMERICAN CHEMICAL SOCIETY

Communication

pubs.acs.org/JACS

Chirality Transfer in 1D Self-Assemblies: Influence of H-Bonding vs Metal Coordination between Dicyano[7]helicene Enantiomers

Aneliia Shchyrba,[†] Manh-Thuong Nguyen,[‡] Christian Wäckerlin,[§] Susanne Martens,[†] Sylwia Nowakowska,[†] Toni Ivas,[†] Jesse Roose,[⊥] Thomas Nijs,[†] Serpil Boz,[†,¶] Michael Schär,[⊥] Meike Stöhr,[∥] Carlo A. Pignedoli,[#] Carlo Thilgen,[⊥] François Diederich,[⊥] Daniele Passerone,[#] and Thomas A. Jung*[,§]

[†]Department of Physics, University of Basel, Klingelbergstrasse 82, 4056 Basel, Switzerland

[‡]The Abdus Salam International Centre for Theoretical Physics, Strada Costiera 11, I-34151 Trieste, Italy

[§]Laboratory for Micro- and Nanotechnology, Paul Scherrer Institute, 5232 Villigen, Switzerland

[⊥]Laboratorium für Organische Chemie, ETH Zurich, Wolfgang-Pauli-Strasse 10, 8093 Zürich, Switzerland

[∥]Zernike Institute for Advanced Materials, University of Groningen, Nijenborgh 4, 9747 AG Groningen, The Netherlands

[#]Empa, Swiss Federal Laboratories for Materials Science and Technology, Überlandstrasse 129, CH-8600 Dübendorf, Switzerland

Supporting Information

ABSTRACT: Chiral recognition as well as chirality transfer in supramolecular self-assembly and on-surface coordination is studied for the enantiopure 6,13-dicyano[7]helicene building block. It is remarkable that, with this helical molecule, both H-bonded chains and metal-coordinated chains can be formed on the same substrate, thereby allowing for a direct comparison of the chain bonding motifs and their effects on the self-assembly in experiment and theory. Conformational flexure and both adsorbate/adsorbent and intermolecular interactions can be identified as factors influencing the chiral recognition at the binding site. The observed H-bonded chains are chiral, however, the overall appearance of Cu-coordinated chains is no longer chiral. The study was performed via scanning tunneling microscopy, X-ray-photoelectron spectroscopy and density functional theory calculations. We show a significant influence of the molecular flexibility and the type of bonding motif on the chirality transfer in the 1D self-assembly.

Controlling and understanding chirality in chemical reactions and during self-assembly is important, in particular if chiral or pro-chiral building blocks are involved.[1,2] Recently, a Pasteur-type[3] spontaneous chiral resolution was shown to occur also in two dimensions, at surfaces.[2a,4] In analogy to the 3D case, the condensation of 2D islands at surfaces can be controlled by the enantiomeric excess[5] of one component or by a chiral auxiliary.[6] Chirality transfer and the long-range expression of chirality in molecular self-assembly have been studied intensively in surface science. These studies involved prochiral molecules[6,7] which become chiral upon conformational changes induced by their interaction with the substrate, as well as inherently chiral molecules. A very interesting model system is [*n*]helicenes, which have been used to study the chirality transfer during nucleation and self-assembly at the solid/liquid interface[8] as well as at the solid/vacuum interface.[9] No chiral interactions were observed for layers of hexathia[11]helicene on Au(111) nor for linear ad molecular chains on Au(110).[10] Parschau et al. studied the chirality transfer of [7]helicene in the growth of 2D islands by van der Waals (vdW) interactions.[11] Later, Stöhr et al. showed the spontaneous resolution of (±)-6,13-dicyano[7]-helicene driven by polar interactions,[12] and Seibel et al. described the 2D separation of pentahelicene into homochiral domains purely through vdW forces.[13] Only a few investigations on chiral molecules self-assembling to structures of further reduced dimensionality, i.e. 1D, have been reported: On calcite, Kühnle et al. observed islands of enantiopure [7]helicene-2-carboxylic acid and chains of the racemate, both stabilized by $\pi-\pi$ stacking.[14] Here we report on the chirality transfer that takes place during the self-assembly of enantiopure dicyanohelicene building blocks into 1D chains, with particular focus on the influence of the intermolecular bonding motif.

With enantiomers of cyano-functionalized helicenes, (*P*)-(+)-6,13-dicyano[7]helicene and (*M*)-(−)-6,13-dicyano[7]-helicene ((*P*)-**1** and (*M*)-**1**, Figure 1), we earlier introduced an inherently chiral molecule with intermolecular bonding capability.[12] In this work we demonstrate that the intermolecular interactions can be tuned by the presence or absence of coordinating metal atoms, i.e. adatoms that can be supplied by

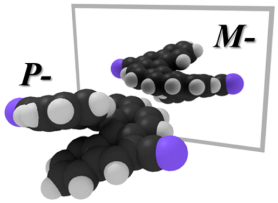

Figure 1. Enantiomers of 6,13-dicyano[7]helicene: (*P*)-**1** and its mirror image (*M*)-**1**.

Received: July 17, 2013
Published: October 3, 2013

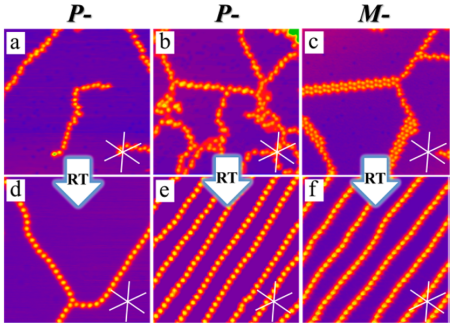

Figure 2. Top: Transition, upon heating, of self-assembled chains of enantiopure **1** created by deposition at low (a) and higher (b,c) coverages of (a,b) (*P*)-**1** or (c) (*M*)-**1** on cold (90 K) Cu(111) substrates. Here coverages are significantly smaller than in our previous work.[12] Bottom: Evolution of the chain morphology after heating to RT. STM images of enantiopure dicyano[7]helicenes taken at 5 K (30 × 30 nm^2, 25 pA, 1.2 V) reflect linear zigzag-shaped H-bonded self-assemblies and the subsequent formation of elongated islands at increased coverage created by deposition of (a,b) (*P*)-**1** and (c) (*M*)-**1** onto a Cu(111) substrate held at 90 K. (d–f) Formation of highly ordered molecular chains after annealing for 1 h at 300 K of the samples shown in (a–c). Chains of both chirality senses, (*P*)-**1** and (*M*)-**1**, are oriented 30° off the Cu(111) high-symmetry directions (indicated by white stars in each STM image).

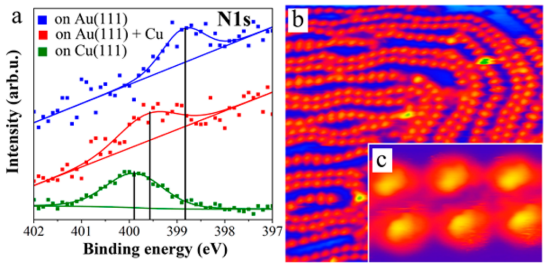

Figure 3. (a) XPS of submonolayer coverage of (*P*)-**1** on Cu(111) (green) and Au(111) before (blue) and after (red) Cu addition. The presence of Cu adatoms significantly increases the N1s BE, confirming the formation of a Cu coordination complex. (b) STM image (35 × 35 nm^2, 77 K) revealing Cu-coordinated (*P*)-**1** chains on Au(111), oriented along the linear domains of the herringbone reconstruction.[20] (c) High-resolution STM image (4.0 × 1.8 nm^2, 77 K) of two neighboring chains on the hcp-domain of the reconstructed Au(111) surface (cf. Figure S6).

means of deposition or by thermally activated release from the substrate. An irreversible conversion of 1D H-bonded assemblies of enantiomerically pure **1** to a Cu-coordinated chain assembly occurs. Surprisingly, in the H-bonded case, the opposite enantiomer leads to chains of inverted symmetry, whereas this is not the case for the metal-coordinated chains.

All samples were prepared and characterized in ultrahigh vacuum. Molecules were deposited onto the substrates held at 90 or 300 K. Morphological assignment of the self-assembled structures was performed via scanning tunneling microscopy (STM) at 5 K, unless mentioned otherwise, and the chemical environment of N-atoms in the CN-groups was characterized by X-ray photoelectron spectroscopy (XPS) at room temperature (RT). Complementary density functional theory (DFT) calculations are used to model possible supramolecular arrangements (see Supporting Information (SI) for experimental and computational details).

STM experiments, performed after deposition of enantiopure (*P*)-**1** or (*M*)-**1** on Cu(111) held at 90 K, reveal assemblies that are modified after heating to RT. STM images of enantiopure **1**, deposited on Cu(111) at 90 K, show a zigzag chain organization for (*P*)-**1** (Figure 2a,b) and (*M*)-**1** (Figure 2c). With increasing coverage, the well-separated zigzag chains (Figure 2a, ∼0.05 mol/nm^2) evolve into irregular networks of chains and linear supramolecular islands (Figure 2b,c; ∼0.17 and ∼0.15 mol/nm^2, respectively). Interestingly, we observe the directions of the chains to be independent of the chirality sense of the constituent molecules, namely along the directions rotated by 30° with respect to the principal axis of the Cu(111) surface. Heating the samples to RT and re-investigating by STM at 5 K reveals a strongly modified morphology: only long and straight chains occur, oriented along the same crystallographic directions as before. The chain direction again does not change with chirality sense ((*P*)-**1**, Figure 2d,e/(*M*)-**1**, Figure 2f). The evolution of zigzag chains to linear chains has also been observed for the racemic mixture (±)-**1** (cf. Figure S1). Importantly, at increased coverage, a new phase consists of large domains of parallel and quasi equidistant linear chains (cf. Figure S2). We attribute this to repulsive electrostatic interactions (Figure 2e,f; see also SI sections 4 and 10), as similarly assigned for Cu-pyridyl coordinated chains.[15] These complex phenomenological changes and the transition from chiral H-bonded zigzag chains to straight linear chains with overall lack of chiral appearance (*vide infra*) hint at modified chain binding motifs after annealing, in agreement with CN-Cu-assisted on-surface assembly.[16]

The chain architecture critically depends on intermolecular interactions. The zigzag structure of the chains formed at low (90 K) sample temperature can be tentatively attributed to a balance between H-bonding (C–H···NC) and vdW interactions. We performed an XPS study to investigate the nature of the interactions in the straight chain assembly. For this purpose, we sublimed (*P*)-**1** onto Cu(111) and Au(111) surfaces kept at 300 K. The N1s binding energies of (*P*)-**1** correspond to 398.85 eV for submonolayer coverage on Au(111) and 399.15 eV for a multilayer on Cu(111) (cf. Figures 3 and S4). These values correspond well with N1s XPS data for cyano substituents.[17] The significantly higher N1s binding energy (BE) for submonolayer coverage of (*P*)-**1** on Cu(111) (399.85 eV) evidences a different chemical environment of the nitrogen. Further, only one N1s peak is observed, revealing equal bonding of both CN groups. Notably, the lone-pair of the N atom might interact with the Cu substrate. However, sp-hybridization of the cyano nitrogen and energetically favorable σ-donor complexation to a metal (M) require a CN–M angle close to 180°. Thus, this arrangement with both cyano groups simultaneously pointing to the surface is barely feasible (cf. Figure 1). In the case of chemisorption of the CN groups and absence of their coordination, a N1s peak at lower BE would be expected.[18] Our observation of the N1s at higher BE provides experimental evidence for the involvement of Cu adatoms in intermolecular bonding and chain formation, supported by the STM manipulations and DFT calculations (cf. Figure S7 and SI section 12).

To confirm the presence of Cu adatoms in the straight chain architecture, we evaporated a trace amount (∼0.07 ML) of Cu onto the submonolayer of (*P*)-**1** on Au(111). In subsequently acquired XPS data, the N1s BE is shifted from 398.85 to 399.65 eV (Figure 3a). STM measurements performed on the same sample at 77 K show straight chains (Figure 3b).

dx.doi.org/10.1021/ja407315f | *J. Am. Chem. Soc.* 2013, 135, 15270–15273

Conversely, in the absence of trace amounts of Cu, STM at 77 K reveals only a 2D condensed phase (cf. Figure S5). These XPS and STM data confirm spontaneous coordination of (*P*)-**1** to Cu adatoms on Au(111). Notably, the Cu-coordinated chains are aligned along the herringbone reconstruction of the substrate (Figure 3b). In particular, the pair of chains in closer proximity (~2 nm) can be located at the linear hcp-domains, and the single chain follows the fcc-domains of the reconstruction (cf. Figures 3c and S6). Another interesting feature is the considerable variation in the intermolecular distance when the chains reorient by following the domains of the surface reconstruction. The range of variation (~1.2−1.5 nm ± 0.1 nm) is atypical for coordination complexes and may be attributed to the flexibility of the helicene backbone.

The observation of straight or zigzag chains dependent on the Cu(111) substrate temperature during deposition of (*P*)-**1** or (*M*)-**1** is consistent with the above-described observations of the Cu coordination occurring after deposition of Cu adatoms on Au(111) held at RT. Notably, we observed the coexistence of linear and zigzag chains after deposition of (*P*)-**1** on Cu(111) held at intermediate sample temperatures (~130 K). The availability of Cu adatoms from surface self-diffusion on Cu(111) depends primarily on the temperature, among other factors. At the substrate temperature used to generate zigzag chains (90 K), the presence of Cu adatoms is significantly lowered;[19] at further elevated temperatures CN-Cu complexes modify the chain (SI section 5).

An important question with regard to the chirality of the building block relates to the degree of chirality transfer observable in the two different architectures, namely the H-bonded vs the Cu-coordinated chains of (*P*)-**1** or (*M*)-**1**. The H-bonded chains of homochiral molecules appear as imperfect regular arrangement of dimers. However, far less defects occur in the chain after coordination to Cu. This is attributed to the thermodynamics of the system after being annealed, as well as to higher BE of the coordination bonds in comparison to H-bonds. Moreover, H-bonding can involve different aryl H atoms resulting in an aperiodic chain.[21] The most important difference between the two chain architectures lies in the presence or absence of mirror symmetry. For the H-bonded chains, the chirality of enantiopure (*P*)-**1** or (*M*)-**1** is reflected in the H-bonding pattern as mirroring of the dimers making the chain (Figure 4a,c). In contrast, no such signature is observable after Cu coordination where the apparent repetitive unit consists of a single molecule only (Figure 4b,d).

DFT calculations were performed to complement the experimental observations on (*M*)-**1** for the H-bonded (Figure 4e) and Cu-coordinated chains (Figure 4f). The superimposed simulated and experimental STM data show good agreement. The calculations confirm the modification of the chain architecture (Figure 4e,f, cf. Figures S7−S9) with the transition of the bonding motif. As demonstrated in the side views in Figure 4e,f, the dimers of the H-bonded chain derive from close contact interactions (H-bond, preferred to CN−Cu bonding and vdW) between two helicene molecules, leading to two nonequivalent positions of the CN groups involved in the bonding. This nonequivalence implies that the chain exhibits a directional sense, and re-orientation of different segments within one chain is improbable due to the different angle formed by the CN groups with respect to the substrate, as observed in Figure 4e. After Cu coordination, this nonequivalence is lifted by the flexure of the molecule to bind to the equidistant Cu adatoms. It seems that the strong coordination bond forces the helicene into the inter-

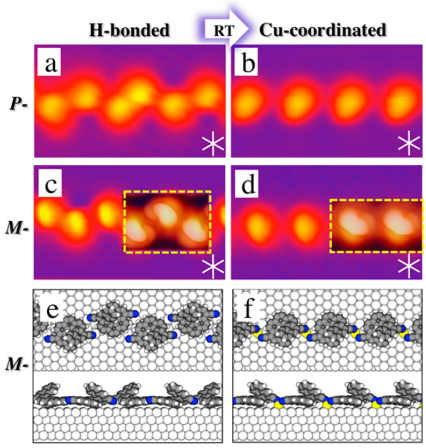

Figure 4. STM images (5.4 nm × 3.2 nm) of (a) (*P*)-**1** and (c) (*M*)-**1** on Cu(111) reveal a mirror-image appearance in H-bonded chains. After coordination with Cu adatoms, the chains have a similar appearance (b,d). Transition from one bonding motif to the other occurs upon annealing for 1 h at 300 K. Simulated STM images (marked by yellow dashed rectangles) of (c) H-bonded and (d) Cu-coordinated chains are superimposed onto the experimental ones. (e,f) DFT models for H-bonded and metal-coordinated (*M*)-**1** chains.

adatom gap which is determined by the lattice registry. This occurs for both enantiomers and also for the racemate (cf. Figure S1). The intermolecular distances, determined from STM data, increase from 1.00 nm for the H-bonded chains to 1.35 nm for the Cu-coordinated chains. Experimental results and calculations of the proposed models are in good qualitative and quantitative agreement (SI section 9).

Concerning the chirality transfer in supramolecular on-surface arrays, the two types of helicene chains provide a very interesting model system: the same molecule forms two different chain arrangements by either weak H-bonding or relatively stronger coordination bonds. In this context, it is important to discuss the intermolecular and molecule/substrate interactions with respect to the orientation of the building blocks within the chain. Note that all adsorbed helicenes of the same chirality sense can be aligned in the same manner by mere rotation and translation. Upon binding in a 1D chain, the CN groups are fixed to the nearest-neighbor molecules and exhibit a CN "tail" and a CN "head" with different angles with respect to the substrate. Thus, different arrangements within one chain are possible. Due to the geometric constraints of the H-bonded architecture, tail-to-tail and head-to-head connections are more plausible than tail-to-head connections. This preference is confirmed in the simulated minimal energy arrangement (Figure 4e, cf. Figure S9). Further evidence is provided by the regularity of chains formed from enantiopure helicenes in comparison to the irregular arrangement of the racemic H-bonded chain on the same substrate.

Switching the point symmetry (chirality sense) of the building block from (*P*)-**1** to (*M*)-**1** leads to exact mirroring of the self-assembled H-bonded chains: the characteristic "dimers" recognized in the STM data are symmetry-inverted. The overall "chain direction" with respect to the surface, however, remains the same. We attribute this observation to the high symmetry of the chain directions, i.e. $\langle 11\bar{2} \rangle$ family of directions, which are mapped onto themselves upon symmetry inversion. After Cu coordination of the enantiopure (*P*)-**1** or (*M*)-**1**, the character-

istic image of the chain is modified, and two different orientations of the building blocks in the chain arrangement can be observed. These orientations are observed in random distribution, so all possible combinations occur: head−head, head−tail, and tail−tail (Figure S12). This behavior indicates that the coordination bond, unlike the H-bond, does not differentiate head−tail, head−head, and tail−tail connections; thus, we do not observe mirror-image patterns in enantiopure Cu-coordinated chains. The racemic helicene forms Cu-coordinated chains along the same $\langle 11\bar{2} \rangle$ directions. Stereoselectivity, a key factor in the assembly of the H-bonded chain, becomes negligible due to the strong influence of the metal coordination bond. This is confirmed in the numerical calculations by the limited flexure in H-bonded chains leading to nonequivalent bonding and by the considerable flexure of the helicenes after the stronger coordination bond is formed. This stronger binding in the chain (i) flexes helicenes, (ii) directs the chain formation despite small energy differences stemming from the different binding motifs (i.e., 3^2 for a racemate), and (iii) overcomes nonequivalences in the molecular footprint of helicene on the corrugated substrate between the adatoms.

In general, molecular superstructures comprised of chiral elements on any surface give rise to mirror-inverted structures when the element of opposite chirality sense is used.[2] Our work demonstrates a remarkable exception, as the direction of helicene chains is independent of the chirality sense (*P* or *M*) of the molecular building block—neither in the case of the H-bonded nor the Cu-coordinated chain. However, locally we observe that the symmetry of the H-bonded dimers is mirrored when the helicene of opposite chirality sense is used. By Cu coordination, the tolerance to symmetry and registry defects is observed to increase considerably. Thus, no spontaneous resolution is expected for 1D arrangements formed by Cu coordination. In conclusion, the complexity of intermolecular interactions—in the present case flexibility and weaker H-bonding vs stronger Cu coordination—significantly affects the possibility of chiral recognition and spontaneous resolution.

■ ASSOCIATED CONTENT

Supporting Information

STM, XPS, and DFT methods and analyses. This material is available free of charge via the Internet at http://pubs.acs.org.

■ AUTHOR INFORMATION

Corresponding Author

thomas.jung@psi.ch

Present Address

[¶]Faculty of Engineering, Gedik University, 34876, Kartal, Istanbul, Turkey.

Notes

The authors declare no competing financial interest.

■ ACKNOWLEDGMENTS

We gratefully acknowledge financial support from the National Centre of Competence in Research Nanosciences (NCCR-Nano), Swiss Nanoscience Institute (SNI), Swiss National Science Foundation (grants No. 200020-137917, 206021-113149, 206021-121461), and Wolfermann Nägeli Foundation, and the Swiss Supercomputing Center (CSCS) for computational support. The authors sincerely thank N. Ballav for fruitful discussions, R. Pawlak, S. Kawai, R. Schelldorfer, and M. Martina for support during measurements, and H. Rossmann for contribution to the graphics. The STM data were processed with the WSXM software.[22]

■ REFERENCES

(1) Shen, Y.; Chen, C.-F. *Chem. Rev.* **2012**, *112*, 1463.

(2) (a) Ernst, K.-H. *Phys. Status Solidi B* **2012**, *249*, 2057. (b) Gingras, M. *Chem. Soc. Rev.* **2013**, *42*, 1051.

(3) Flack, H. D. *Acta Crystallogr. A* **2009**, *65*, 371.

(4) (a) Santagata, N. M.; Lakhani, A. M.; Davis, B. F.; Luo, P.; Buongiorno Nardelli, M.; Pearl, T. P. *J. Phys. Chem. C* **2010**, *114*, 8917. (b) Ortega Lorenzo, M.; Baddeley, C. J.; Muryn, C.; Raval, R. *Nature* **2000**, *404*, 376. (c) Barlow, S. M.; Louafi, S.; Le Roux, D.; Williams, J.; Muryn, C.; Haq, S.; Raval, R. *Langmuir* **2004**, *20*, 7171.

(5) (a) Parschau, M.; Romer, S.; Ernst, K.-H. *J. Am. Chem. Soc.* **2004**, *126*, 15398. (b) Parschau, M.; Kampen, T.; Ernst, K.-H. *Chem. Phys. Lett.* **2005**, *407*, 433.

(6) De Cat, I.; Guo, Z.; George, S. J.; Meijer, E. W.; Schenning, A. P. H. J.; De Feyter, S. *J. Am. Chem. Soc.* **2012**, *134*, 3171.

(7) Mugarza, A.; Lorente, N.; Ordejón, P.; Krull, C.; Stepanow, S.; Bocquet, M.-L.; Fraxedas, J.; Ceballos, G.; Gambardella, P. *Phys. Rev. Lett.* **2010**, *105*, 115702.

(8) Balandina, T.; van der Meijden, M. W.; Ivasenko, O.; Cornil, D.; Cornil, J.; Lazzaroni, R.; Kellogg, R. M.; De Feyter, S. *Chem. Commun.* **2013**, *49*, 2207.

(9) (a) Fasel, R.; Parschau, M.; Ernst, K.-H. *Angew. Chem. Int. Ed.* **2003**, *42*, 5178. (b) Fasel, R.; Parschau, M.; Ernst, K.-H. *Nature* **2006**, *439*, 449.

(10) Taniguchi, M.; Nakagawa, H.; Yamagishi, A.; Yamada, K. *J. Mol. Catal. A Chem.* **2003**, *199*, 65.

(11) Parschau, M.; Fasel, R.; Ernst, K.-H. *Cryst. Growth Des.* **2008**, *8*, 1890.

(12) Stöhr, M.; Boz, S.; Schär, M.; Nguyen, M.-T.; Pignedoli, C. A.; Passerone, D.; Schweizer, W. B.; Thilgen, C.; Jung, T. A.; Diederich, F. *Angew. Chem. Int. Ed.* **2011**, *50*, 9982.

(13) Seibel, J.; Allemann, O.; Siegel, J. S.; Ernst, K.-H. *J. Am. Chem. Soc.* **2013**, *135*, 7434.

(14) (a) Hauke, C. M.; Rahe, P.; Nimmrich, M.; Schütte, J.; Kittelmann, M.; Stará, I. G.; Starý, I.; Rybáček, J.; Kühnle, A. *J. Phys. Chem. C* **2012**, *116*, 4637. (b) Rahe, P.; Nimmrich, M.; Greuling, A.; Schütte, J.; Stará, I. G.; Rybáček, J.; Huerta-Angeles, G.; Starý, I.; Rohlfing, M.; Kühnle, A. *J. Phys. Chem. C* **2010**, *114*, 1547. (c) Rybáček, J.; Huerta-Angeles, G.; Kollárovič, A.; Stará, I. G.; Starý, I.; Rahe, P.; Nimmrich, M.; Kühnle, A. *Eur. J. Org. Chem.* **2011**, *2011*, 853.

(15) Heim, D.; Écija, D.; Seufert, K.; Auwärter, W.; Aurisicchio, C.; Fabbro, C.; Bonifazi, D.; Barth, J. V. *J. Am. Chem. Soc.* **2010**, *132*, 6783.

(16) (a) Pawin, G.; Wong, K. L.; Kim, D.; Sun, D.; Bartels, L.; Hong, S.; Rahman, T. S.; Carp, R.; Marsella, M. *Angew. Chem. Int. Ed.* **2008**, *47*, 8442. (b) Sirtl, T.; Schlögl, S.; Rastgoo-Lahrood, A.; Jelic, J.; Neogi, S.; Schmittel, M.; Heckl, W. M.; Reuter, K.; Lackinger, M. *J. Am. Chem. Soc.* **2013**, *135*, 691. (c) Pivetta, M.; Pacchioni, G. E.; Schlickum, U.; Barth, J. V.; Brune, H. *Phys. Rev. Lett.* **2013**, *110*, 086102.

(17) Lindberg, B. J.; Hedman, J. *Chem. Scr.* **1975**, *7*, 155.

(18) (a) Sexton, B. A.; Hughes, A. E. *Surf. Sci.* **1984**, *140*, 227. (b) Piantek, M.; Miguel, J.; Krüger, A.; Navío, C.; Bernien, M.; Ball, D. K.; Hermann, K.; Kuch, W. *J. Phys. Chem. C* **2009**, *113*, 20307.

(19) Wang, W.; Shi, X.; Wang, S.; Van Hove, M. A.; Lin, N. *J. Am. Chem. Soc.* **2011**, *133*, 13264.

(20) (a) Fernandez-Torrente, I.; Monturet, S.; Franke, K.; Fraxedas, J.; Lorente, N.; Pascual, J. *Phys. Rev. Lett.* **2007**, *99*, 176103. (b) Böhringer, M.; Morgenstern, K.; Schneider, W.-D.; Wühn, M.; Wöll, C.; Berndt, R. *Surf. Sci.* **2000**, *444*, 199. (c) Yu, M.; Kalashnyk, N.; Barattin, R.; Benjalal, Y.; Hliwa, M.; Bouju, X.; Gourdon, A.; Joachim, C.; Lægsgaard, E.; Besenbacher, F.; Linderoth, T. R. *Chem. Commun.* **2010**, *46*, 5545.

(21) Wintjes, N.; Hornung, J.; Lobo-Checa, J.; Voigt, T.; Samuely, T.; Thilgen, C.; Stöhr, M.; Diederich, F.; Jung, T. A. *Chem.—Eur. J.* **2008**, *14*, 5794.

(22) Horcas, I.; Fernández, R.; Gómez-Rodríguez, J. M.; Colchero, J.; Gómez-Herrero, J.; Baro, A. M. *Rev. Sci. Instrum.* **2007**, *78*, 013705.

Supporting Information

Chirality Transfer in 1D Self-Assemblies: Influence of H-bonding vs Metal Coordination between Dicyano[7]helicene Enantiomers

Aneliia Shchyrba,[1] Manh-Thuong Nguyen,[2] Christian Wäckerlin,[3] Susanne Martens,[1] Sylwia Nowakowska,[1] Toni Ivas,[1] Jesse Roose,[4] Thomas Nijs,[1] Serpil Boz,[1,#] Michael Schär,[4] Meike Stöhr,[5] Carlo A. Pignedoli,[6] Carlo Thilgen,[4] François Diederich,[4] Daniele Passerone,[6] and Thomas A. Jung[3]*

1. Department of Physics, University of Basel, Klingelbergstrasse 82, 4056 Basel, Switzerland

2. The Abdus Salam, International Centre for Theoretical Physics, Strada Costiera 11, I - 34151 Trieste, Italy

3. Laboratory for Micro- and Nanotechnology, Paul Scherrer Institute, 5232 Villigen PSI, Switzerland

4. Laboratorium für Organische Chemie, ETH Zurich, Wolfgang-Pauli-Str. 10, 8093 Zürich, Switzerland

5. Zernike Institute for Advanced Materials, University of Groningen, Nijenborgh 4, 9747 AG Groningen, The Netherlands

6. Empa, Swiss Federal Laboratories for Materials Science and Technology, nanotech&surfaces laboratory, Überlandstrasse 129, 8600 Dübendorf, Switzerland

[#] Present Adress: Faculty of Engineering, Gedik University, 34876, Kartal, Istanbul, Turkey

Corresponding Author

*Tel: +41 56 310 4518; Fax: +41 56 210 2646; E-mail: thomas.jung@psi.ch

Table of Contents

1. General Methods

STM. Our investigations were carried out in ultra-high vacuum (UHV) with a base pressure of 5×10^{-11} mbar, equipped with low-temperature scanning tunneling microscope (STM), X-Ray Photoelectron Spectroscopy (XPS), facilities for substrate preparation, and molecule deposition. Atomically flat Cu(111) and Au(111) surfaces were made by repeated cycles of 1000 eV Ar^+ bombardment at 300 K and subsequent annealing at 800 K. To form self-assembled structures of 6,13-dicyano[7]helicene (**1**) molecules, enantiomerically pure (*P*)-**1**, (*M*)-**1**, and racemic (±)-**1** were deposited by thermal evaporation from commercial Kentax equipment (Kentax GmbH, Germany) on the substrates held at 90 K or 298 K. Glass crucibles with compound **1** were heated up for sublimation to approximately 450 K. The amount of molecular adsorbate was controlled by means of a quartz crystal microbalance (QCMB). STM images were obtained in a constant current mode (typical tunneling current 25 pA, sample bias 1.2 V) at 5 K and 77 K. Probe tips were made from Pt-Ir wire (90% Pt, 10% Ir) by means of simple mechanical cutting and cleaned by subsequent sputtering.

XPS. The X-ray photoelectron spectroscopy (XPS) measurements were performed in the Laboratory for Micro- and Nano-technology at the Paul Scherrer Institute (PSI; vide supra). The facility provides all required systems for the surface preparation, molecule and metal deposition, and analysis techniques like XPS and STM. XPS (Monochromatic Al Kα X-rays) energy resolution gives 1.0 eV full width at half maximum (FWHM). The energy calibration was performed using a Au reference. All XP spectra were obtained at 300 K.

DFT. Our calculations were carried out using the CP2K package.[1] We exploited the Perdew-Burke-Ernzerhof (PBE) GGA exchange-correlation functional[2] and corrected with a semi-empirical dispersion potential[3]. We utilized the Gaussian and plane-wave (GPW) hybrid basis set, namely, the DZVP basis set for Cu and the TZV2P basis for H, N, C and O; all basis sets are optimized for molecular systems.[4] Ions were represented through the norm-conserving pseudopotentials of the Goedecker-Teter-Hutter (GTH) type.[5] To describe the substrate, we use the repeated slab approach.

The metallic substrate in the simulation cells consists of 4 atomic layers. The size of super-cells is detailed below for the different cases.c In geometry optimizations only two outermost surface layers are relaxed to preserve a bulk-like region in the slab.

2. Racemic 6,13-Dicyano[7]helicene ((±)-1)

Comparison of the behavior of (*P*)-**1**, (*M*)-**1**, and (±)-**1** reveal similar behaviour of self-assembly on the Cu(111) substrate investigated by STM. Deposition of (±)-**1** onto the Cu(111) surface at 90 K results in the formation of worm-like H-bonded chains, randomly distributed over the surface along the same directions, rotated 30° with respect to the principal Cu(111) axis (Fig. S1a). The architecture of the chains contains 'dimeric' building blocks (Fig. S1a, inset), which are aligned along the principal Cu(111) axis, marked by yellow lines (Fig. 1a).

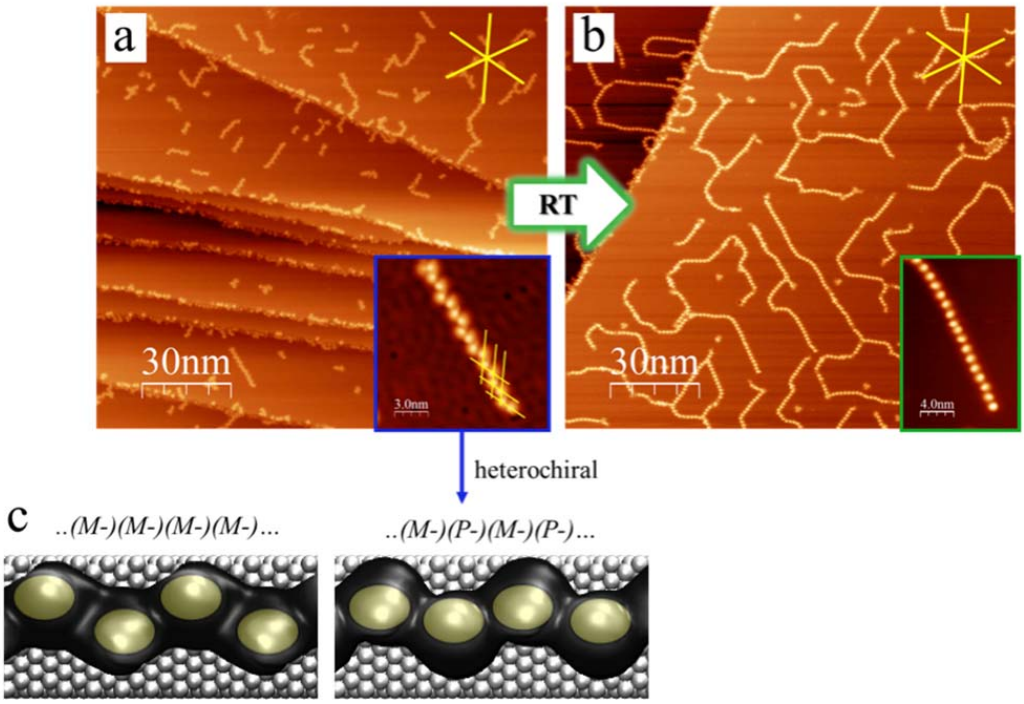

Figure S1. STM images at 5 K: (a) (±)-**1** deposited on Cu(111) at 90 K forms H-bonded chains. Inset: The irregular appearance of the chain is attributed to homochiral and heterochiral segments due to irregular arrangement of the enantiomers from the racemate. b) The same sample after annealing at 300 K for 1 h; complexation to Cu adatoms occurs. The formed chains follow directions rotated by

30° with respect to the Cu(111) principal axis (marked by the yellow star). Inset: The Cu coordination forces the racemic helicene in a straighter chain. (c) DFT models for a homochiral H-bonded chain (left) and alternatively, a heterochiral H-bonded chain (right): the brighter (darker) parts represent higher (lower) parts of the chains. The brighter parts suggest a different STM-appearance of the heterochiral chain in comparison to the homochiral chain which explains the irregular appearance of the randomly sorted chain observed in the experiment

Annealing for 1 h at 300 K leads to coordination to Cu adatoms generated by the substrate (see also Chapter 5 of the SI). Through coordination, the H-bonded chains transform into the linear Cu-coordinated 1D-arrangements (Fig. S1b). From Fig. S1b it can also be seen that the molecular coverage is not sufficiently high for the formation of long-range ordered domains. Reasons for the ordering into quasi-equidistant parallel chains at increased coverages are described later in the SI (Chapters 4, 10). Additionally, the presence of a small amount of impurities on the surface must be taken into account as an additional factor that can block the growth of the chain.

Important to note that 'dimers' inside of the H-bonded racemic (±)-**1** chain (Fig. S1a) do not look as well-pronounced zig-zag, as in the case of the enantiomerically pure assembly ((±)-**1** (Fig. S1a *vs.* (*P*)-**1** Fig. 4a; (*M*)-**1** Fig. 4c). We have performed the DFT-calculations (see details in the Chapter 9 of the SI) to explain this effect. Interestingly, we found that a heterochiral chain, i.e. …(*M*-)(*P*-)(*M*-)(*P*-)… , is more stable than a homochiral chain …(*M*-)(*M*-)(*M*-)(*M*-)… (Fig. S1c). This leads to a better alignment of the more elevated parts of molecules **1** and reduces the effect of the well-pronounced zig-zag appearance in the STM-images.

3. Large-scale STM-image of (*M*)-1

Increasing the coverage of (*M*)-**1** on Cu(111) leads to parallel chains that exhibit long-range order on the surface. The large-scale STM-image at 5 K reveals the domain of Cu-coordinated chains of (*M*)-**1** aligned in the directions rotated by 30° with respect to the Cu(111) principal axes (Fig. S2).

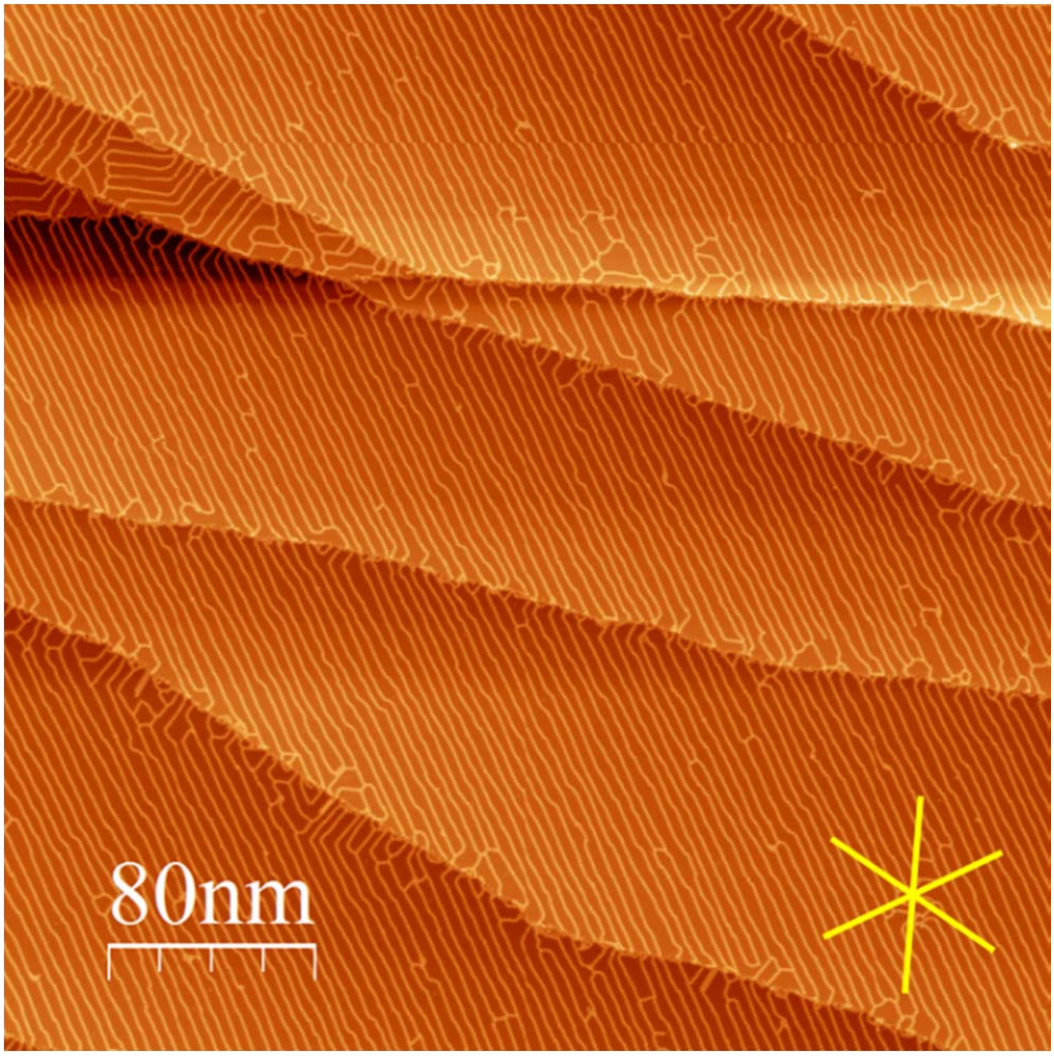

Figure S2. STM image (400 nm x 400 nm) taken at 5 K: Long-range ordered domain of Cu-coordinated parallel chains of (*M*)-**1**. Principal axes of Cu(111) are marked by the yellow cross.

4. Parallel arrangement of the Cu-coordinated chains

We observe a transition of the **1** self-assembly from the zig-zag shaped to long straight Cu-coordinated chains upon heating for 1h at RT (Fig. 2 in the main text). Interestingly, the latter phase becomes highly ordered and leads to extended domains of parallel quasi-equidistant chains (Fig. S2). Large-scale domains of parallel chains have been reported earlier in the literature and were mostly attributed to surface commensurability[6–10] or alignment by steps on high-index substrates.[11] In the present case of quasi equidistant chains on Cu(111), we assign the alignment to registry with the substrate and the equidistance to a presence of a repulsive interaction,[12] which could either stem from Coulomb forces or from surface state-mediated long-range interactions.[13] To assign the dominant mechanism, we have analyzed the chain separation statistically (Fig. S3a) within two molecular coverages. At a coverage of ~0.150 mol nm^{-2} of (*P*)-**1** on Cu(111) (Fig. S3b), measurements were done at 77 K. The spacing between the chains was analyzed within defect-free domains, perpendicular to the chains.

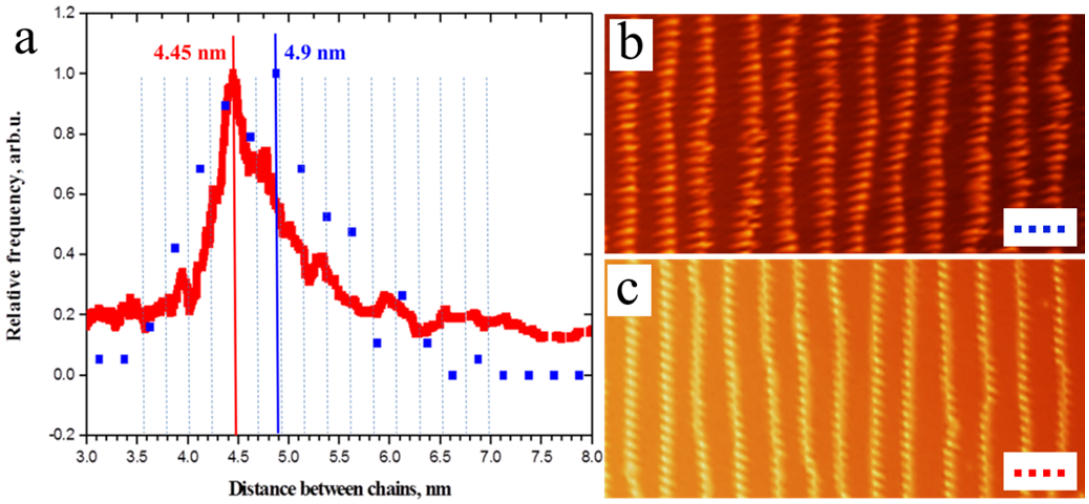

Figure S3. (a) Relative frequency vs. inter-chain distance for neighboring parallel chains. Histograms were plotted for two different coverages and reveal mainly a single broad peak in each case (red plot: ~0.162 mol/nm^2 (*M*)-**1**, corresponding to STM image (c) at 5K (60 nm x 30 nm); blue plot: ~0.150 mol/nm^2 (*P*)-**1**, corresponding to STM image (b) at 77K (60 nm x 30 nm). The main driving force for the parallel arrangement is assigned to repulsive electrostatic interactions. The blue dashed lines in (a) represent the surface registry of Cu(111).

The STM tip has more interaction with the chain during the measurement at 77 K (streaks along the molecules on the STM images (Fig. S3b)) than at 5 K (Fig S3c), and as a result, the deviation in the inter-chain distance from the equal spacing occurs more often. However we can still detect the most frequent inter-chain distance (≈ 4.9 nm) from a frequency vs. distance histogram (Fig.S3, blue points). A similar analysis, including more data points for a sample of (*M*)-(–)-**1** on Cu(111) with slightly higher coverage (Fig. S3c), is shown in (Fig. S3a, red line). Note that samples of different chirality sense can be compared due to identical self-assembling behavior at sub-ML coverage. The plot exhibits mainly one intensive peak in this case as well (average interchain distance of 4.45 nm). The grid of blue dashed lines (Fig. 3a) reproduces the neighbor-to-neighbor atom distance on the Cu(111) surface. The data points in the histogram agree quite well (+-0.1nm) to the expected registry with the Cu substrate as marked by the grid of blue dashed lines.The histogram of the STM data taken at 77K (blue dots in Fig. S3) exhibits a wider peak in comparison to the histogram of the data taken at 5K. The histogram (cf. Fig. S3) exhibits only a single peak which moves to shorter inter-chain distances with increasing coverage. Notably, no discrete favored distances apart from the substrate registry have been observed, as would be expected for a surface-state mediated ordering mechanism. Therefore, we attribute the equidistant ordering of the chains to electrostatic interactions (also supported by calculations, see chapter 10 of SI), which appear only after heating of the samples.

5. Availability of Cu adatoms and formation of Cu-CN complex

The changing chain morphology after heating as well as the modified ordering behavior at elevated temperatures hints at a transition of the main bonding motif, as was already pointed out in the main text (Fig. 2, 4). The influence of the Cu(111) substrate temperature on the architecture of the chains can be explained by the significant difference in the availability of free Cu adatoms on the surface and the consequent formation of CN-Cu adatom coordination complexes. Different threshold temperatures for the availability of native Cu adatoms by the Cu(111) surface have been reported.[12,14–18] Note that depending on the reactive functional group involved (e.g. carboxy, amino, imino), chemical reactions such as dehydrogenation may be

required before coordination to form a chain or network.[19–22] Moreover, even for CN-Cu complexes forming on the Cu(111) surface, the reported temperatures at which coordination occurs - differ significantly (180–300 K).[15,17,18] Hence, a number of additional factors deserve attention here to explain this variation in the temperature: i) the presence or absence of impurities modifying the rate of adatom generation,[23–25] ii) the possible removal of adatoms from step-edges and kinks by the direct interaction of the ad-molecules with these specific sites at temperatures below the threshold temperature for adatom generation, and iii) the coverage dependence of adatom and ad-molecule diffusion due to the progressively increased fractional occupancy of nearest neighbor sites.

6. XPS of a multilayer of (*P*)-1 on Au(111)

Measurement of a reference value for the binding energy (BE) of the N1s in **1**, as well as sublimation control were performed by XPS on multilayered (*P*)-(+)-**1** on Au(111). In the C1s core level spectra, two peaks corresponding to the aromatic and the cyano group carbon atoms are observed (Fig. S4a). According to the chemical formula $C_{30}H_{16}(CN)_2$, one peak is expected for N1s and two peaks for C1s (15:1, small peak at higher BE) with a C:N ratio of 16:1, which was experimentally confirmed (Fig. S4 a,b). The binding energy is lower for helicenes **1** adsorbed on Au(111) as compared to Cu(111).

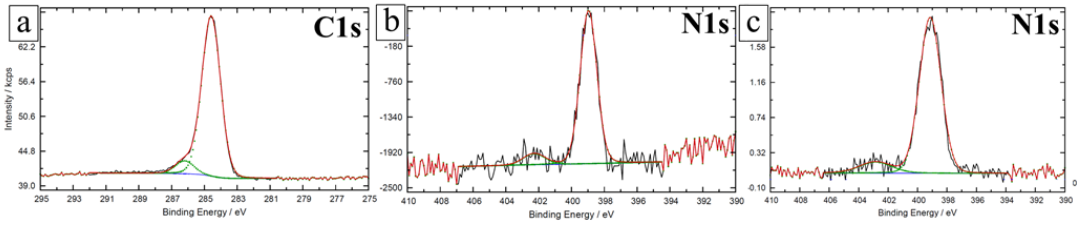

Figure S4. XPS references for a multilayer of (*P*)-**1** on Au(111): (a) C1s and (b) N1s spectra. The 16:1 ratio expected on stoichiometric grounds for C and N is observed experimentally. (c) XPS reference for a multilayer of (*P*)-**1** on Cu(111): N1s spectrum.

7. Condensed phase of (*P*)-1 on Au(111)

A condensed phase of (*P*)-**1** is observed on Au(111) at 77 K (Fig. S5a). Mobility of **1** on this surface is higher than on Cu(111), the nucleated islands that occur at low temperature are not very stable and require gentle scanning parameters (relatively low scanning speed <50 nm/s, tunnel current <40 pA; bias voltage 1.4 V) to avoid rearrangement of the edges of the islands or, as observed in some cases, hopping of the molecule to the tip. The main contributing binding motifs can be attributed to H-bonding and van-der-Waals forces. As can be observed, the structure of the islands has well-ordered row character, and each row consists of (*P*)-**1** 'dimers' (marked by green dashed circles on Fig. S5b).

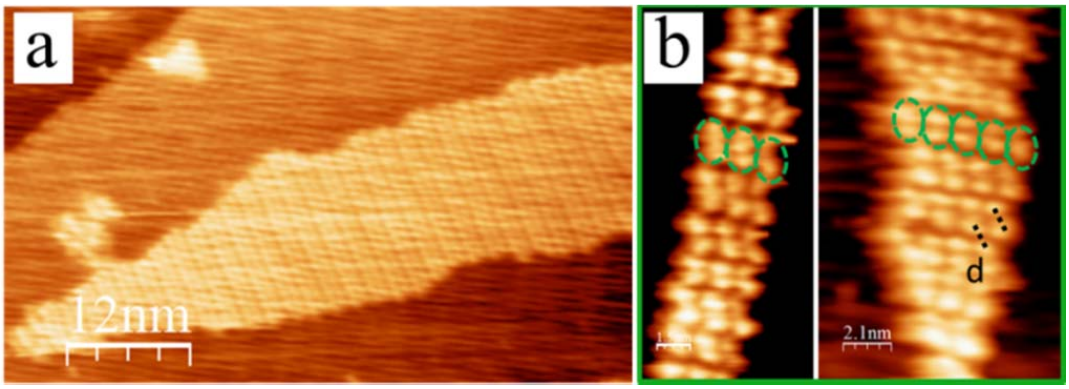

Figure S5. STM images of (*P*)-**1** at 77 K: (a) H-bonded island on Au(111), row structure is observed in the arrangement; (b) zoom of different islands, revealing the formation of dimers (marked by green dashed circles) with an intermolecular distance $d = 1.0 \text{ nm} \pm 0.2 \text{ nm}$.

The structure observed in the H-bonded islands is similar to that observed at full monolayer coverage on Cu(111).[26]

8. Orientation of the Cu-coordinated (*P*)-1 chains on Au(111)

It is well known that the surface of Au(111) reconstructs in the herringbone structure. The fcc stacking of the bulk alternates with narrower reconstructed hcp stacking regions. The domain boundaries between these two regions appear bright because the gold atoms are lifted by few tenths of an Å due to the absent registry in this area. STM images suggest that (*P*)-**1** chains use the reconstructed gold surface as a template and follow the herringbone structure (Fig. S6).

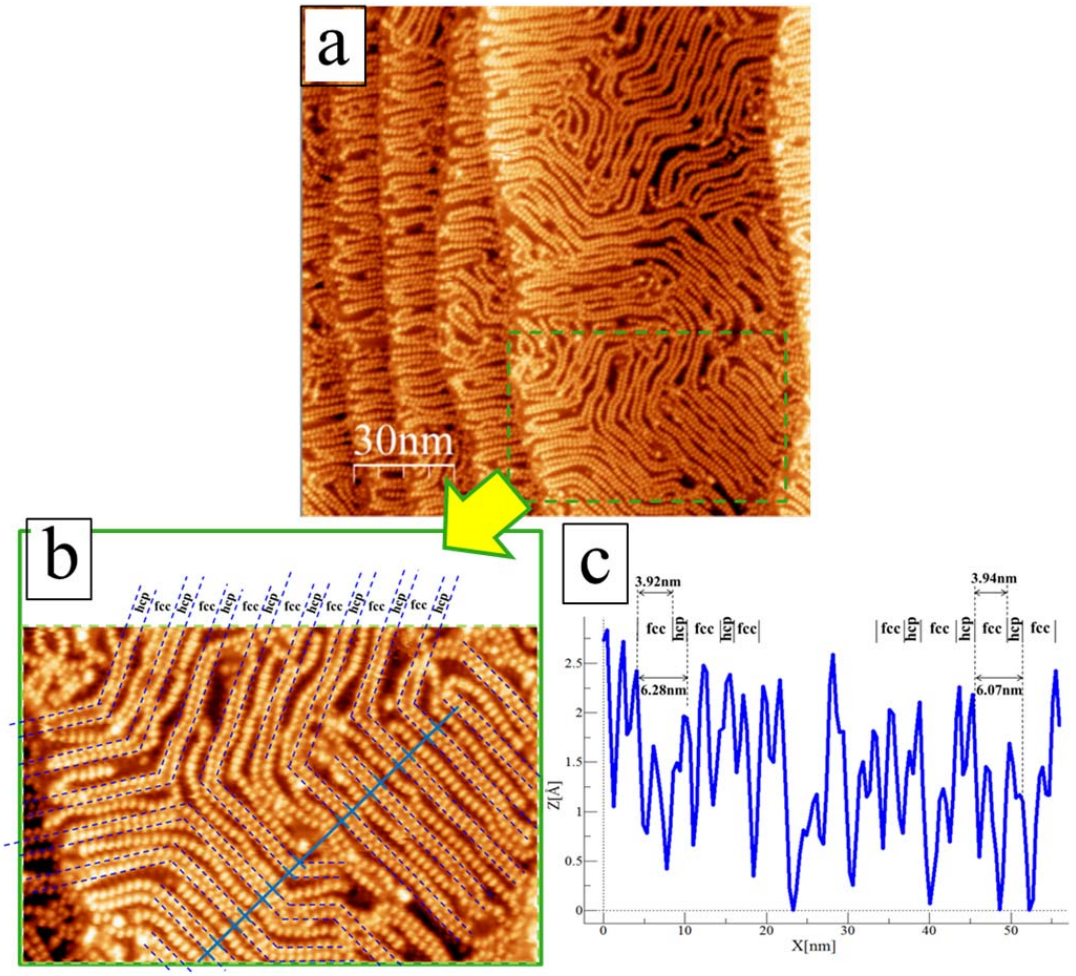

Figure S6. (a) STM micrograph (77 K) of Cu-coordinated chains of (*P*)-**1** on Au(111). (b) STM zoom (79.4 nm x 51.5 nm) of the green dashed area of (a) with overlaid theoretical Au(111) herringbone reconstruction (blue mesh, representing the spacing of the fcc/hcp domain boundaries). (c) Cross-section (cf. blue solid line in (b)) over two different domains, with highlighted fcc regions and repetition patterns. Indication of fcc and hcp regions as in (b).

STM data of (*P*)-**1** (Fig. S6) confirm that the chains follow the soliton walls of herringbone-reconstructed Au(111), which are marked by superimposed blue dashed mesh (Fig. S6b). This mesh, based on the theoretical values for the herringbone structure, matches very well with the observed arrangement of molecules, which is supported by the experimental inter-chain distances (see blue profile in Fig. S6c). Even though two different domains bridged by a defect area, sizes and directions of the alternating fcc and hcp regions still fit. We measured a total average distance of 61.5 Å between repetitive units, which is, within the margin of tolerance of our STM, in good agreement with the distance of repetitive units of the pure gold reconstruction (63 Å).[27] Also, the width of the fcc region (38 Å)[28] matches well the distance between two "double" chains of **1** (we measure a total average of 39 Å). In the fcc region, additional single chains of **1** are observed. The latter are shifted from the fcc/hcp domain boundaries of the Au(111)(22x$\sqrt{\ }$3) surface reconstruction, but nevertheless, follow the herringbone reconstruction. Not only from the geometric but also from an energetic point of view these chains fit in the fcc region. It is reported in the literature that fcc is an electron-poor, and hcp an electron-rich region.[28] On the other hand, a higher mobility was observed by STM for single as compared to double chains. This could be explained by the expected lower mechanical stability or the less favorable electronic interactions with the fcc surface.

It is important to note that the intermolecular distance inside the chain varies significantly by ~12÷15 Å ± 1 Å (see main text of MS), and corresponds well to the 5 ÷ 6 neighbour-neighbour atomic distances (the NN distance along the reconstruction is ~ 2.7 Å), depending on the selected region (5x NNd = 13.5 Å; 6x NNd = 16.2 Å), straight part of the reconstruction or an elbow. In comparison, a distance from molecule to molecule inside the chain on Cu(111) is around 13 Å± 1 Å, which corresponds to 6 neighbour-neighbour atomic distances (NNd = 2.25 Å).

9. DFT Calculations

Single (*M*)-(–)-1 Molecules

Based on geometric considerations, **1** has a "face-on" ("lying") adsorption geometry on surfaces due to the considerable interaction between π-orbitals of the aromatic rings and the metallic surface, as was already shown for a non-functionalized [7]helicene on Cu(111).[29] Additionally, cyano (-CN) groups of an adsorbate may strongly bind to a surface atom forming an anchoring point, as seen for example for tetrafluorotetracyanoquinodimethane on Cu(111), tetracyanoethylene on Cu(100), or 1,4,5,8,9,11-hexaazatriphenylene-hexacarbonitrile on Ag(111).[30–32] Based on these findings, three different binding modes for (*M*)-**1** were computed by DFT calculations (Figure S7). After the introduciton of two Cu adatoms on Cu(111) the following situations were considered:

1). The adatoms do not coordinate to the cyano groups, that are both bound to the surface (Fig. S7, left).

2). Two adatoms coordinate to CN groups (Fig. S7, right).

The calculated structures are displayed in Fig. S7 together with their relative total energies of 1.4 eV and 0.0 eV. The adsorption energy of a helicene molecule in the configuration S7a amounts to 2.56 eV. Our calculations confirm that the energetically most favorable structure has both cyano groups coordinated to Cu adatoms.

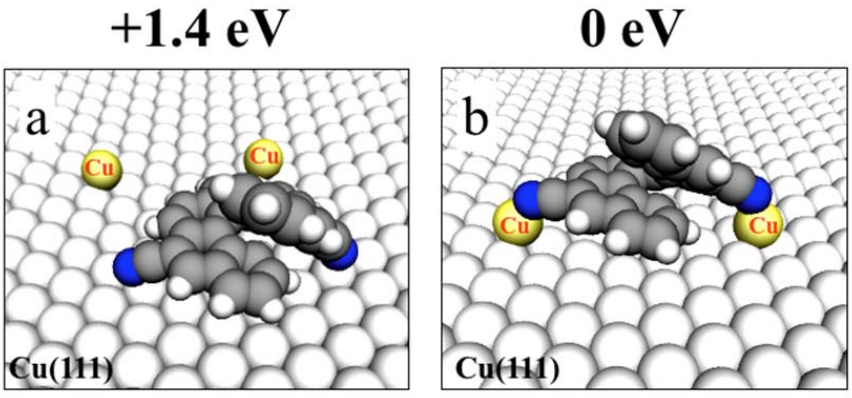

Figure S7. DFT-calculated structure of a single (*M*)-**1** molecule on Cu(111) in the presence of two Cu adatoms: (a): CN groups directly coordinated to the surface; (b) coordinated to one Cu adatom; (b): cyano groups coordinated to two Cu adatoms.

From the calculations, we conclude that the molecule gains 1.4 eV through a geometrically more favorable coordination to the Cu-adatoms, even though the helical backbone is significantly bent.
The same type of calculations was applied to a single molecule (*M*)-**1** adsorbed on Au(111) and similar results were found.

H-bonded and Cu-coordinated chains

We have performed calculations on the possible models for the H-bonded and Cu-coordinated chains in the way described below. First, we consider a situation in which the adsorbate is not coordinated to Cu adatoms on Cu(111). For the face-on helicene geometry, we proposed two possible chain structures based on CN···HC(Ar) hydrogen bonding (Fig. S8
), and taking as building block the structure of the isolated helicene molecule directly bound to the surface (Fig. S7a). If we denote the CN group parallel to the surface as "tail" and the other one (which is forced to bend toward the surface) as "head", the following minimum energy models were obtained: 1)....-tail-head-tail-head-... structure, in which the center-to-center distance between two molecules in the unit cell corresponding in both cases to energy minima is about 5 Å along the y direction and 11.5 Å along the chain direction. The latter case clearly resembles the "dimerization effect observed by STM on Cu(111).

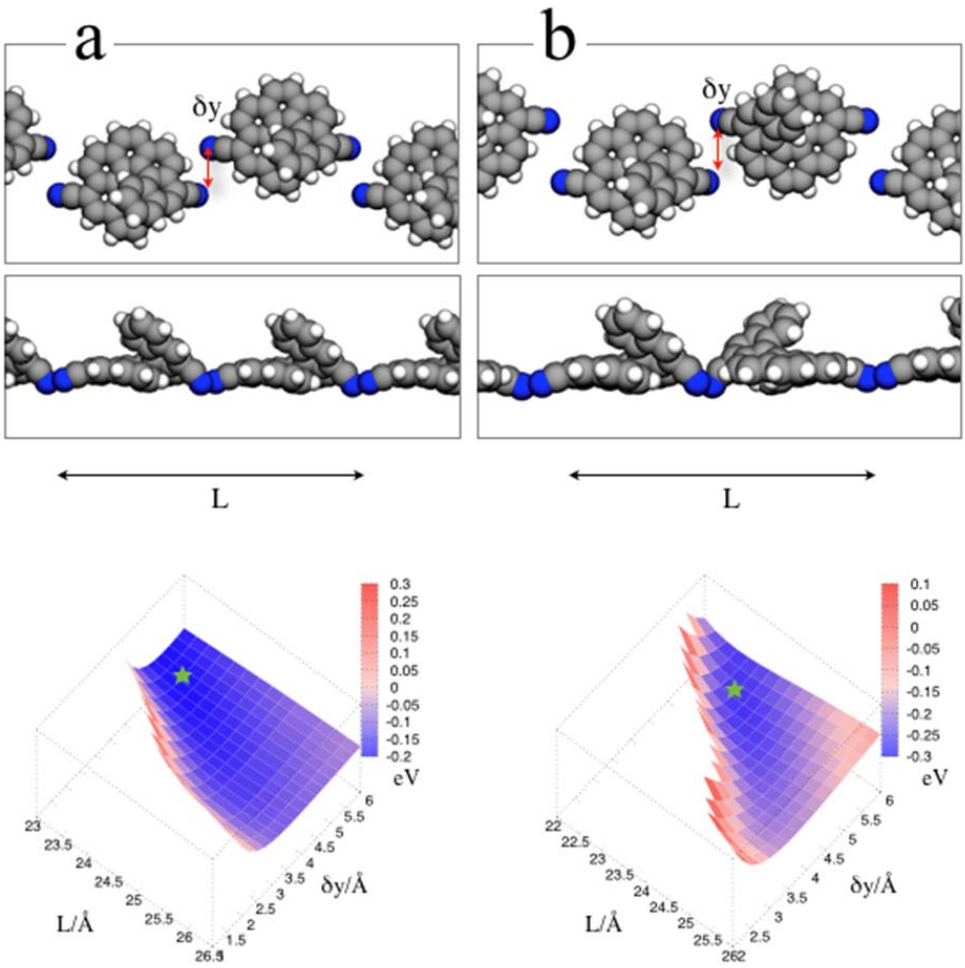

Figure S8. Proposed models (top view and side view) for the H-bonded dicyanohelicene chains in the vacuum. Binding energies per molecule are plotted below for the geometry of single face-on molecules at the Cu(111) surface. L/2 is the intermolecular center-to-center distance along the x-direction; L is the size of the unit cell, which contains two molecules (*M*)-**1** along the x-direction; δy is the intermolecular N···N distance along the y-direction. The small stars indicate the position of the minima in the potential energy surfaces.

Subsequently, we investigated chains of the type "zig-zag" (Fig. S8b) when placed on a Cu(111) surface with full structural optimization. Depending on the initial conditions, we found two distinct minima with slightly different geometry. In one case (Fig. S9, bottom panel, red molecule) one of the two CN groups for each molecule binds to the surface. In the other, more favorable case (Fig S9, top panel,

blue molecule) all CN groups are hydrogen bonded to the neighbors. The competition between deformation, bonding to the surface, van der Waals interactions is subtle and lead to an energy gain of 0.13 eV per pair of molecules, with a total interaction energy gain of 0.2 eV per pair. The fully hydrogen bonded chain also shows a more distinct dimerized STM footprint, in agreement with the experiment, and we favor this model for the low-temperature phase (see Fig. 4 in the main text). A more detailed study of the possible chains including the effects of substrate registry and relative orientation is in progress to completely rule out other bonding mechanisms. The calculated intermolecular center-to-center distances (10 Å) and the length of the H-bond (2.7 Å on average) are in agreement with the experimental data.

Finally, the geometry of the fully Cu adatom coordinated chains was computed. The calculated intermolecular center-to-center distances within a chain amount to 13.4 Å and the N-Cu-N angle to 91°.

Calculated coordinates were used to simulate the STM images for the H-bonded and Cu-coordinated case (cf. Fig. 4 c, d of the main text).

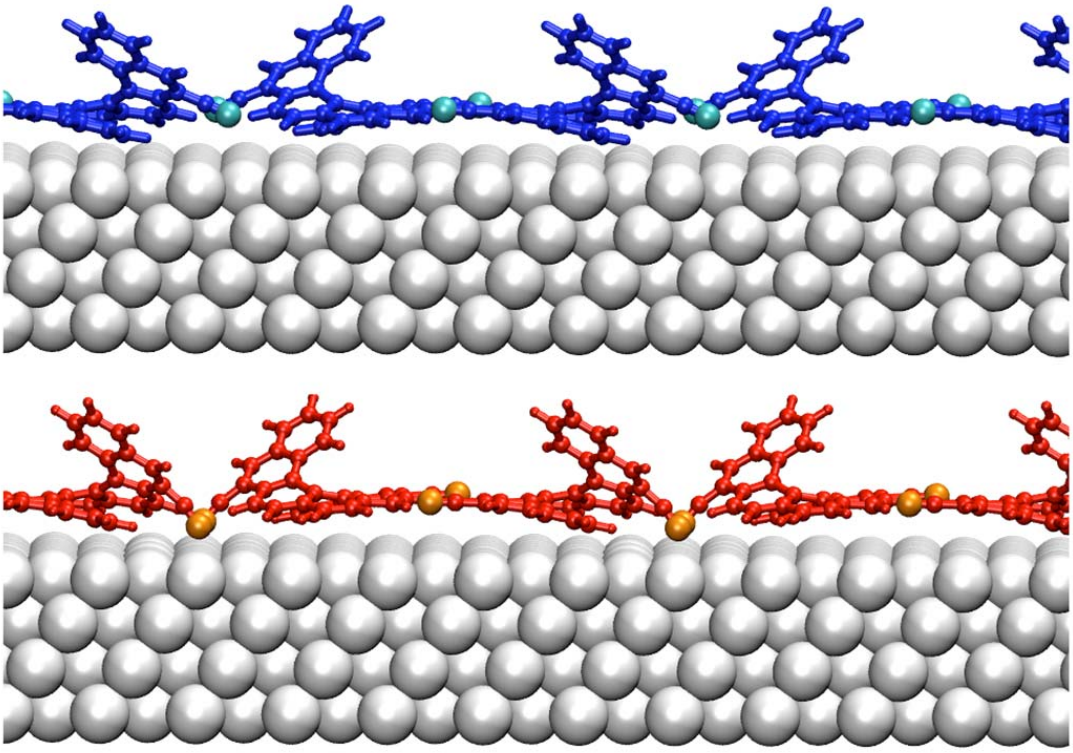

Figure S9. Optimized structures of the chain models, with different bonding mechanisms: fully hydrogen bonded, the most energetically favorable (above) and mixed hydrogen and surface bonded (below). The N atoms are highlighted in both lateral views.

10. Electrostatic interactions

Two parallel chains with a spacing R are considered, and the quantities to be determined are the van der Waals (vdW) and electrostatic interactions between them. For reasons of simplicity, we shall consider the interactions between a molecule **A** plus the Cu adatom bound to **A** (note that in the considered Cu-coordinated chains, Cu adatoms and dicyanohelicene molecules occur in a 1:1 ratio, and a Cu adatom bound to it) in one chain and all the molecules B in another chain. The distance between A and B is

$$d = \sqrt{R^2 + (n\Delta x)^2},$$

where $n = -\infty, ..., -1, 0, 1, ..., +\infty$. (Fig. S10)

Given coefficients C_6 of all the chemical elements involved, it is straightforward to calculate the vdW potential between two molecules. Since the inter-chain distance is large (ca. 5 nm) classical electrostatic interactions are considered, as following.

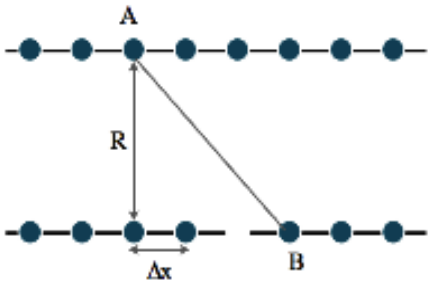

Figure S10. Parallel chains: R is the inter-chain distance, Δx is intermolecular distance in a chain.

First, we consider the partial atomic charge on each atom of the molecule. These atomic charges are calculated in the Cu-coordinated chain on Cu(111), using the Bader analysis.[33,34] Once a set of atomic charges $\{q_{real}\}$ is known, the charge-charge interactions between molecule A and molecules B are given by:

$$V_{charge} = V_{real} + V_{im},$$

where V_{real} is the Coulomb interaction of these charges and, V_{im} the Coulomb potential when image charges are taken into account.

We have

$$V_{real} = \sum_n \sum_{ij} \frac{q_i^{A,real} q_j^{B(n),real}}{r_{ij}},$$

where A refers to molecule A, B(n) refers to molecules B, r_{ij} is the distance between charges i and j. Next,

$$V_{im} = \sum_n \left[\frac{1}{2} \sum \frac{q_i^{A,im} q_j^{B(n),real}}{r_{ij}} + \frac{1}{2} \sum \frac{q_i^{A,real} q_j^{B(n),im}}{r_{ij}} \right],$$

the image charge $q_{im} = -q_{real}$, and the image plane is chosen 1.16 Å above Cu(111)[35].

For R > 4 nm, our calculations show that the van der Waals potential is smaller than the point charge potentials by three orders of magnitude, and we neglect this contribution.

Since the surface mediated potential was already ruled out as the original for the equidistance of the parallel chains, we conclude that electrostatic repulsion should play the major role in defining the interchain interactions (Fig. S11).

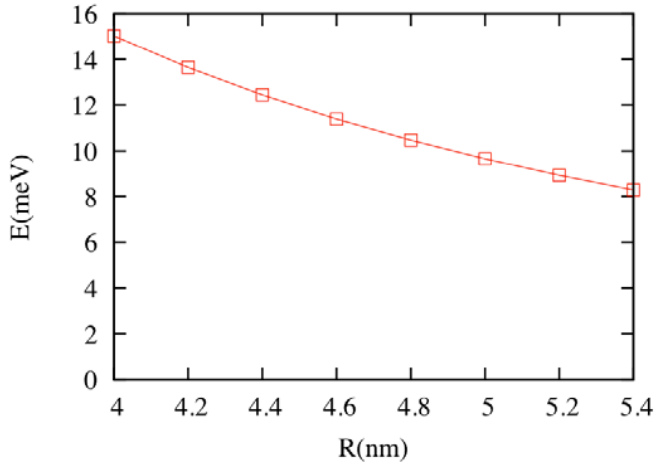

Figure S11. Electrostatic potentials between a single molecule and a chain plotted as a function of their distance R.

11. Two molecular orientations inside of Cu-coordinated (*M*)-1 chain

High resolution STM-images reveal two possible molecular orientations within a chain of Cu-coordinated dicyanohelicenes (Fig. S12a). The observation of head-to-tail next to head-to-head and tail-to-tail interconnections shows that flipped molecules can occur within the self-assembled chains of Cu-coordinated enantiopure (*M*)-**1** (Fig. S12a). Two possible molecular orientations are marked by arrows of different colours and directions for better visualization (yellow and blue arrows on Fig. S12a). Schematic representation of (*M*)-**1** flipped molecule, highlighted by a red rectangle, in the chain is shown in Fig. S12b.

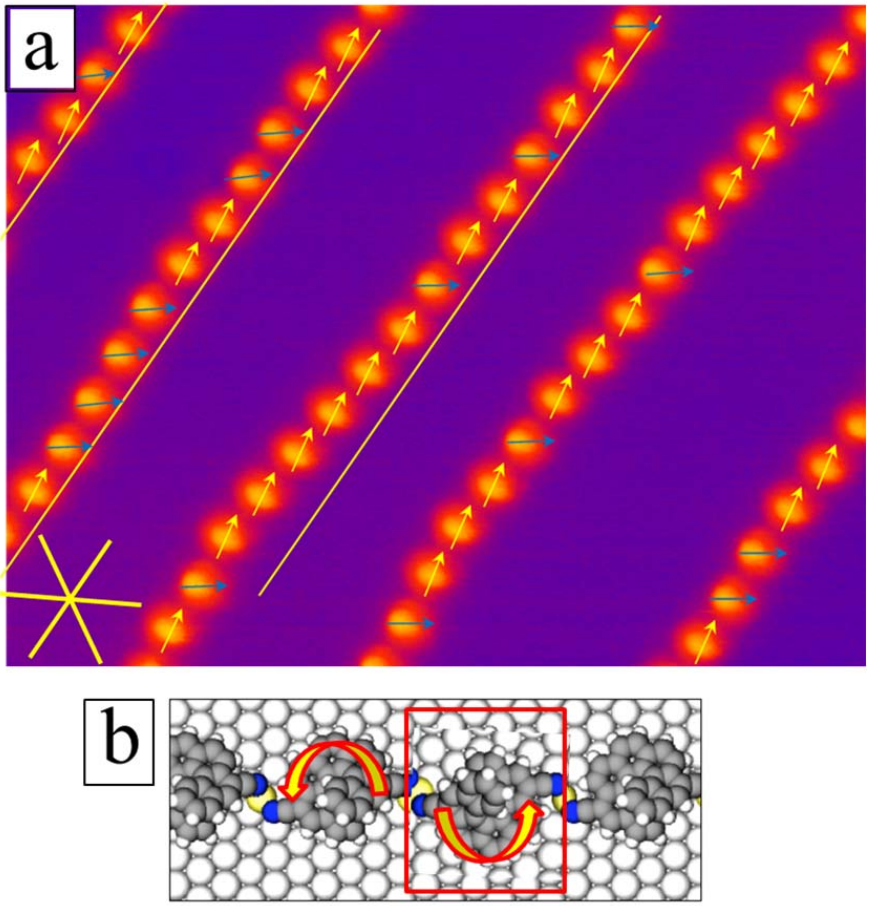

Figure S12. (a) Two possible orientations of (*M*)-**1** within Cu-coordinated dicyanohelicene chains on Cu(111) are seen by high resolution STM at 5 K (19.99 nm x 15.36 nm); (b) Schematic representation of a flipped molecule (red rectangle) within a Cu-coordinated chain of (*M*)-**1**.

12. Involvement of Cu adatoms in the CN-Cu complex

Straight parallel chains on the Cu(111) substrate contain molecules (*M*)-**1** which are interlinked via CN-Cu-adatom coordination complexation. This assignment is supported by XPS and STM evidence (see main text of the manuscript) and, additionally, by STM manipulation experiments of the chains.

We performed 2 types of manipulation experiments: 1) across the molecule to slide the chain on the surface; 2) across the interconnection between 2 molecules – to cut single molecule for the STM imaging (Fig. S13). Manipulation experiments were performed with the feed-back loop switched off at typical tunneling parameters: 500pA; 5mV.

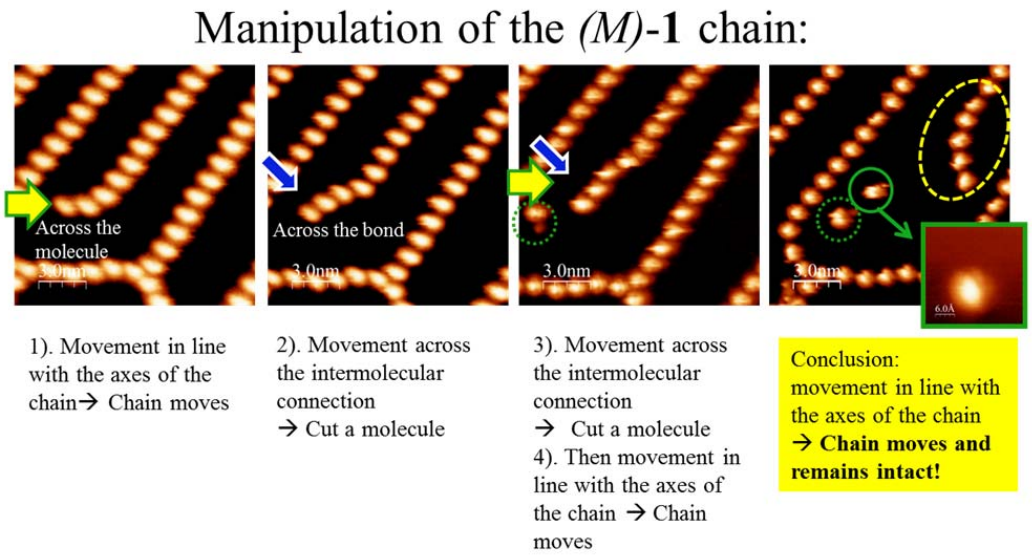

Figure S13 Manipulation experiments of the straight Cu-coordinated *(M)*-**1** chain on Cu(111) surface in line with the axes of the chain (yellow arrow) and across the CN-Cu bond between molecules (blue arrow) result in sliding of the chain as a whole (marked by the yellow dashed oval) and separated single molecules for the STM imaging (green dotted circles and green frame in-set), respectively.

Interestingly, lateral manipulation with the STM tip across the molecule leads to sliding of the chain. The manipulated chain, which remains intact in this sequence, provides additional experimental evidence (see XPS and STM in MS) for the presence of Cu-adatoms inside the chains of molecules *(M)*-**1** interlinked via Cu-CN complexation.

13. References

(1) VandeVondele, J.; Krack, M.; Mohamed, F.; Parrinello, M.; Chassaing, T.; Hutter, J. *Comput. Phys. Commun.* **2005**, *167*, 103–128.
(2) Perdew, J. P.; Burke, K.; Ernzerhof, M. *Phys. Rev. Lett.* **1996**, *77*, 3865–3868.
(3) Grimme, S.; Antony, J.; Ehrlich, S.; Krieg, H. *J. Chem. Phys.* **2010**, *132*, 154104.
(4) VandeVondele, J.; Hutter, J. *J. Chem. Phys.* **2007**, *127*, 114105.
(5) Goedecker, S.; Teter, M.; Hutter, J. *Phys. Rev. B* **1996**, *54*, 1703–1710.
(6) Haq, S.; Hanke, F.; Dyer, M. S.; Persson, M.; Iavicoli, P.; Amabilino, D. B.; Raval, R. *J. Am. Chem. Soc.* **2011**, *133*, 12031–12039.
(7) Hanke, F.; Haq, S.; Raval, R.; Persson, M. *ACS Nano* **2011**, *5*, 9093–9103.
(8) Lipton-Duffin, J. A.; Ivasenko, O.; Perepichka, D. F.; Rosei, F. *Small* **2009**, *5*, 592–597.
(9) Classen, T.; Fratesi, G.; Costantini, G.; Fabris, S.; Stadler, F. L.; Kim, C.; De Gironcoli, S.; Baroni, S.; Kern, K. *Angew. Chem. Int. Ed.* **2005**, *44*, 6142–6145.
(10) Tait, S. L.; Langner, A.; Lin, N.; Stepanow, S.; Rajadurai, C.; Ruben, M.; Kern, K. *J. Phys. Chem. C* **2007**, *111*, 10982–10987.
(11) Saywell, A.; Schwarz, J.; Hecht, S.; Grill, L. *Angew. Chem. Int. Ed.* **2012**, *51*, 5096–5100.
(12) Heim, D.; Écija, D.; Seufert, K.; Auwärter, W.; Aurisicchio, C.; Fabbro, C.; Bonifazi, D.; Barth, J. V. *J. Am. Chem. Soc.* **2010**, *132*, 6783–6790.
(13) Hyldgaard, P.; Einstein, T. L. *J. Cryst. Growth* **2005**, *275*, e1637–e1642.
(14) Wang, W.; Hong, Y.; Shi, X.; Minot, C.; Van Hove, M. A.; Tang, B. Z.; Lin, N. *J. Phys. Chem. Lett.* **2010**, *1*, 2295–2298.
(15) Pawin, G.; Wong, K. L.; Kim, D.; Sun, D.; Bartels, L.; Hong, S.; Rahman, T. S.; Carp, R.; Marsella, M. *Angew. Chem. Int. Ed.* **2008**, *47*, 8442–8445.
(16) Lin, T.; Shang, X. S.; Adisoejoso, J.; Liu, P. N.; Lin, N. *J. Am. Chem. Soc.* **2013**, 130221174928002.
(17) Sirtl, T.; Schlögl, S.; Rastgoo-Lahrood, A.; Jelic, J.; Neogi, S.; Schmittel, M.; Heckl, W. M.; Reuter, K.; Lackinger, M. *J. Am. Chem. Soc.* **2013**, *135*, 691–695.
(18) Pivetta, M.; Pacchioni, G. E.; Schlickum, U.; Barth, J. V.; Brune, H. *Phys. Rev. Lett.* **2013**, *110*.
(19) Dougherty, D. B.; Maksymovych, P.; Yates, J. T. *Surf. Sci.* **2006**, *600*, 4484–4491.
(20) Dmitriev, A.; Lin, N.; Weckesser, J.; Barth, J. V.; Kern, K. *J. Phys. Chem. B* **2002**, *106*, 6907–6912.
(21) Diller, K.; Klappenberger, F.; Marschall, M.; Hermann, K.; Nefedov, A.; Wöll, C.; Barth, J. V. *J. Phys. Chem.* **2012**, *136*, 014705.
(22) Pan, S.; Fu, Q.; Huang, T.; Zhao, A.; Wang, B.; Luo, Y.; Yang, J.; Hou, J. *PNAS* **2009**, *106*, 15259–15263.
(23) Feibelman, P. *Phys. Rev. Lett.* **1998**, *81*, 168–171.
(24) Kalff, M.; Comsa, G.; Michely, T. *Phys. Rev. Lett.* **1998**, *81*, 1255–1258.
(25) Kyuno, K.; Ehrlich, G. *Phys. Rev. Lett.* **1998**, *81*, 5592–5595.
(26) Stöhr, M.; Boz, S.; Schär, M.; Nguyen, M.-T.; Pignedoli, C. A.; Passerone, D.; Schweizer, W. B.; Thilgen, C.; Jung, T. A.; Diederich, F. *Angew. Chem. Int. Ed.* **2011**, *50*, 9982–9986.
(27) Barth, J.; Brune, H.; Ertl, G.; Behm, R. *Phys. Rev. B* **1990**, *42*, 9307–9318.

(28) Chen, W.; Madhavan, V.; Jamneala, T.; Crommie, M. *Phys. Rev. Lett.* **1998**, *80*, 1469–1472.
(29) Fasel, R.; Parschau, M.; Ernst, K.-H. *Nature* **2006**, *439*, 449–452.
(30) Romaner, L.; Heimel, G.; Brédas, J.-L.; Gerlach, A.; Schreiber, F.; Johnson, R.; Zegenhagen, J.; Duhm, S.; Koch, N.; Zojer, E. *Phys. Rev. Lett.* **2007**, *99*.
(31) Bedwani, S.; Wegner, D.; Crommie, M.; Rochefort, A. *Phys. Rev. Lett.* **2008**, *101*.
(32) Bröker, B.; Hofmann, O. T.; Rangger, G. M.; Frank, P.; Blum, R.-P.; Rieger, R.; Venema, L.; Vollmer, A.; Müllen, K.; Rabe, J. P.; Winkler, A.; Rudolf, P.; Zojer, E.; Koch, N. *Phys. Rev. Lett.* **2010**, *104*.
(33) Bader, R. F. W. *Atoms in molecules: a quantum theory*; The International series of monographs on chemistry; Clarendon Press ; Oxford University Press: Oxford [England] : New York, 1994.
(34) Tang, W.; Sanville, E.; Henkelman, G. *J. Phys. Condens. Mat.* **2009**, *21*, 084204.
(35) Chulkov, E. V.; Silkin, V. M.; Echenique, P. M. *Surf. Sci.* **1999**, *437*, 330–352.

Controlling the dimensionality of on-surface coordination polymers via endo- or exoligation

Summary:

In this study we report on a new metal-specific on-surface reaction, occurring between amino-functionalized perylene derivative (4,9-diaminoperylene-quinone-3,10-diimine (DPDI)) and transition metal adatoms (Co, Fe, Ni, Cu). Surprisingly, we find that the precursor molecule undergoes different dehydrogenation steps depending on the supplied transition metal adatom: $-H_2$ (with Co, Fe, Ni) and $-3H_2$ (with Cu). Consequently, the modified molecule can be triggered to either act as an endo- or as an exo-ligand. The selected metal controls the stage of dehydrogenation of the building block precursor and thereby defines the dimensionality of the coordination polymer (1D or 2D). These findings present a new alternative way to control self-assembled molecular architectures at surfaces.

Manuscript [[2]] has been published in the Journal of the American Chemical Society in 2014. Contribution of Aneliia Shchyrba: carried out the experimental investigation (STM, XPS, NEXAFS), analysed the data, wrote the manuscript.

JACS
JOURNAL OF THE AMERICAN CHEMICAL SOCIETY

Article

pubs.acs.org/JACS

Controlling the Dimensionality of On-Surface Coordination Polymers via Endo- or Exoligation

Aneliia Shchyrba,*[,†] Christian Wäckerlin,[‡,▲] Jan Nowakowski,[‡] Sylwia Nowakowska,[†] Jonas Björk,[§] Shadi Fatayer,[†] Jan Girovsky,[‡] Thomas Nijs,[†] Susanne C. Martens,[†,#] Armin Kleibert,[⊥] Meike Stöhr,[∥] Nirmalya Ballav,[¶] Thomas A. Jung,*[,‡] and Lutz H. Gade*[,#]

[†]Department of Physics, University of Basel, Klingelbergstrasse 82, 4056 Basel, Switzerland

[‡]Laboratory for Micro- and Nanotechnology, Paul Scherrer Institute, 5232 Villigen PSI, Switzerland

[§]Department of Physics, Chemistry and Biology, IFM, Linköping University, Linköping 581 83, Sweden

[⊥]Swiss Light Source, Paul Scherrer Institute, 5232 Villigen PSI, Switzerland

[∥]Zernike Institute for Advanced Materials, University of Groningen, Nijenborgh 4, 9747 AG Groningen, The Netherlands

[¶]Department of Chemistry, Indian Institute of Science Education and Research, Pune 411008, India

[#]Anorganisch-Chemisches Institut, Universität Heidelberg, Im Neuenheimer Feld 270, 69120 Heidelberg, Germany

Supporting Information

ABSTRACT: The formation of on-surface coordination polymers is controlled by the interplay of chemical reactivity and structure of the building blocks, as well as by the orientating role of the substrate registry. Beyond the predetermined patterns of structural assembly, the chemical reactivity of the reactants involved may provide alternative pathways in their aggregation. Organic molecules, which are transformed in a surface reaction, may be subsequently trapped via coordination of homo- or heterometal adatoms, which may also play a role in the molecular transformation. The amino-functionalized perylene derivative, 4,9-diaminoperylene quinone-3,10-diimine (DPDI), undergoes specific levels of dehydrogenation (−1 H_2 or −3 H_2) depending on the nature of the present adatoms (Fe, Co, Ni or Cu). In this way, the molecule is converted to an endo- or an exoligand, possessing a concave or convex arrangement of ligating atoms, which is decisive for the formation of either 1D or 2D coordination polymers.

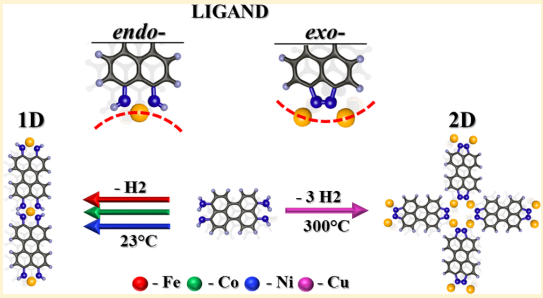

INTRODUCTION

Organic and metal−organic networks[1−18] generated on metal surfaces have been shown to alter the electronic properties of the substrate and to serve as templates for the formation of host−guest complexes,[19−26] giving rise to complex forms of aggregation.

The mechanisms of on-surface reactions may differ significantly from those in solution,[27] thereby creating the opportunity to explore new "on-surface phenomena".[28] Coordination between organic molecular ligands and metal adatoms,[12,29−38] on one hand, and on-surface coupling and breaking of covalent bonds,[18,28,39−58] on the other, have both been found to give rise to stable, well-ordered structures. There are thus several levels of chemical transformations and bonding interactions determining the assembly of molecular on-surface structures. Through reaction with surface adatoms, the building block or synthon can be modified prior to coordinative polymerization, as exemplified by the deprotonation of COOH to the ligating COO^- in carboxylate-based surface coordination polymers.[35,59−61] In previous work, the nature of the metal adatom exhibited only a minor influence on the topology of the 2D layer,[62−64] which is commonly predicted on the basis of the organic ligand only.

In this work, we demonstrate how two nitrogen-containing functional groups in a polycyclic aromatic architecture undergo modification depending on the specific reactivity of the available metal adatoms. Previously, we reported the formation of a highly stable porous network upon deposition of 4,9-diaminoperylene quinone-3,10-diimine (DPDI) onto a Cu(111) surface and subsequent annealing.[65] A closer inspection of the transformation of this planar organic molecule has revealed that it undergoes thermal dehydrogenation generating deh-DPDI (−1 H_2) and, potentially, subsequent ring closure and further dehydrogenation to the polyazocyclic compound 3deh-DPDI (−3 H_2) (Figure 1).

Whereas deh-DPDI may act as a chelating *endoligand* on a metal surface, coordinating single metal atoms or forming 1D

Received: February 26, 2014
Published: June 24, 2014

dx.doi.org/10.1021/ja5020103 | J. Am. Chem. Soc. 2014, 136, 9355−9363

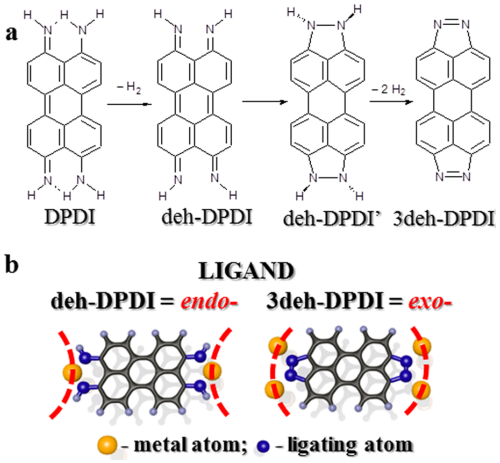

Figure 1. Dehydrogenation of DPDI to a quinoidal bisimino form deh-DPDI, which may act as an *endoligand* on a metal surface, and further cyclization and dehydrogenation resulting in triply dehydrogenated DPDI (3deh-DPDI) (a). In the latter, the diazo units may act as bridging ligands between metal centers, rendering 3deh-DPDI an *exoligand* capable of forming 2D coordination networks (b).

chain structures, the diazo units at both ends in 3deh-DPDI may bridge metal centers, rendering the latter a bridging *exoligand* capable of forming 2D coordination networks. We will show that the observed reactivity and thus the degree of dehydrogenative conversion is specifically determined by the co-deposited or substrate-supplied transition metal adatoms. The geometry of the resulting coordination polymer depends also on the type (Au or Cu) and crystal index ((111), (100)) of the substrate.

In this report, we focus on the assembly of on-surface coordination polymers by a two-stage reactive dehydrogenation of the amine and imine functional groups in DPDI. To investigate the impact of transition metal adatoms on the transformation of the building block and on the formed coordination architecture, we employ a broad portfolio of surface analytical techniques: scanning tunneling microscopy (STM), X-ray photoelectron spectroscopy (XPS), near-edge X-ray absorption fine structure (NEXAFS) measurements in combination with density functional theory (DFT) computational modeling.

EXPERIMENTAL SECTION

All samples were prepared and investigated under ultrahigh vacuum (UHV) conditions with a base pressure of ~10^{-10} mbar. The crystal substrates were cleaned by cycles of sputtering with Ar^+ ions and subsequent annealing to ~450 °C. The molecules were deposited on the surface by means of thermal evaporation at ~240 °C from a commercial evaporator (Kentax GmbH, Germany) and metal adatoms by e-beam evaporator (Oxford Applied Research, United Kingdom). The amount of the sublimed compound was controlled by a quartz crystal microbalance.

STM images were obtained at 5 K, 77 K, or at room temperature (RT) in constant current mode (typical tunneling current 20−50 pA), and the sample bias was selected in the range of 5 mV to 3 V, such that the molecules appear in high contrast. Scanning probe tips were made from Pt−Ir wire (90% Pt, 10% Ir) and cleaned by sputtering with Ar^+ ions.

XPS was used to estimate the coverage of DPDI and to verify the stoichiometry after deposition. Also by XPS, the element-specific chemical environment (analysis of C1s and N1s signatures), in particular, the coordination of DPDI with different metal adatoms, was tracked. A monochromatized Al Kα X-ray source was used. The instrumental setup gives a full width at half-maximum (FWHM) of 1.0 eV. The energy calibration was performed using a Au(111) reference. All XPS data were obtained at RT, and the spectra were recorded in normal emission unless stated otherwise.

The NEXAFS measurements were performed on samples held at RT at the Surfaces/Interfaces: Microscopy (SIM) beamline of the Swiss Light Source (SLS) using total electron yield acquisition mode.[66] The spectra were divided by the background obtained on the clean substrate and normalized to pre-edge. The fitting analysis of the spectra was performed by asymmetric Gaussian functions with linearly increasing FWHM for higher photon energies.[67] The onset of the ionization potential was fitted by a broadened step function.

Periodic DFT modeling was performed with the VASP code[68] using the projector-augmented wave method[69] for describing ion-core interactions. The van der Waals interactions were included using the van der Waals density functional,[70] while local correlation was described by local density approximations (LDA). The semilocal exchange was described in the generalized gradient approximation (GGA) using an optimized form of the Becke 86 functional.[71]

The Cu(111) surface was modeled by a four-layered slab separated by 15 Å of vacuum, with a $p(10 \times 10)$ surface unit cell for the 3deh-DPDI honeycomb network, as previously determined.[65] For the deh-DPDI chains, we used the unit cell illustrated in Figure S7 of Supporting Information (SI), which gave the most stable structure (see SI for calculations with other unit cells). The calculated lattice constant, obtained with the methods described here, of 3.598 Å was used. In all calculations, the plane waves were expanded to a kinetic energy cutoff of 500 eV. For the honeycomb network, the first Brillouin zone was sampled by the Γ point only, while for the Co-coordinated deh-DPDI chains, a 3×2 k-point sampling was used. All structures were structurally optimized until the residual forces of all atoms, except for the bottom two layers of the slab, kept fixed, were smaller than 0.01 eV/Å.

Simulated core-level shifts were obtained by comparing total energy differences between core-ionized and ground state systems. The total energies of core-ionized systems were computed by using a core-ionized PAW potential for the core-ionized atom as described by Köhler and Kresse.[72]

RESULTS AND DISCUSSION

Dehydrogenation of DPDI and Endo/Exoligand Formation, Controlled by the Type of Adatoms Present on the Surface. First, we investigated the dehydrogenation of adsorbed DPDI on Cu surfaces. The changes in the chemical environment of N upon reaction of DPDI with adatoms were monitored by XPS (N1s peak) and are represented in Figure 2. Unreacted DPDI, after deposition on Cu(111) and Cu(100) substrates, gives rise to two peaks in the N1s spectrum corresponding to the coexisting amino (~399.4 eV) and imino group (~397.5 eV) (Figure 2a; cf. Figure S1 in SI). The observed XPS peak positions correspond well to the values reported in the literature (see XPS values in Tables S1 and S2 of the SI).[73,74] In spite of the 1:1 stoichiometry between amino and imino nitrogen, we observe unequal intensities of the amine and imine peak even in the native multilayer (cf. Figure S3). We tentatively attribute this to intramolecular hydrogen bonding ($-NH_2\cdots N=$, cf. Figure 1a) which has been found to yield significant peak shifts[75,76] and potentially photoelectron scattering effects.[77] The position of the observed N1s peaks of the DPDI monolayer on Cu(111) corresponds well to the XPS data of the DPDI multilayer, indicating that neither dehydrogenation nor Cu coordination occurs at RT (Figure

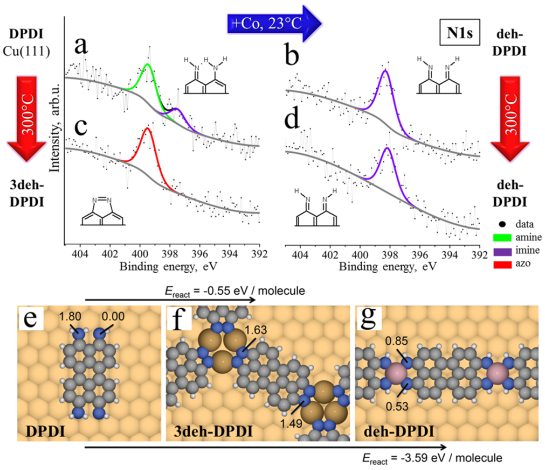

Figure 2. Identification of the various N species in the N1s XP spectra of DPDI on Cu(111). (a) Native DPDI is characterized by two peaks corresponding to amino (green) and imino (violet) groups. (b) Upon addition of Co adatoms to native DPDI on Cu(111) at RT, the dehydrogenation occurs readily as recognized by the dominant NH peak (violet). (c) Annealing of native DPDI on Cu(111) to 300 °C leads to a different reaction product: one peak is visible in the N1s XPS data at higher binding energy (BE), which is attributed to azo nitrogen (N═N). (d) Annealing of the DPDI/Cu(111) in the presence of Co adatoms to 300 °C does not modify a deh-DPDI product. Chemical schemes: Note that the arrangement of the free electron pairs of the ═NH (imine) and N═N (azo) ligands determines the role of deh-DPDI as an endoligand and of 3deh-DPDI as an exoligand, respectively. The DFT models with calculated reaction energies: (e) isolated DPDI, (f) Cu-coordinated 3deh-DPDI, and (g) Co-coordinated deh-DPDI cases. The average N1s core-level shifts with respect to the imine-N atoms of native DPDI are +1.56 eV for 3deh-DPDI and +0.69 eV for deh-DPDI.

S3). Even after deposition of Cu adatoms onto the monolayer of DPDI on Cu(111), there is no significant modification of the chemical environment of N as monitored by the N1s peaks (cf. Figure S4 in SI). Thus, DPDI remains unreacted irrespective of whether it is adsorbed on Cu at RT or whether higher thermal energy adatoms from a sublimation source are provided.

Annealing to 300 °C promotes a chemical transformation of DPDI on the Cu(111) and Cu(100) substrates and leads to characteristic changes in the N1s XPS signature. The modified spectrum is characterized by a *single* N1s peak at ∼399.4 eV, reflecting an identical chemical environment of the N atoms contained in 3deh-DPDI (Figure 2c and Figure S1). The N1s binding energy of Cu-coordinated 3deh-DPDI corresponds well to the energies reported for related azo-functionalized species.[78] Moreover, we calculated the average N1s core-level shift between imine N contained in isolated DPDI on the surface and the azo-N contained in Cu-coordinated 3deh-DPDI. The resulting shift of +1.56 eV is within the experimental error margin. This reaction is exothermic with a reaction energy of −0.55 eV per molecule. The transformation of DPDI into 3deh-DPDI, containing azo-N at both ends, is also supported by the NEXAFS data (vide infra).

Notably, deposition of Cu adatoms onto DPDI on the more inert Au(111) substrate triggers the same chemical reaction leading to 3deh-DPDI−Cu complexes upon annealing to ∼300 °C (however, the reaction proceeds only for a part of the compound; cf. S5 and discussion in the SI).

The reaction products after annealing DPDI at 300 °C on both Cu(111) and Cu(100) substrates were visualized by RT STM. These experiments reveal the formation of a highly ordered 2D hexagonal porous network on Cu(111)[65] and a moderately ordered 2D rectangular network on Cu(100), respectively (Figure 3). The XPS data confirm that both

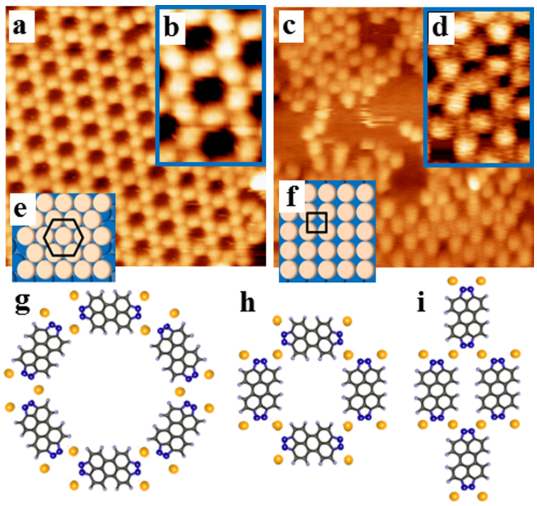

Figure 3. Annealing of native DPDI at 300 °C on Cu substrates leads to the formation of exoligating 3deh-DPDI. The resulting Cu-coordinated 2D polymer reflects the symmetry of the underlying substrate: (a,b) hexagonal pores are formed on the Cu(111) surface and (c,d) rectangular pores on the Cu(100) surface, as depicted in the STM images (19 × 19 nm^2 and 4 × 6 nm^2). The hexagonal and rectangular symmetry for Cu(111) and Cu(100) surfaces are depicted in the insets (e) and (f), respectively. Schematic models: (g) hexagonal 3deh-DPDI pore; (h,i) rectangular pores in two configurations with parallel or perpendicular orientation and corresponding rectangular or square symmetry of the coordination polymer, respectively.

networks consist of 3deh-DPDI in the role of an exoligand (cf. Figure 2 and SI). The symmetry of the surface is directly reflected by the symmetry of the network (Figure 3a,b,e and 3c,d,f, respectively). Due to the reduced commensurability of the rectangular coordination network with the Cu(100) surface lattice and the coexistence of square and rectangular pores (Figure 3h,i), the amount of defects is greater and long-range order is accordingly reduced compared to the corresponding structure on Cu(111).

The role of the open d-shell metals, such as Co, Fe, and Ni, in the on-surface reaction of DPDI on Cu(111) was studied in a dedicated series of experiments: After deposition of DPDI and subsequent deposition of cobalt atoms at RT, the N1s XPS spectrum, presented in Figure 2b, shows significant changes from native DPDI. The amino peak, which is characteristic for the unreacted compound, disappears (Figure 2b), and only a single N1s peak is observed at ∼398.3 eV. The energy position differs significantly (1.1 eV lower), from the one observed after Cu coordination of 3deh-DPDI on Cu(111), and is assigned to imino-nitrogen atoms.[79,80] Upon annealing at ∼300 °C, the N1s peak remains virtually unchanged (∼398.1 eV) (Figure 2d). The core-level shift between this Co-coordinated imine

dx.doi.org/10.1021/ja5020103 | J. Am. Chem. Soc. 2014, 136, 9355−9363

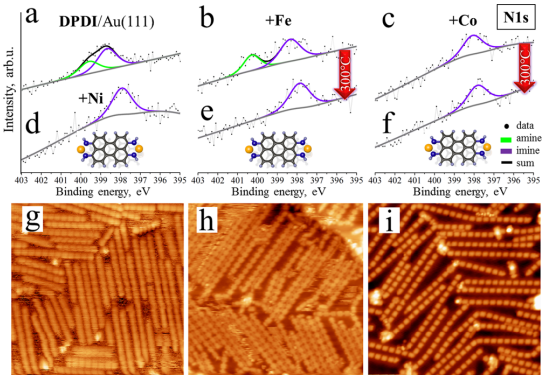

Figure 4. Transformation of DPDI into deh-DPDI (an endoligand) in the presence of Ni, Fe, and Co on Au(111). This transformation occurs at RT in an on-surface reaction between DPDI and transition metal adatoms as recognized by the change of (a) initial two peaks in N1s spectrum of DPDI on Au(111) into (b–f) dominant N1s XPS peak of imine character. (b) Shoulder of the amine corresponds to small amounts of the unreacted DPDI, which disappear after annealing. The resulting chelating ligand coordinates with adatoms and arranges into a chain architecture. (g–i) STM micrographs of the polymers, created by co-deposition of DPDI with (g) Ni, (h) Fe, and (i) Co adatoms on Au(111) at RT ((g) 30 × 30 nm^2 at RT; (h,i) 30 × 30 nm^2 at 5 K). Note, the polymers observed in STM are not modified upon annealing.

and the uncoordinated imine-N has been calculated to be 0.69 eV (Figure 2e,g), which compares well to the experimental data. Based on DFT modeling, the calculated reaction energy is −3.59 eV for transforming DPDI into Co-coordinated deh-DPDI.

The same type of transformation occurs for DPDI on a Au(111) substrate (Figure 4a) in the presence of Co adatoms (Figure 4c,f). Moreover, other open 3d-shell transition metal adatoms, such as Fe and Ni, initiate an identical transformation of DPDI on Au(111) as recognized in the XPS data showing the dominant imino peak at low binding energy, ∼398 eV (Figure 4d for Ni and Figure 4b,e for Fe).

Annealing of the samples to 300 °C only completes a conversion of the unreacted compound (e.g., Figure 4e); however, it does not change the final reaction product. The dominant XPS signature is assigned to deh-DPDI (see Figure 1), which is reminiscent of the ubiquitous *acac* (acetylacetonato) ligands in coordination chemistry. This ligand is able to act as a ditopic chelating endoligand for the co-deposited transition metals. Therefore, the formation of metal complexes, with two of these bis(imine) units in a square-planar coordination geometry on the different substrates, gives rise to 1D coordination polymers as depicted by STM in Figure 4g–i.

The analysis of the XPS data reveals two types of reaction products for closed versus open d-shell adatoms coordinating with DPDI. Cu adatoms transform DPDI into 3deh-DPDI that may act as a bridging exoligand with its convex arrangement of donor atoms. On the other hand, in the presence of Co, Fe and Ni adatoms, the less dehydrogenated species deh-DPDI, which acts as a ditopic bis(chelating) endoligand, are trapped by coordination to the heterometal atoms, forming the chain-like 1D coordination polymers. The adatom-dependent transformations of DPDI to deh-DPDI or 3deh-DPDI and coordination to the respective transition metals represent complex multistep processes. Only detailed computational modeling of all possible reaction pathways/sequences on the metal surface(s) would provide insight into the factors governing the final product(s) observed in the transformations described above.

NEXAFS Study of the Surface-Transformed DPDI: Identification of Amino-, Imino-, and Azo-Nitrogen. To confirm the assignment of the deh-DPDI and 3deh-DPDI dehydrogenation product in the on-surface coordination polymers, we have employed NEXAFS. The method provides a characteristically different probing mechanism from XPS in that transitions from occupied N1s to unoccupied N2p orbitals are examined. The method is sensitive to both the chemical environment and the orientation of the molecule. Figure 5 displays the NEXAFS data obtained for three samples, (a)

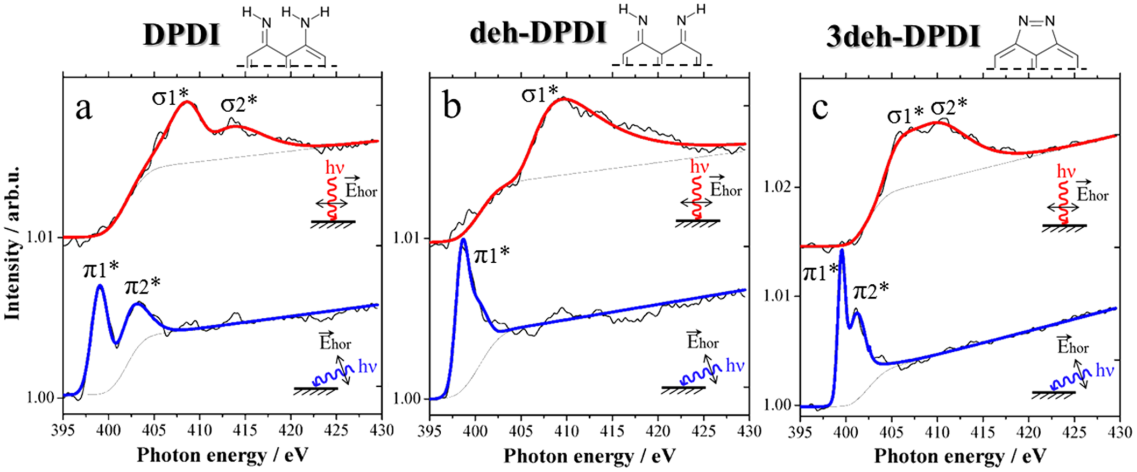

Figure 5. NEXAFS data revealing different DPDI species. In-plane σ^* and out-of-plane π^* resonances are reflected by red and blue curves, respectively. (a) Spectra of unreacted DPDI on Cu(100) contain both amino and imino peaks; (b) spectra of deh-DPDI coordinated to Co via imino-nitrogen; (c) spectra of 3deh-DPDI coordinated to Cu via azo-nitrogen.

dx.doi.org/10.1021/ja5020103 | J. Am. Chem. Soc. 2014, 136, 9355–9363

unreacted DPDI/Cu(100) (not annealed), (b) DPDI + Co/Cu(111), and (c) DPDI/Cu(111) (annealed to liberate Cu adatoms and to activate the on-surface reaction). The data are summarized in Table 1, along with the corresponding assignments of the peaks.

Table 1. Energies of the NEXAFS N1s Peaks, Obtained from the Fit of Data, Correspond to Amino, Imino, and Azo Groups

molecule/NEXAFS	π_1* (eV)	π_2* (eV)	σ_1* (eV)	σ_2* (eV)
(a) DPDI	399.1	403.2	408.6	414.4
(b) deh-DPDI	398.7		409.6	
(c) 3deh-DPDI	399.6	401.2	407.0	410.7

The relative orientation of the unoccupied states with respect to the incident X-ray beam, as determined in angle-dependent NEXAFS experiments, modifies the magnitude of the spectral features. In the present case, electronic states with their nodal plane in out-of-plane orientation were probed in grazing incidence (70° off the surface-normal) with the linear polarization perpendicular to the surface plane (blue curves in Figure 5). In comparison, the signature of electronic states with their nodal plane oriented in-plane were probed in normal incidence with the polarization of the incident X-ray light oriented parallel to the surface plane (red curves in Figure 5). The signature of the transitions states derived from C−N and N−N bonds (vida infra) clearly establishes that the molecules are oriented in the surface plane.

For the identification of the different N species, we analyze the nitrogen K-edge NEXAFS signature of native DPDI on Cu(100) as presented in Figure 5a. We observe two N species via their π* states (403.2 and 399.1 eV) as well as by their σ* states (414.4 and 408.6 eV). The transition energies correspond well with the literature values reported for N atoms of amine and imine character[81,82] (SI Table S3). Note that XPS of unreacted DPDI deposited on Cu(100) also revealed two different N1s signals, corresponding to the amine and imine nitrogen atoms (SI Figure S1a). In case of co-deposited DPDI and Co on Cu(111), the observed N K-edge NEXAFS signal differs significantly (Figure 5b).

The spectrum corresponding to DPDI with Co adatoms revealed only a single π* peak (398.7 eV) and a single σ* peak (409.6 eV), which is consistent with only one type of (imine) nitrogen.[80] This confirms the structural assignment provided above on the basis of the XPS data: The 1D coordination polymer is assigned to Co−deh-DPDI. The 2D coordination polymer formed by DPDI/Cu(111) after annealing has been assigned to a porous 3deh-DPDI−Cu network. In this case, the N K-edge NEXAFS signature reveals again very different features compared to the previous cases. Split peaks corresponding to the transitions between the π* (401.2 and 399.6 eV) and σ* states (410.7 and 407.0 eV) (Figure 5c) are observed. Their energies correspond well to the proposed azo-bridges[78,83−85] formed upon three-fold dehydrogenation of the DPDI molecules, as identified already on the basis of XPS.

The assignment of unreacted DPDI and of deh-DPDI in the NEXAFS data is unambiguous. The NEXAFS signals attributed to the azo-N atoms in 3deh-DPDI, in contrast, requires additional analysis. The observation of the split π* N peak in case of Cu-coordinated 3deh-DPDI on Cu(111) is unexpected on the grounds of the N species alone. We relate this to "donation/back-donation" effects coming from the coordination of 3deh-DPDI with the copper atoms.[78] Specifically, the occupied/unoccupied metal centered orbitals mix with the lowest unoccupied molecular orbital (LUMO)/highest occupied molecular orbital (HOMO) of the molecule, respectively. In the case at hand, this would primarily involve the azo-bridge of 3deh-DPDI and the Cu adatoms. In order to support the proposed donation/back-donation model as a reason for the split π* N peak, a DFT modeling study was carried out.

The extended degeneracy of the molecular orbitals across the Cu-coordinated 3deh-DPDI on Cu(111) can be recognized in the numerical simulations, as well. In Figure 6, the electron density of the frontier orbitals of the freestanding 3deh-DPDI network is illustrated which reflects the bonding in the network: the p_z states of the molecule mix with the d states of the Cu atoms. Notably, both the HOMO and the LUMO consist of three electronic states (one per molecule in the unit cell) with their degeneracy lifted due to the molecule−adatom interactions as represented in Figure 7a,b.

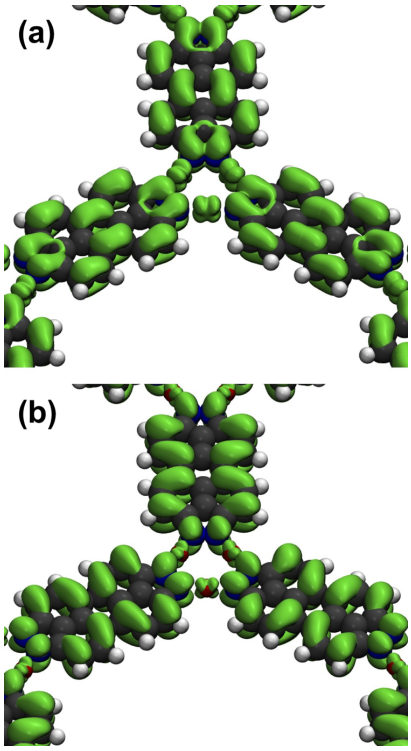

Figure 6. Numerical simulation of Cu-coordinated 3deh-DPDI: Absolute contour plots of the (a) HOMO and (b) LUMO of the freestanding 3deh-DPDI network, represented by the band-decomposed density of states closest to the Fermi level below and above the Fermi level, respectively. The value of the contours is 0.005 e/Å^3.

The partial density of states (PDOS) of the molecule's N atoms is significantly altered due to the interaction with the coordinating Cu adatoms. The calculations of the 3deh-DPDI reveal a splitting of the peaks in the p_z component of the PDOS localized on the N atoms in vacuum (Figure 7a) after Cu coordination (Figure 7b). This splitting pertains when including the Cu(111) surface in the simulations (Figure 7c).

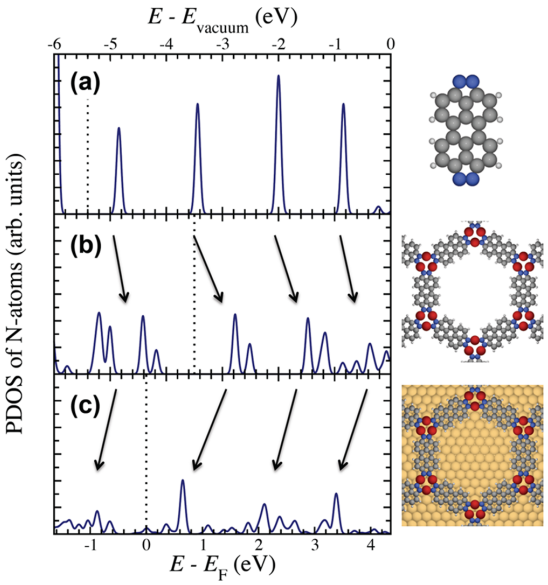

Figure 7. Donation/back-donation effect upon Cu coordination of 3deh-DPDI causes a split in the π^* state, which appears as a double peak in the N K-edge NEXAFS. The partial density of states (PDOS) (a) of the p_z component on the N atoms of the 3deh-DPDI becomes modified by coordination to Cu adatoms for the (b) freestanding and (c) the surface-supported coordination polymer.

Notably, Co-coordinated deh-DPDI chains on Cu(111) give rise to a single (not split) peak in the p_z component of the PDOS of nitrogen (see Figure S9 of SI).

Endo/Exo-DPDI Coordination Defines the Dimensionality of the On-Surface Polymer. In the case at hand, the surface-deposited DPDI molecule acts as a ligand precursor, which is transformed to a ligating structural building block by adatom-specific dehydrogenation (-1 H_2 or -3 H_2). Please note that the hydrogen may be lost as atomic (presumably forming metal hydrides) or as molecular hydrogen (H_2 gas). The control of polymer topology via endo/exoligation provides an example of site-specific chemistry in an oligomerization reaction (Figure 8). The linear polymeric structures formed by deh-DPDI are imposed by the ditopic nature of the chelating endoligand, which connects metal centers via the two inward-pointing free electron pairs belonging to the N atoms at either end of the DPDI molecule (Figure 8, left). The 3deh-DPDI, which is generated in the presence of Cu adatoms, exhibits a characteristically different arrangement of the free N electron pairs while acting as exoligand in the coordination. The construction of the network node also depends on the symmetry of the substrate: On Cu(111), three adatoms connect three 3deh-DPDI molecules in the form of a hexagonal network (Figure 8f and Figure 3a,b,g). On Cu(100), four adatoms interconnect four 3deh-DPDI molecules in each node, thereby forming a tetragonal network (Figure 8d and Figure 3c,d,h,i). At low coverage of 3deh-DPDI on Cu(100) substrates, however, oligomers nucleate in a bridge-to-bridge fashion, initiating a 1D arrangement (Figure 8e and Figure S2 in SI). The N1s peak in the XPS data is not modified with increasing submonolayer coverage indicating that the chemical environment of the nitrogen atoms remains the same irrespective of whether a 1D or a 2D coordination polymer is present. This supports the notion that the 3deh-DPDI ligands are fully Cu-decorated at all coverages. We note that initiating the reaction with Cu adatoms requires the highest temperature (300 °C). This is consistent with the position of Cu on the scale of the second ionization energies of the different atoms studied here. The oxidation state of the coordinating atom in the "*on-surface*" configuration is not trivial to define, as the intermixing between the electronic states of the reacted molecules and the surface has to be taken into account.[86,87]

The interconnection of the exocoordinated ligands via Cu adatoms depends critically on the chemical nature of the substrate. In spite of the Cu-coordination of 3deh-DPDI, as seen by XPS, no RT-stable arrangements were observed on Au(111) by STM. However, after the sample was cooled to 5 K, single coordinated molecules as well as their vdW condensed islands (Figure 8g and Figure S3c–e) were visualized. The fact that 3deh-DPDI molecules do not form a coordination polymer on this substrate may be related to one or more of the following factors: (1) a mismatch between the surface registry and the length of the coordination bond, (2) an interaction between an electronic state of the substrate and the coordinated ligand, or (3) the modified interaction between Cu adatoms and the Au substrate in comparison to the Cu substrate.

CONCLUSIONS

The on-surface reactivity of DPDI molecules, and thus the degree of dehydrogenative conversion into either an endo- or exoligand depends neither on the nature (Au or Cu) nor on the crystal index (111, 100) of the substrate but is exclusively determined by the metal adatoms. In the presence of Fe, Co, and Ni adatoms, the reaction proceeds to deh-DPDI as a ditopic chelating endoligand. This ligand is "trapped" by coordination with the metal adatoms in the formation of 1D coordination polymers. Only in presence of Cu adatoms and at elevated temperatures, the dehydrogenation proceeds to 3deh-DPDI containing two N_2 azo units. Here the two ligating N atoms are linked to two Cu atoms in a convex arrangement at either end of the 3deh-DPDI. Therefore, two types of molecular building blocks are generated, which differ in the encoded structural information: Due to the characteristic difference in the orientation of the ligating functional groups, the endoligand deh-DPDI forms 1D coordination polymers, while the exoligating 3deh-DPDI acts as bridging building block in 2D surface networks. In the latter case, the resulting architecture also depends critically on the chosen substrate: While the reaction with Cu adatoms progresses in the same way on Cu(111), Cu(100) and Au(111), the porous network is observed only on the Cu substrates.

In conclusion, DPDI provides an instructive example of on-surface reactivity which crucially depends on the adatom chemistry. The combined interplay of all critical factors leads to a remarkable structural variety and the possibility to control the dimensionality and architecture of the surface aggregates. Future research will focus inter alia on the reaction mechanisms leading to such new architectures, including detailed theoretical modeling of the reaction sequences involved, and on the exploration of the structure–property relationships. This is geared toward designing novel surface materials with tunable characteristic properties resulting from the interaction of the coordination polymers with the surface.

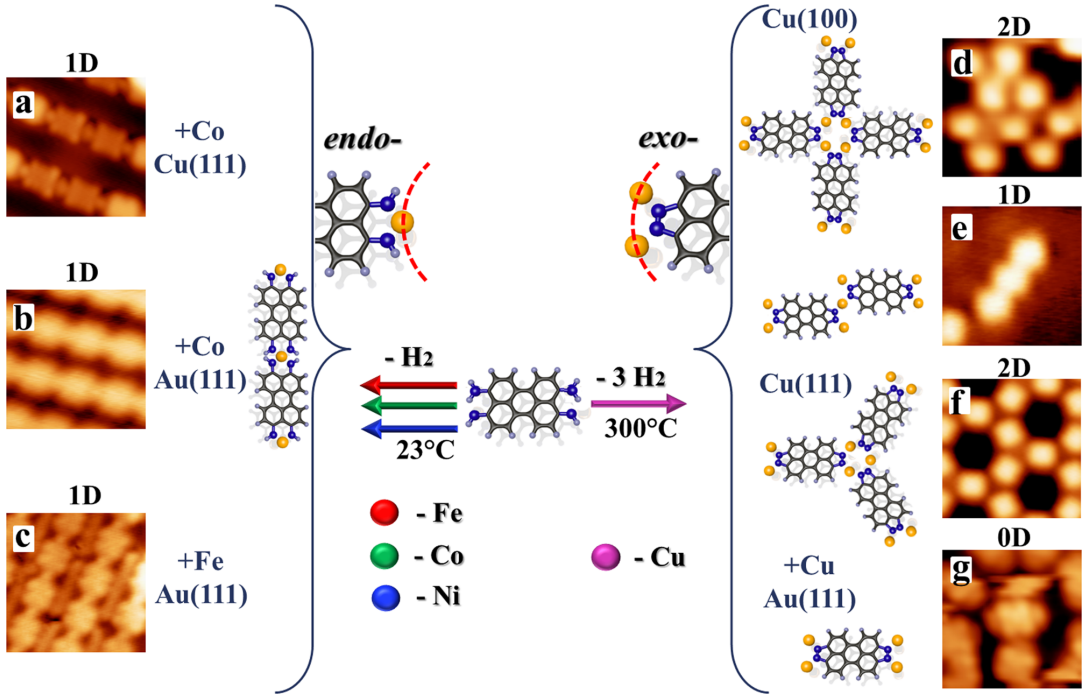

Figure 8. Depending on their reaction partner, dehydrogenated DPDI molecules can act as either endo- or exoligands in the formation of on-surface coordination polymers. (Top center) Two possible polymerization reactions depend on the involved adatoms (Fe, Co, Ni, Cu) as indicated by the schematic representation and the arrows. Colors indicate the chemical species of adatoms as depicted in the legend; (left) deh-DPDI, an endoligand, forms 1D coordination polymers, while 3deh-DPDI (right), an exoligand, forms 2D coordination polymers. STM images ((a–d,f,g) 4×4 nm^2, (e) 5×5 nm^2 taken at 5 K) reveal the chain vs network character of the formed polymers. (a–c) Co or Fe adatoms transform DPDI into deh-DPDI already at RT. In all these cases, the endotype ligation leads to the formation of straight chains on Cu(111) and Au(111). (d) Annealing of DPDI on Cu(100) promotes a formation of an exoligated poly-Cu–3deh-DPDI network with rectangular symmetry. (e) At low coverage, the bridge-to-bridge 1D arrangement is observed. (f) Annealing of DPDI on Cu(111) promotes a formation of an exoligated poly-Cu–3deh-DPDI network with hexagonal symmetry. (g) Sublimation of DPDI and Cu adatoms on Au(111) and subsequent annealing to 300 °C promotes the formation of isolated, but fully Cu-coordinated 3deh-DPDI. The tunneling parameters for the STM imaging were optimized for visualization of the coordinating metal adatoms, which appear as protrusions. Notably for poly-Cu–3deh-DPDI, no adatoms have been visualized by STM.[36]

■ ASSOCIATED CONTENT

Supporting Information

Additional XPS and STM data, tables of XPS values and references; NEXAFS table of references; DFT models; PDOS graphs. This material is available free of charge via the Internet at http://pubs.acs.org.

■ AUTHOR INFORMATION

Corresponding Authors

aneliia.shchyrba@unibas.ch
thomas.jung@psi.ch
lutz.gade@uni-hd.de

Present Address

▲Institute of Condensed Matter Physics (ICMP), Ecole Polytechnique Fédérale de Lausanne (EPFL), Station 3, CH-1015 Switzerland.

Notes

The authors declare no competing financial interest.

■ ACKNOWLEDGMENTS

We gratefully acknowledge the financial support from the National Centre of Competence in Research "Nanoscience" (NCCR-Nano), Swiss Nanoscience Institute (SNI), Swiss National Science Foundation (Grant Nos. 200020-149713, 206021-113149, 206021-121461) and the São Paulo Research Foundation (Grant No. 2013/04855-0). We also thank the University of Heidelberg for funding. The XPS measurements were performed at the Laboratory for Micro- and Nano-technology at the Paul Scherrer Institute (PSI). The authors sincerely thank R. Schelldorfer and M. Martina for the technical support during measurements, as well as H. Peters for their contributions to the experiments at an initial stage of the project. M.S. acknowledges support from The Netherlands Organization for Scientific Research (Chemical Sciences, VIDI Grant No. 700.10.424) and the European Research Council (ERC-2012-StG 307760-SURFPRO). The STM data were processed with the WSXM software.[88]

■ REFERENCES

(1) Elemans, J. A. A. W.; Lei, S.; De Feyter, S. *Angew. Chem., Int. Ed.* **2009**, *48*, 7298.
(2) Klappenberger, F. *Prog. Surf. Sci.* **2014**, *89*, 1.
(3) Koepf, M.; Chérioux, F.; Wytko, J. A.; Weiss, J. *Coord. Chem. Rev.* **2012**, *256*, 2872.
(4) Müllen, K.; Rabe, J. P. *Acc. Chem. Res.* **2008**, *41*, 511.

(5) Treier, M.; Fasel, R. *Chimia* **2009**, *63*, 122.
(6) Yokoyama, T.; Yokoyama, S.; Kamikado, T.; Okuno, Y.; Mashiko, S. *Nature* **2001**, *413*, 619.
(7) Yu, M.; Xu, W.; Kalashnyk, N.; Benjalal, Y.; Nagarajan, S.; Masini, F.; Lægsgaard, E.; Hliwa, M.; Bouju, X.; Gourdon, A.; Joachim, C.; Besenbacher, F.; Linderoth, T. R. *Nano Res.* **2012**, *5*, 903.
(8) Henningsen, N.; Rurali, R.; Limbach, C.; Drost, R.; Pascual, J. I.; Franke, K. J. *J. Phys. Chem. Lett.* **2011**, *2*, 55.
(9) Kley, C. S.; Čechal, J.; Kumagai, T.; Schramm, F.; Ruben, M.; Stepanow, S.; Kern, K. *J. Am. Chem. Soc.* **2012**, *134*, 6072.
(10) Kunkel, D. A.; Hooper, J.; Simpson, S.; Beniwal, S.; Morrow, K. L.; Smith, D. C.; Cousins, K.; Ducharme, S.; Zurek, E.; Enders, A. *J. Phys. Chem. Lett.* **2013**, *4*, 3413.
(11) Pawin, G.; Wong, K. L.; Kim, D.; Sun, D.; Bartels, L.; Hong, S.; Rahman, T. S.; Carp, R.; Marsella, M. *Angew. Chem., Int. Ed.* **2008**, *47*, 8442.
(12) Schlickum, U.; Decker, R.; Klappenberger, F.; Zoppellaro, G.; Klyatskaya, S.; Ruben, M.; Silanes, I.; Arnau, A.; Kern, K.; Brune, H.; Barth, J. V. *Nano Lett.* **2007**, *7*, 3813.
(13) Shi, Z.; Lin, N. *J. Am. Chem. Soc.* **2010**, *132*, 10756.
(14) Stepanow, S.; Lin, N.; Barth, J. V. *J. Phys.: Condens. Matter* **2008**, *20*, 184002.
(15) Tait, S. L.; Wang, Y.; Costantini, G.; Lin, N.; Baraldi, A.; Esch, F.; Petaccia, L.; Lizzit, S.; Kern, K. *J. Am. Chem. Soc.* **2008**, *130*, 2108.
(16) Wang, Y.; Fabris, S.; Costantini, G.; Kern, K. *J. Phys. Chem. C* **2010**, *114*, 13020.
(17) Xu, W.; Wang, J.; Yu, M.; Lægsgaard, E.; Stensgaard, I.; Linderoth, T. R.; Hammer, B.; Wang, C.; Besenbacher, F. *J. Am. Chem. Soc.* **2010**, *132*, 15927.
(18) Zhang, X.; Zeng, Q.; Wang, C. *Nanoscale* **2013**, *5*, 8269.
(19) Cheng, Z.; Luo, M.; Wyrick, J.; Sun, D.; Kim, D.; Zhu, Y.; Lu, W.; Kim, K.; Einstein, T. L.; Bartels, L. *Nano Lett.* **2010**, *10*, 3700.
(20) Kühne, D.; Klappenberger, F.; Krenner, W.; Klyatskaya, S.; Ruben, M.; Barth, J. V. *Proc. Natl. Acad. Sci. U.S.A.* **2010**, *107*, 21332.
(21) Lei, S.; Tahara, K.; Feng, X.; Furukawa, S.; De Schryver, F. C.; Müllen, K.; Tobe, Y.; De Feyter, S. *J. Am. Chem. Soc.* **2008**, *130*, 7119.
(22) MacLeod, J. M.; Ivasenko, O.; Fu, C.; Taerum, T.; Rosei, F.; Perepichka, D. F. *J. Am. Chem. Soc.* **2009**, *131*, 16844.
(23) Ruben, M.; Payer, D.; Landa, A.; Comisso, A.; Gattinoni, C.; Lin, N.; Collin, J.-P.; Sauvage, J.-P.; De Vita, A.; Kern, K. *J. Am. Chem. Soc.* **2006**, *128*, 15644.
(24) Spillmann, H.; Kiebele, A.; Stöhr, M.; Jung, T. A.; Bonifazi, D.; Cheng, F.; Diederich, F. *Adv. Mater.* **2006**, *18*, 275.
(25) Stöhr, M.; Wahl, M.; Spillmann, H.; Gade, L. H.; Jung, T. A. *Small* **2007**, *3*, 1336.
(26) Wintjes, N.; Bonifazi, D.; Cheng, F.; Kiebele, A.; Stöhr, M.; Jung, T.; Spillmann, H.; Diederich, F. *Angew. Chem., Int. Ed.* **2007**, *46*, 4089.
(27) Björk, J.; Hanke, F. *Chem.—Eur. J.* **2014**, *20*, 928.
(28) Bartels, L. *Nat. Chem.* **2010**, *2*, 87.
(29) Grumelli, D.; Wurster, B.; Stepanow, S.; Kern, K. *Nat. Commun.* **2013**, *4*, 2094.
(30) Faraggi, M. N.; Jiang, N.; Gonzalez-Lakunza, N.; Langner, A.; Stepanow, S.; Kern, K.; Arnau, A. *J. Phys. Chem. C* **2012**, *116*, 24558.
(31) Shchyrba, A.; Nguyen, M.-T.; Wäckerlin, C.; Martens, S.; Nowakowska, S.; Ivas, T.; Roose, J.; Nijs, T.; Boz, S.; Schär, M.; Stöhr, M.; Pignedoli, C. A.; Thilgen, C.; Diederich, F.; Passerone, D.; Jung, T. A. *J. Am. Chem. Soc.* **2013**, *135*, 15270.
(32) Sirtl, T.; Schlögl, S.; Rastgoo-Lahrood, A.; Jelic, J.; Neogi, S.; Schmittel, M.; Heckl, W. M.; Reuter, K.; Lackinger, M. *J. Am. Chem. Soc.* **2013**, *135*, 691.
(33) Hanke, F.; Haq, S.; Raval, R.; Persson, M. *ACS Nano* **2011**, *5*, 9093.
(34) Saywell, A.; Greń, W.; Franc, G.; Gourdon, A.; Bouju, X.; Grill, L. *J. Phys. Chem. C* **2014**, *118*, 1719.
(35) Clair, S.; Bedwani, S.; Fabris, S.; Baroni, S.; Brune, H.; Kern, K.; Barth, J. V. *J. Phys. Chem. B* **2006**, *110*, 5627.
(36) Björk, J.; Matena, M.; Dyer, M. S.; Enache, M.; Lobo-Checa, J.; Gade, L. H.; Jung, T. A.; Stöhr, M.; Persson, M. *Phys. Chem. Chem. Phys.* **2010**, *12*, 8815.
(37) Lin, N.; Stepanow, S.; Vidal, F.; Kern, K.; Alam, M. S.; Strömsdörfer, S.; Dremov, V.; Müller, P.; Landa, A.; Ruben, M. *Dalton Trans.* **2006**, 2794.
(38) Fan, Q.; Wang, C.; Han, Y.; Zhu, J.; Kuttner, J.; Hilt, G.; Gottfried, J. M. *ACS Nano* **2014**, *8*, 709.
(39) Björk, J.; Zhang, Y.-Q.; Klappenberger, F.; Barth, J. V.; Stafström, S. *J. Phys. Chem. C* **2014**, *118*, 3181.
(40) Liu, X.-H.; Guan, C.-Z.; Ding, S.-Y.; Wang, W.; Yan, H.-J.; Wang, D.; Wan, L.-J. *J. Am. Chem. Soc.* **2013**, *135*, 10470.
(41) Lin, T.; Shang, X. S.; Adisoejoso, J.; Liu, P. N.; Lin, N. *J. Am. Chem. Soc.* **2013**, *135*, 3576.
(42) Li, Q.; Owens, J. R.; Han, C.; Sumpter, B. G.; Lu, W.; Bernholc, J.; Meunier, V.; Maksymovych, P.; Fuentes-Cabrera, M.; Pan, M. *Sci. Rep.* **2013**, *3*, 2102.
(43) El Garah, M.; MacLeod, J. M.; Rosei, F. *Surf. Sci.* **2013**, *613*, 6.
(44) Lafferentz, L.; Eberhardt, V.; Dri, C.; Africh, C.; Comelli, G.; Esch, F.; Hecht, S.; Grill, L. *Nat. Chem.* **2012**, *4*, 215.
(45) Bieri, M.; Nguyen, M.-T.; Gröning, O.; Cai, J.; Treier, M.; Aït-Mansour, K.; Ruffieux, P.; Pignedoli, C. A.; Passerone, D.; Kastler, M.; Müllen, K.; Fasel, R. *J. Am. Chem. Soc.* **2010**, *132*, 16669.
(46) Gutzler, R.; Walch, H.; Eder, G.; Kloft, S.; Heckl, W. M.; Lackinger, M. *Chem. Commun.* **2009**, 4456.
(47) Weigelt, S.; Busse, C.; Bombis, C.; Knudsen, M. M.; Gothelf, K. V.; Lægsgaard, E.; Besenbacher, F.; Linderoth, T. R. *Angew. Chem., Int. Ed.* **2008**, *47*, 4406.
(48) Matena, M.; Riehm, T.; Stöhr, M.; Jung, T. A.; Gade, L. H. *Angew. Chem., Int. Ed.* **2008**, *47*, 2414.
(49) Gourdon, A. *Angew. Chem., Int. Ed.* **2008**, *47*, 6950.
(50) Grill, L.; Dyer, M.; Lafferentz, L.; Persson, M.; Peters, M. V.; Hecht, S. *Nat. Nanotechnol.* **2007**, *2*, 687.
(51) Zhang, Y.-Q.; Kepčija, N.; Kleinschrodt, M.; Diller, K.; Fischer, S.; Papageorgiou, A. C.; Allegretti, F.; Björk, J.; Klyatskaya, S.; Klappenberger, F.; Ruben, M.; Barth, J. V. *Nat. Commun.* **2012**, *3*, 1286.
(52) Faury, T.; Dumur, F.; Clair, S.; Abel, M.; Porte, L.; Gigmes, D. *CrystEngComm* **2013**, *15*, 2067.
(53) Gao, H.-Y.; Wagner, H.; Zhong, D.; Franke, J.-H.; Studer, A.; Fuchs, H. *Angew. Chem., Int. Ed.* **2013**, *52*, 4024.
(54) Gao, H.-Y.; Franke, J.-H.; Wagner, H.; Zhong, D.; Held, P.-A.; Studer, A.; Fuchs, H. *J. Phys. Chem. C* **2013**, *117*, 18595.
(55) Schlögl, S.; Heckl, W. M.; Lackinger, M. *Surf. Sci.* **2012**, *606*, 999.
(56) Fischer, S.; Papageorgiou, A. C.; Lloyd, J. A.; Oh, S. C.; Diller, K.; Allegretti, F.; Klappenberger, F.; Seitsonen, A. P.; Reichert, J.; Barth, J. V. *ACS Nano* **2014**, *8*, 207.
(57) Marele, A. C.; Mas-Ballesté, R.; Terracciano, L.; Rodríguez-Fernández, J.; Berlanga, I.; Alexandre, S. S.; Otero, R.; Gallego, J. M.; Zamora, F.; Gómez-Rodríguez, J. M. *Chem. Commun.* **2012**, *48*, 6779.
(58) Xu, L.; Zhou, X.; Yu, Y.; Tian, W. Q.; Ma, J.; Lei, S. *ACS Nano* **2013**, *7*, 8066.
(59) Classen, T.; Fratesi, G.; Costantini, G.; Fabris, S.; Stadler, F. L.; Kim, C.; de Gironcoli, S.; Baroni, S.; Kern, K. *Angew. Chem.* **2005**, *117*, 6298.
(60) Barth, J. V.; Weckesser, J.; Lin, N.; Dmitriev, A.; Kern, K. *Appl. Phys. A: Mater. Sci. Process.* **2003**, *76*, 645.
(61) Stepanow, S.; Strunskus, T.; Lingenfelder, M.; Dmitriev, A.; Spillmann, H.; Lin, N.; Barth, J. V.; Wöll, C.; Kern, K. *J. Phys. Chem. B* **2004**, *108*, 19392.
(62) Abdurakhmanova, N.; Floris, A.; Tseng, T.-C.; Comisso, A.; Stepanow, S.; De Vita, A.; Kern, K. *Nat. Commun.* **2012**, *3*, 940.
(63) Dmitriev, A.; Spillmann, H.; Lin, N.; Barth, J. V.; Kern, K. *Angew. Chem., Int. Ed.* **2003**, *42*, 2670.
(64) Tseng, T.-C.; Abdurakhmanova, N.; Stepanow, S.; Kern, K. *J. Phys. Chem. C* **2011**, *115*, 10211.
(65) Stöhr, M.; Wahl, M.; Galka, C. H.; Riehm, T.; Jung, T. A.; Gade, L. H. *Angew. Chem., Int. Ed.* **2005**, *44*, 7394.

Supporting information

Controlling the dimensionality of on-surface coordination polymers via endo- or exo-ligation

Aneliia Shchyrba,*[,†] Christian Wäckerlin,[#,&] Jan Nowakowski,[#] Sylwia Nowakowska,[†] Jonas Björk,[$] Shadi Fatayer,[†] Jan Girovsky, [#] Thomas Nijs,[†] Susanne C. Martens,[†,§] Armin Kleibert,[£] Meike Stöhr,[ǁ] Nirmalya Ballav,[‡] Thomas A. Jung*[,#] and Lutz H. Gade*[,§]

[†] Department of Physics, University of Basel, Klingelbergstrasse 82, 4056 Basel, Switzerland
[#] Laboratory for Micro- and Nanotechnology, Paul Scherrer Institute, 5232 Villigen PSI, Switzerland
[$] Department of Physics, Chemistry and Biology, IFM, Linköping University, Linköping 581 83, Sweden
[£] Swiss Light Source at Paul Scherrer Institute, 5232 Villigen PSI, Switzerland
[ǁ] Zernike Institute for Advanced Materials, University of Groningen, Nijenborgh 4, 9747 AG Groningen, The Netherlands
[‡] Department of Chemistry, Indian Institute of Science Education and Research, Pune 411008, India
[§] Anorganisch-Chemisches Institut, Universität Heidelberg, Im Neuenheimer Feld 270, 69120 Heidelberg, Germany

Table of Contents

1. Thermally induced dehydrogenation of DPDI at Cu(100) surface

The investigation of thermally activated reaction between **DPDI** and Cu adatoms on the Cu surfaces of different symmetry gives a better understanding of the creation of 2D-polymers, where the DPDI derived molecular sub-unit acts as an exo-ligand. The deposition of **DPDI** onto Cu(111) and Cu(100) and subsequent annealing to 300 °C yields the same type of the reaction, resulting in the formation of **3deh-DPDI** (see main text). The change of the N chemical environment from amino-/imino- (Fig. S1a) into azo-character (Fig. S1b) is supported by the characteristic positions of N1s XPS peaks (see also Table 1). Prior annealing both unreacted systems possessed two peaks at 397.7 eV and at 399.4 eV, corresponding to the =NH, and the -NH_2 group respectively. After annealing, the XPS features change significantly. In both cases, the N1s spectrum contains one peak at the binding energy of ~399.3 eV, which we attribute to the azo-group of the **3deh-DPDI**, and a component with minor intensity, which may be attributed to unreacted **DPDI**.

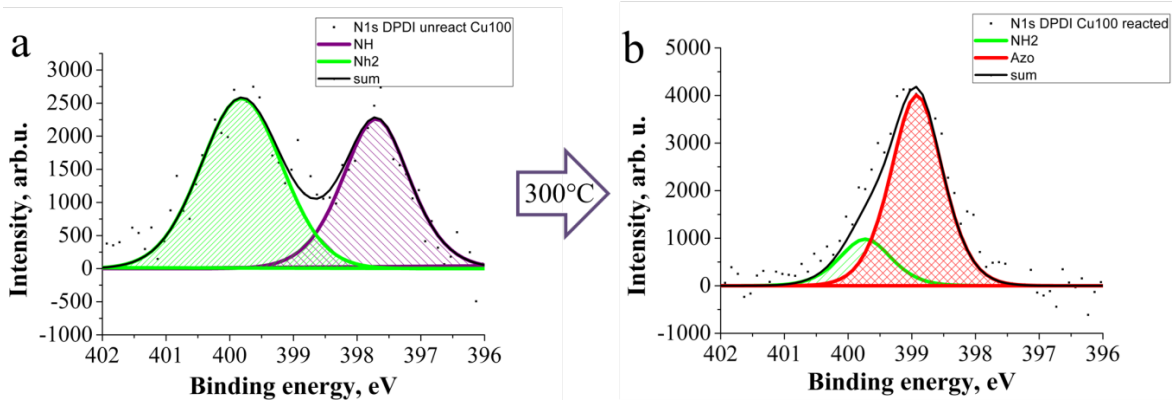

Figure S1: XP spectra of DPDI on Cu(100) before and after annealing. (a) XPS spectra of DPDI prior to annealing contains two components of the N 1s signal, corresponding to the =NH (397.7 eV) and the -NH_2 (399.4 eV) group. (b) After annealing, there is dominant peak at the 399.3 eV corresponding to an azo-group of the 3deh-DPDI. The small shoulder is attributed to the unreacted compound (green).

Although the on-surface transformation of **DPDI** into exo-ligand in presence of Cu adatoms is the same, the geometry of 2D-polymer depends on the symmetry of the substrate (cf. Fig. 3 of the main text). Note that the initial growth of **3deh-DPDI** at low molecular coverage differs between Cu(111) and Cu(100) substrates. The symmetry of the (111) substrate gives rise to ligand-to-ligand binding in the hexagonal shape, whereas on the (100) substrate **3deh-DPDI** starts to bind in the bridge-to-bridge fashion (Fig. S2 STM image and corresponding model), which at increased coverage leads to the rectangular pores (cf. Fig. 3c,d of the main text).

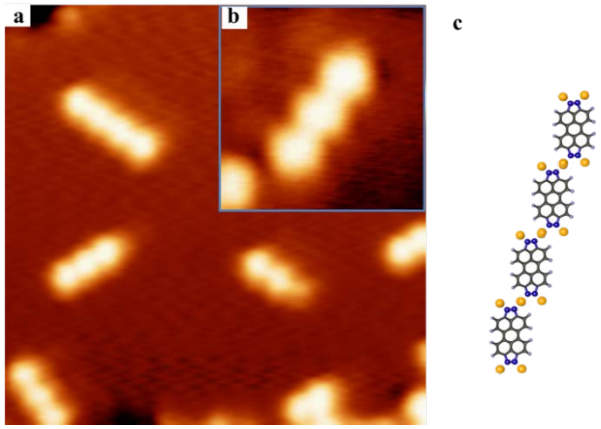

Figure S2: The different symmetry of Cu(100) surface in comparison with Cu(111) surface, directs a nucleation of the exo-ligands. (a,b) Cu-coordinated polymers, formed after annealing of DPDI to 300°C at low coverage on Cu(100), are reflected in the STM images (18x18 nm² and 5x5 nm², respectively). (c) The corresponding tentative model of the interconnected in the bridge-to-bridge fashion exo-ligands at the start of the nucleation process.

2. Multilayer DPDI on Cu(111) studied by XPS

Sub-monolayer amounts of **DPDI** on Cu(111), as probed by XPS, are characterized by two peaks of nitrogen in N1s spectrum (at 399.4 eV and 397.7 eV, see main text and Fig. 2a). Multilayer **DPDI** (ca. 10 monolayers), which was deposited on Cu(111), contains two nitrogen species characterized by the same binding energies in XPS, as evidenced by the N1s spectrum shown in Figure S3.

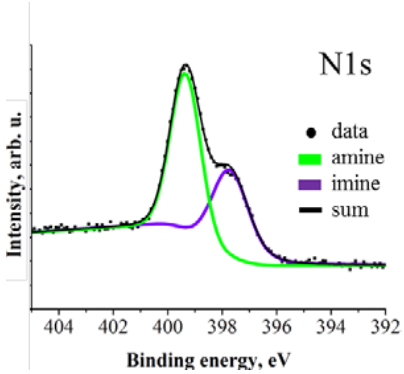

Figure S3: N1s XPS of the DPDI multilayer deposited on Cu(111) surface at room temperature (RT).

3. Deposited Cu adatoms vs. Cu adatoms present on Cu(111) surface

A sub-monolayer of DPDI was deposited onto Cu(111) surface and analyzed by XPS. The spectra of N1s and C1s are shown in Figure S3a. The evaporation of free Cu atoms (from an electron-beam heated metal evaporator source) was performed onto the sample in order to evaluate their influence. The thermal energy during evaporation is higher than for adatoms inherently present on the Cu surface. The corresponding C1s, N1s spectra in Figure S4b do not reveal any significant changes of the carbon or nitrogen chemical environment. The positions of the C1s peaks in both cases are ~ 285.9eV and 284.8 eV (dark green and blue peaks correspondingly in Fig. S4). The two N1s peaks, corresponding to amino- (light green, 399.43 eV) and imino- group (violet, 397.73 eV) are remaining also at the same position.

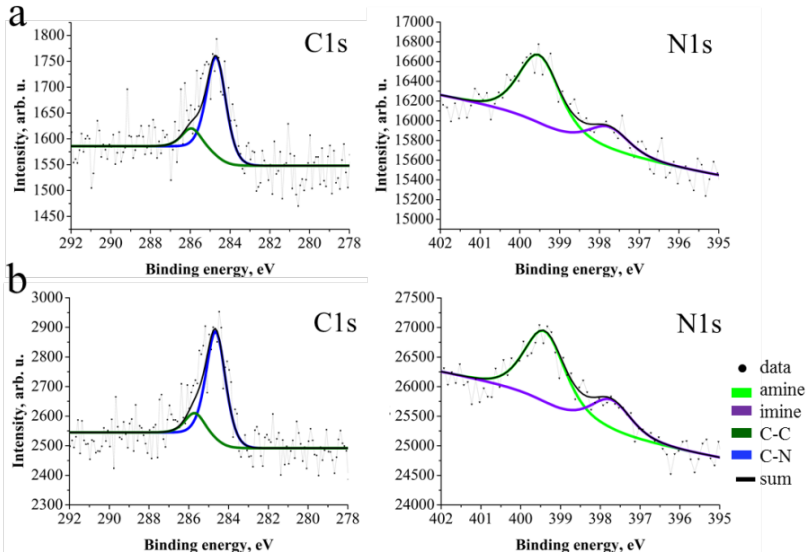

Figure S4: Comparison of the Cu adatoms effect, in dependence whether atoms are inherently present on the surface or deposited from e-beam evaporator source, on DPDI molecules at room temperature (RT). DPDI was deposited on Cu(111) surface, where the thermally generated Cu adatoms are in excess at RT, and was analysed by XPS. Afterwards, additional Cu adatoms were deposited on the same sample by means of evaporation. The C1s and N1s spectra of DPDI on Cu(111) for (a) natively present Cu and (b) additionally deposited adatoms.

4. Coordination of 3deh-DPDI to Cu adatoms on Au(111)

In order to investigate the possibility of the Cu adatoms to promote an on-surface **DPDI** transformation into exo-ligand on a less reactive surface, we have chosen a Au(111) substrate. The XP spectrum of **DPDI** shows two peaks at 399.8 eV and 398.8 eV for amine- and imine group with a ratio of 29.2% and 70.8%, respectively (Fig. S5a). Deposition of Cu adatoms on the Au(111) substrate held at RT does not modify the spectra significantly suggesting that the compound does not change in the presence of Cu adatoms, as has been also shown for Cu adatoms on Cu(111) (chapter 3 of SI). Annealing of the sample to 300 °C modifies the ratio between two peaks (40.4% and 59.6%). Moreover the increased nitrogen-component appears at different binding energy, i.e. 399.5 eV. These findings hint towards modification of **DPDI** and conversion of the **DPDI** molecule into exo-ligand (**3deh-DPDI**), in analogy to the case on Cu surfaces. The remaining decreased imine-peak can be attributed to the unreacted compound. Note that, annealing of DPDI on Au(111) in absence of Cu results in the desorption of the molecule.

In the STM images we did not observe any stable structures at RT. Cooling down to 5 K allowed us to visualize single as well as condensed in islands coordinated molecules (Fig. S5 b-d). Single molecules are imaged with a bright protrusion on each side, corresponding to coordinated copper adatoms.

The different behavior of the exo-ligating **3deh-DPDI** on Au(111) in comparison to Cu(111), can be explained on the basis of i) commensurability and/or ii) a stronger interaction of the coordinated Cu-adatoms with the Cu substrate then with the Au substrate. i) The Cu-Cu nearest neighbor distance and its relation to a **3deh-DPDI** size (1.2 nm) appears to be a better match in the case of Cu(111) compared to Au(111). ii) Another important parameter, namely the electronic configuration of the system, should be considered. The interaction between the copper adatom and the exo-ligand is different in the case of Cu(111) compared to Au(111). In the latter case the charge state of a metal adatom can be no more favorable for the connection between two exo-ligands. Therefore it seems that a success of the 2D-coordinated polymer formation depends not only on the resulting reaction product, substrate symmetry, their commensurability, but also on the specific adatom-substrate interaction.

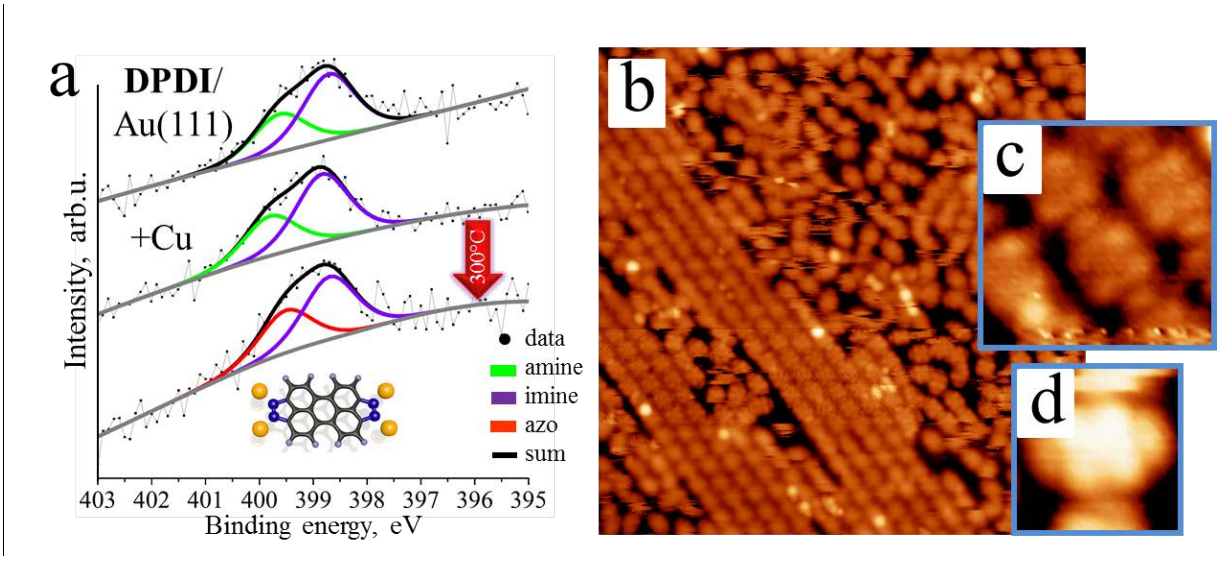

Figure S5: (a) Native DPDI molecules on Au(111) are not modified upon adding Cu adatoms, as can be seen from the corresponding unmodified amine- and imine-nitrogen N1s peaks in XPS data (399.8 eV, green ; 398.8 eV, violet). Annealing of the sample to ~300°C modifies the ratio between the two components, i.e. the imine peak decreases and remains at the same energy (398.8 eV, violet), whereas the peak at higher binding energy increases and shifts by ~0.3 eV (399.5 eV, red). The latter component may be attributed to the azo-nitrogen, characteristic for exo-ligating 3deh-DPDI. Note, annealing should be performed with a slowly increasing temperature otherwise the molecules desorb from the surface. (b-d) Single, coordinated exo-ligands are mobile at RT, whereas at 5 K they are partially condensed into islands, as reflected in the STM images (2.5V, 10pA; b: 30x30 nm^2; c: 3x3 nm^2 and d: 2x2 nm^2).

5. XPS Tables of values and references

In order to test the transformation of DPDI molecule into endo-/exo- ligands with regard to the different transition metals used, we have performed XPS measurements of N 1s. The measured average positions for N1s of imino-, amino, and azo- groups (Table 1) correspond well with the ones reported in literature (Table 2).

Table S1: XPS N 1s peak positions for the amino-, imino- and azo- nitrogens of the DPDI and its derivatives were obtained from the fit.

Molecule/Substrate	**-NH_2, eV**	**=NH, eV**	**N=N, eV**
Multilayer DPDI/Cu(111)	399.4	397.7	-
DPDI/Cu(111)	399.4	397.5	-
deh-DPDI+Co/Cu(111)	-	398.3	-
deh-DPDI+Co/Cu(111) annealed		398.1	
3deh-DPDI/Cu(111)	-	-	399.4

Table S2: XPS N 1s values from amino-, imino- and azo-groups presented in literature.

	-NH_2, eV	**=NH, eV**	**N=N, eV**
Binding Energy	400, 399.5[2] 399.6[3] 400.0[4] 399.5[6]	398.3 [4]	399.5[7] 399.8[8] 399.2[9]

6. NEXAFS table of references

Complementary to XPS, verification of the resulting reaction products, i.e. endo-/exo- type of the ligand in the metal coordination complex, was performed with Near Edge X-ray Absorption Fine Structure (NEXAFS) measurements at the Swiss Light Source (SLS). In all investigated by NEXAFS samples (see main text) π* or σ* states are observed exclusively in the grazing and normal beam incidence confirming the flat orientation of DPDI and its derivatives on the surface. The experimental positions for π* and σ* resonances for the amino-, imino- and azo- nitrogen (cf. Table 1 of the main text) are in good agreement with the values reported in literature (Table 3).

Table S3: NEXAFS N 1s values deriving from amino-, imino- and azo-groups as presented in literature.

-NH_2		**=NH**		**N=N**	
π*, eV	**σ*, eV**	**π*, eV**	**σ*, eV**	**π*, eV**	**σ*, eV**
402[10]	407[10]	398.5[11]	412[10]	398.2[12] 399.7[7] 398.2[8]	408[8] 404.6[7]

7. DFT calculations for Co-coordinated deh-DPDI chain: models and energies

The addition of Co adatoms to the DPDI molecules at Cu(111) surface leads to the formation of linear chains, as shown in the main text and on the large-scale STM overview in Figure S6.

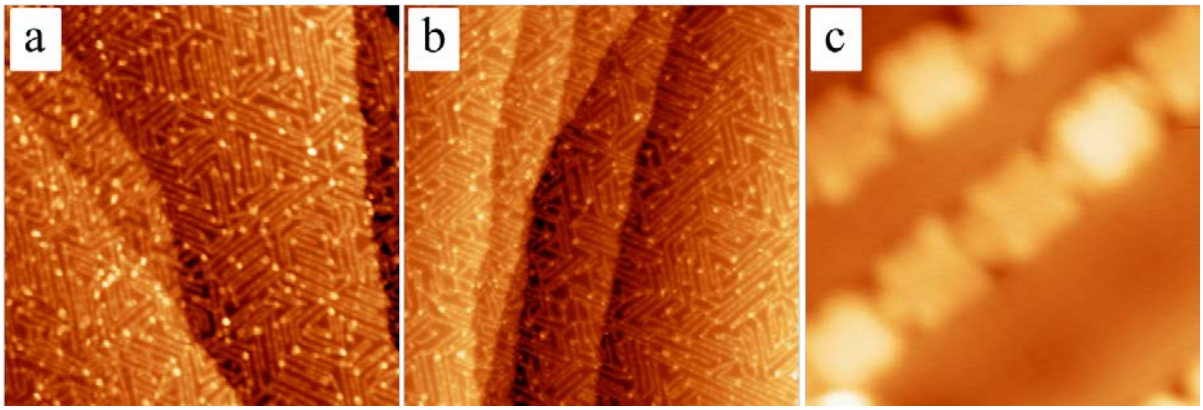

Figure S6: Deposition of Co adatoms onto DPDI/Cu(111) at RT results in 1D deh-DPDI chain structures observed in the STM micrographs: (a, b) 100 x 100 nm^2, (c) 4 x 4 nm^2.

Spectroscopic probing of nitrogen before and after the reaction have revealed a modified nitrogen environment and the resulting reaction product was assigned to imino-type of nitrogen (XPS and NEXAFS – see Figure 2 and Figure 4 of the main text). In order to get more insight into the on-surface reaction, we did calculations for several Co-coordinated deh-DPDI chain models using different unit cells. The resulting models are illustrated in Figures S7-9 together with their corresponding unit cells and reaction energies. Energy of the reaction E_{react} was calculated as

$$E_{react} = E_{tot} - E_{Co@Cu(111)} - (E_{DPDI@Cu(111)} - E_{Cu(111)}) + 2(E_{H@Cu(111)} - E_{Cu(111)}),$$

where E_{tot} is the total energy of the Co-coordinated deh-DPDI chain, $E_{Co@Cu(111)}$ the total energy of a system with a Co adatom on Cu(111), $E_{DPDI@Cu(111)}$ the total energy of an intact isolated DPDI molecule on Cu(111), $E_{H@Cu(111)}$ the total energy of a H atom adsorbed on Cu(111), and $E_{Cu(111)}$ the total energy of the clean Cu(111) surface. In this way, the reaction energy is defined with respect to an isolated intact DPDI molecule and an isolated Co atom on the surface, and that the abstracted H atoms adsorb on Cu(111) subsequent to the reaction. We find that the structure illustrated in Figure S7b is the most stable one. It runs along the high symmetry direction of the substrate, e.g. [1-10]-direction, where each repeated unit has a length of 12.72 Å, close to the experimentally estimated value of 11.6±1.0 Å.

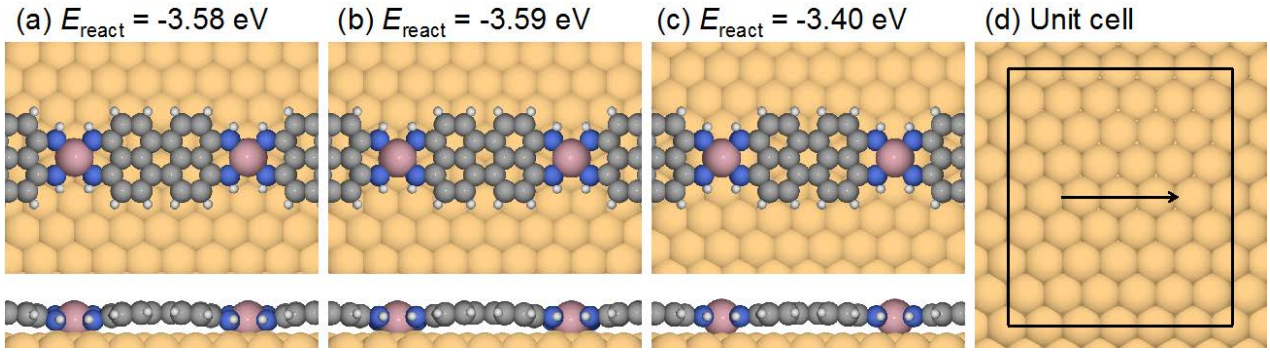

Figure S7: (a-c) Calculated DFT models of the Co-coordinated deh-DPDI chains on Cu(111). The unit cell, which was used for calculations, is shown in (d) with a use of a 3×2 k-point sampling. The chain runs in the direction of the arrow. For each of the structures (a-c) the reaction energy is indicated.

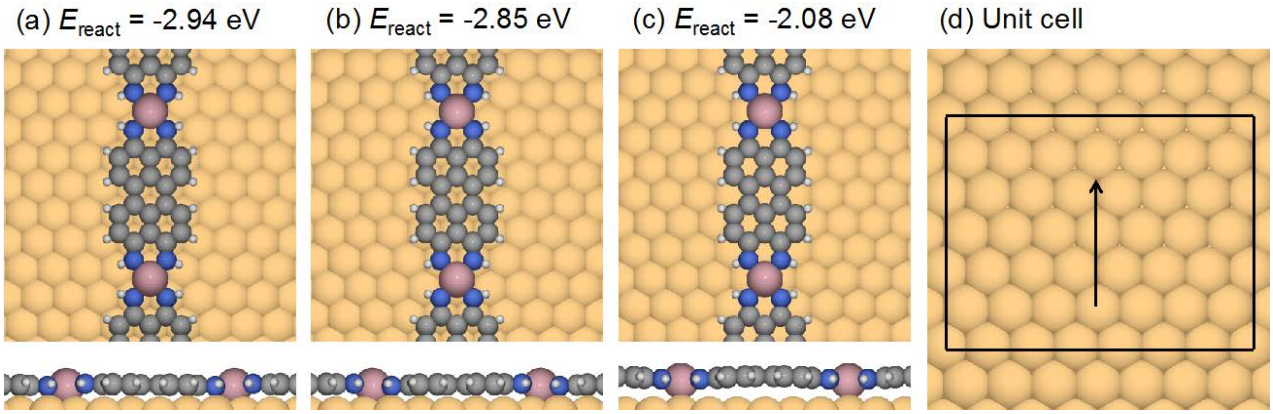

Figure S8: (a-c) Calculated DFT models of the Co-coordinated deh-DPDI chains on Cu(111). The unit cell, which was used during calculations, is shown in (d) with a use of a 2×3 k -point sampling. The chain runs in the direction of the arrow. For each of the structures (a-c)the reaction energy is indicated.

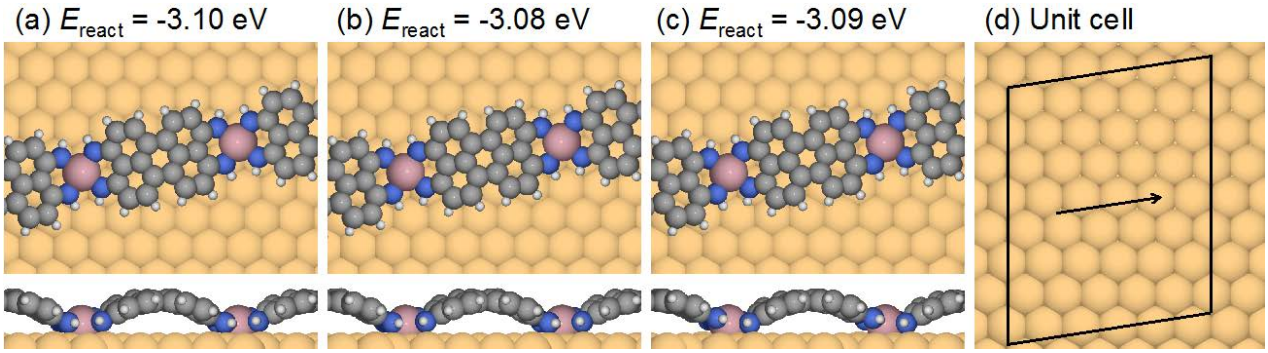

Figure S9: (a-c) Calculated DFT models of the Co-coordinated deh-DPDI chains on Cu(111). The unit cell, which was used during calculations, is shown in (d) with a use of a 3×2 k -point sampling. The chain runs in the direction of the arrow. For each of the structures (a-c)the reaction energy is indicated.

Additionally, we calculated the partial density of states (PDOS) for the Co-coordinated DPDI chain, focusing on the p_z components on the nitrogen atoms. The PDOS diagrams for the chain in gas phase and on Cu(111) reflect no split of the peak components (Figure S10) like in the case of Cu-coordinated 3deh-DPDI, described in the main text (Figure 7). These findings support an appearance of the single peak observed in NEXAFS. Thus, the calculations support the model of the Co-coordinated deh-DPDI chain, assigned from the experimental observations..

Furthermore, we have calculated the atomic orbital projected density of states (AO-PDOS) of the transition metals atoms inside the coordination complex (Figure S11): (a) Cu atoms in the freestanding **3deh-DPDI** honeycomb network and (b) the Co atoms in the freestanding **deh-DPDI** chains. The AO-PDOS is compared to the energy levels of the isolated atoms (illustrated by the shaded curves on Figure S11). The spin-orbit coupling was not included into the calculation, thereby the 3d spin-down orbitals for the isolated Co atom are degenerated in energy. Both spin-components for the 4s orbital of Cu split below and above the Fermi level, additionally the 3d orbitals have contribution above the Fermi level (which is less pronounced). Split in the components reflects the donation/back-donation effect, described in the main text of the manuscript. In case of Co atom, both 3d and 4s orbitals show a significant split induced by the coordination with the nitrogen atoms, with components both above and below the Fermi level, suggesting a presence of the donation/back-donation effect also in this system.

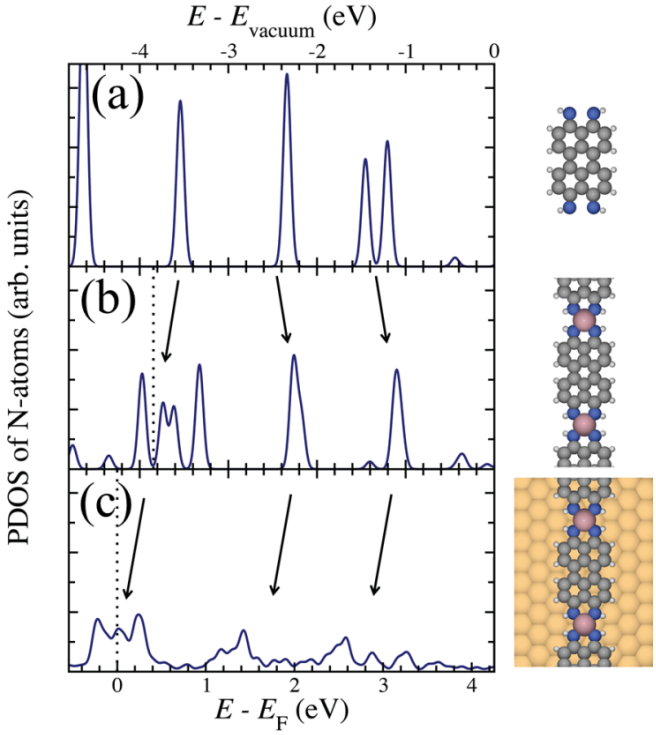

Figure S10: Calculated PDOS of the p_z components on the nitrogen atoms for (a) deh-DPDI in gas phase, (b) Co-coordinated deh-DPDI chain in gas phase, (c) Co-coordinated deh-DPDI chain on Cu(111). In both cases no split in peaks was observed.

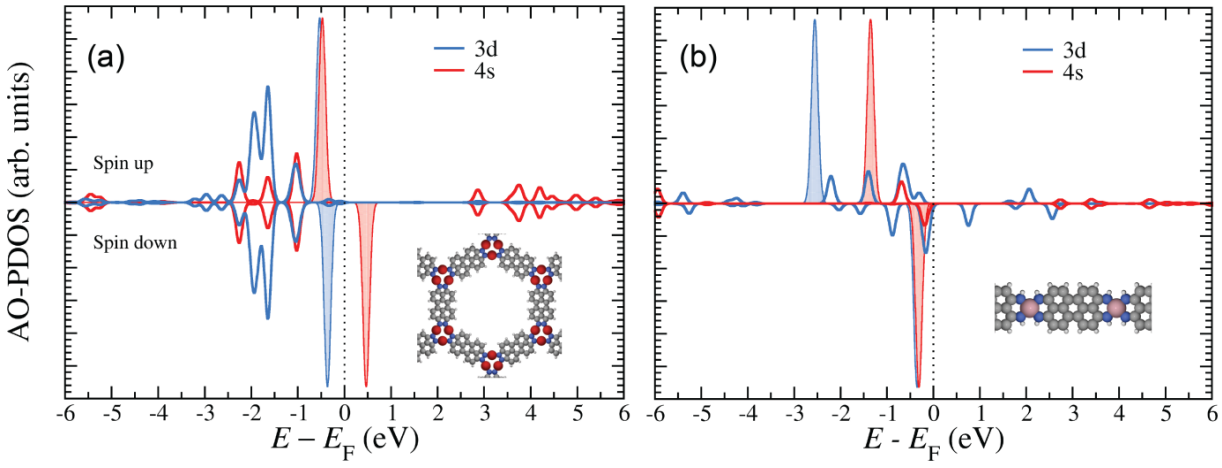

Figure S11: Atomic orbital projected density of states (AO-PDOS) of the Cu atoms in the freestanding 3deh-DPDI honeycomb network (a) and the Co atoms in the freestanding 1deh-DPDI chains (b), compared to the energy levels of the isolated atoms illustrated by the shaded curves. For the isolated Co atom, the 3d spin-down orbitals are degenerated in energy since no spin-orbit coupling was included in the calculations. The donation/back-donation effect is particularly visible for the 4s orbital of Cu (a), where both spin-components split below and above the Fermi level, but also the 3d orbitals have contribution above the Fermi level (which is less pronounced). For the Co atom (b) both 3d and 4s orbitals show significant splitting induced by the coordination with the nitrogen atoms, with components both above and below the Fermi level, indicating the donation/back-donation effect in this system.

8. References:

(1) Dietrich, P. M.; Graf, N.; Gross, T.; Lippitz, A.; Krakert, S.; Schüpbach, B.; Terfort, A.; Unger, W. E. S. *Surf. Interface Anal.* **2010**, *42*, 1184.
(2) Eralp, T.; Shavorskiy, A.; Held, G. *Surf. Sci.* **2011**, *605*, 468.
(3) Shavorskiy, A.; Eralp, T.; Schulte, K.; Bluhm, H.; Held, G. *Surf. Sci.* **2013**, *607*, 10.
(4) Lin, Y.-P.; Ourdjini, O.; Giovanelli, L.; Clair, S.; Faury, T.; Ksari, Y.; Themlin, J.-M.; Porte, L.; Abel, M. *J. Phys. Chem. C* **2013**, *117*, 9895.
(5) Fischer, S.; Papageorgiou, A. C.; Marschall, M.; Reichert, J.; Diller, K.; Klappenberger, F.; Allegretti, F.; Nefedov, A.; Wöll, C.; Barth, J. V. *J. Phys. Chem. C* **2012**, *116*, 20356.
(6) Schiffrin, A.; Reichert, J.; Pennec, Y.; Auwärter, W.; Weber-Bargioni, A.; Marschall, M.; Dell'Angela, M.; Cvetko, D.; Bavdek, G.; Cossaro, A.; Morgante, A.; Barth, J. V. *J. Phys. Chem. C* **2009**, *113*, 12101.
(7) Piantek, M.; Miguel, J.; Krüger, A.; Navío, C.; Bernien, M.; Ball, D. K.; Hermann, K.; Kuch, W. *J. Phys. Chem. C* **2009**, *113*, 20307.
(8) Brete, D.; Przyrembel, D.; Eickhoff, C.; Carley, R.; Freyer, W.; Reuter, K.; Gahl, C.; Weinelt, M. *J. Phys. Condens. Matter* **2012**, *24*, 394015.
(9) Elbing, M.; Błaszczyk, A.; von Hänisch, C.; Mayor, M.; Ferri, V.; Grave, C.; Rampi, M. A.; Pace, G.; Samorì, P.; Shaporenko, A.; Zharnikov, M. *Adv. Funct. Mater.* **2008**, *18*, 2972.
(10) Feyer, V.; Plekan, O.; Šutara, F.; Cháb, V.; Matolín, V.; Prince, K. C. *Surf. Sci.* **2011**, *605*, 361.
(11) Gahl, C.; Brete, D.; Leyssner, F.; Koch, M.; McNellis, E. R.; Mielke, J.; Carley, R.; Grill, L.; Reuter, K.; Tegeder, P.; Weinelt, M. *J. Am. Chem. Soc.* **2013**, *135*, 4273.
(12) Schmidt, R.; Hagen, S.; Brete, D.; Carley, R.; Gahl, C.; Dokić, J.; Saalfrank, P.; Hecht, S.; Tegeder, P.; Weinelt, M. *Phys. Chem. Chem. Phys.* **2010**, *12*, 4488.

Covalent assembly of a two-dimensional molecular “sponge” on a Cu(111) surface: Confined electronic surface states in open and closed pores

Summary:

This article reports on new on-surface boron-chemistry and bi-component covalent reactions. We find that the borylene-functionalized perylene derivative and trimesic acid readily react upon annealing. The covalent B-O connection exhibits a high flexibility, which leads to the formation of pores exhibiting various sizes and shapes. We used the ‘sponge-like’ molecular network to investigate the quantum confinement effect of the surface state electrons by the pores of different size and geometry. By using Scanning Tunneling Spectroscopy (STS), we found an increase in energy of the confined peak with decreasing pore area. We analysed the confinement within a 2D particle-in-a box model. The study revealed propagation of the surface state across the barrier imposed by its interaction with the polymer back-bone. Additionally, we address the different degree of partial confinement imposed by molecular pores with missing barriers, to the best of our knowledge for the first time. We found that the absence of one or two barriers in the hexagonal pore does not affect the energy of the confined surface state but only increases the width of the confined peak. This system serves as a unique example of the ‘templating’ effect in a 2D polygonal box with missing borders. Thereby these results confirm that STM probes a superposition of states in different in-plane directions, which are in one direction fully and in the other direction partially confined – as expected on the basis of quantum mechanics.

Paper [[3]] has been published in Chemical Communications in 2014. Contribution of Aneliia Shchyrba: carried out the experimental investigation (STM, STS), analysed the data, wrote the manuscript.

[Aneliia Shchyrba *et al.*, *Chem. Commun.*, 2014, 50, 7628-7631] - Published by The Royal Society of Chemistry.

ChemComm

COMMUNICATION

View Article Online
View Journal | View Issue

Cite this: *Chem. Commun.*, 2014, **50**, 7628

Received 3rd April 2014,
Accepted 18th May 2014

DOI: 10.1039/c4cc02463j

www.rsc.org/chemcomm

Covalent assembly of a two-dimensional molecular "sponge" on a Cu(111) surface: confined electronic surface states in open and closed pores†

Aneliia Shchyrba,[a] Susanne C. Martens,[ab] Christian Wäckerlin,‡[c] Manfred Matena,[a] Toni Ivas,[a] Hubert Wadepohl,[b] Meike Stöhr,[d] Thomas A. Jung*[c] and Lutz H. Gade*[b]

We present a new class of on-surface covalent reactions, formed between diborylene-3,4,9,10-tetraaminoperylene and trimesic acid on Cu(111), which gives rise to a porous 2D-'sponge'. This aperiodic network allowed the investigation of the dependence of electron confinement effects upon pore size, shape and even in partial confinement.

Covalent coupling reactions between molecular units adsorbed at surfaces have recently received increasing attention, in particular in the context of two-dimensional (2D) networks.[1] The most established approaches include Ullman coupling,[1a,b,d–f,2] Schiff base reaction,[3] Glaser coupling,[4] click-reaction[5] or polyester condensation.[6] The synthesis of covalently linked oligo- or polymeric structures is based on the coupling between planar polyfunctional building blocks which require a connectivity greater than two to form 2D assemblies. There are only a few examples of boron-based covalent chemistry to form aperiodic 2D networks.[7]

We previously reported the synthesis of *N*,*N*′;*N*″,*N*‴-diborylene-3,4,9,10-tetraaminoperylene derivatives (**DIBOTAPs**), which contain two borylene groups (BR) (Fig. 1).[8] The parent compound (R = H) **1** was found to react readily with alcohols and carboxylic aids (R–OH), eliminating H_2 and forming B–O–R bonds. This clean coupling along with the elimination of a gaseous co-product (H_2) was thought to provide the basis for an on-surface synthesis of polymeric structures. In combination with a trifunctional carboxylic acid, such as trimesic acid (**TMA**), the linear **DIBOTAP** could couple to give a porous surface network. The relative angular flexibility of the C(O)–O–B junctions between the building blocks allows for the pore formation of variable size (and shape), resulting in a 'sponge'-like covalent polymer.

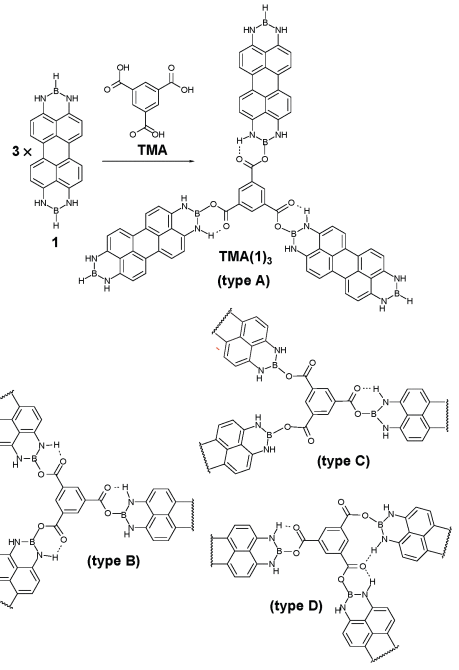

Fig. 1 *N*,*N*′,*N*″,*N*‴-Diborylene-3,4,9,10-tetraaminoperylene (**1**) and benzene-1,3,5-tricarboxylic acid (**TMA**) on Cu(111) form **TMA(1)$_3$** by covalent reaction after thermal activation at ~120 °C. The length of **1** is H**B**–B**H** 13.724 Å; B–B 11.433 Å and the width is H3–H9 6.564 Å; H2A–H8 6.570 Å (X-ray diffraction study in the ESI†). The flexibility of the covalent link formed by **TMA** deprotonation allows for a wide range of bonding geometries categorized as **types A–D**.

Two-dimensional networks provide confinements for the scattering of electrons localized in the Shockley type surface state on noble metal (111) surfaces. Whereas the interaction

[a] *Department of Physics, University of Basel, Klingelbergstrasse 82, 4056 Basel, Switzerland. E-mail: aneliia.shchyrba@unibas.ch*
[b] *Anorganisch-Chemisches Institut, Universität Heidelberg, Im Neuenheimer Feld 270, 69120 Heidelberg, Germany. E-mail: lutz.gade@uni-heidelberg.de*
[c] *Laboratory for Micro- and Nanotechnology, Paul Scherrer Institute, 5232 Villigen PSI, Switzerland. E-mail: thomas.jung@psi.ch*
[d] *Zernike Institute for Advanced Materials, University of Groningen, Nijenborgh 4, 9747 AG Groningen, The Netherlands*

† Electronic supplementary information (ESI) available: Experimental details, additional XPS and STM data. Data of the X-ray diffraction study of **1** (CIF format). CCDC 988044. For ESI and crystallographic data in CIF or other electronic format see DOI: 10.1039/c4cc02463j

‡ Present address: Institute of Condensed Matter Physics, Ecole Polytechnique Fédérale de Lausanne, 1015 Lausanne, Switzerland.

with small scatterers (*e.g.* metal atoms) is well established,[9] the scattering and confinement mechanisms for 2D molecular architectures[10] are less understood. Therefore it is desirable to create a sample with coexisting pores of different size and shape, which are formed by the same polymer backbone. The investigation of the confined surface states in different open and closed pores by scanning tunnelling spectroscopy (STS) allows to draw conclusions regarding the size and shape dependence of the confinement effect.

Deposition of **1** and then **TMA** on Cu(111) at room temperature (RT) and subsequent annealing at ~120 °C resulted in the formation of porous networks (Fig. 2a, experimental details in ESI†). The pores of the network exhibited different shapes, as expected in view of the flexibility of the intermolecular joints discussed above. At least six different pore geometries could be identified as sketched in Fig. 2d (*cf.* Fig. S4, ESI†). Notably, the same type of network can also be formed under analogous preparation conditions on the less reactive Ag(111) substrate (*cf.* Fig. S5, ESI†).

In order to determine the chemical integrity of the on-surface polymer we probed the chemical environment of C, N, O and B atoms of both **TMA**, **1** as well as of the {**TMA(1)$_3$**} polymer by XPS (Fig. 2b and c). The C1s and N1s spectra are displayed in Fig. S2 (ESI†) and all XPS peak positions are summarized in Table S1 (ESI†). The unreacted compound **1** gives rise to N1s and B1s peaks at binding energy (BE) of 399.4 eV and 190.2 eV, respectively. For the native **TMA** molecule on Cu(111) two O1s peaks are observed at 531.6 eV and 533.5 eV. The signal at lower (higher) BE is assigned to oxygen in the carbonyl (hydroxyl) group. The observed ratio between the two oxygen species is different from 1 : 1 due to partial deprotonation of the COOH-groups after **TMA** adsorbs on Cu(111).[11] The on-surface {**TMA(1)$_3$**} polymer is identified by a shift (+1.35 eV) of the B1s peak towards higher binding energy (Fig. 2b). This upshift is attributed to the significant difference in electronegativity between boron and oxygen leading to a partial positive charge on boron after formation of the O–B bond. Moreover, the O1s spectra clearly show a modified balance of the two oxygen species corresponding to C–O–B (533.3 eV) and C═O (532 eV) after polymerisation (Fig. 2c). The position of the N1s peak on the other hand remains unmodified (399.4 eV) (*cf.* Fig. S2, ESI†). Thus, the XPS analysis confirms the formation of an on-surface polymer based on covalent oxygen boron (O–B) bonds.

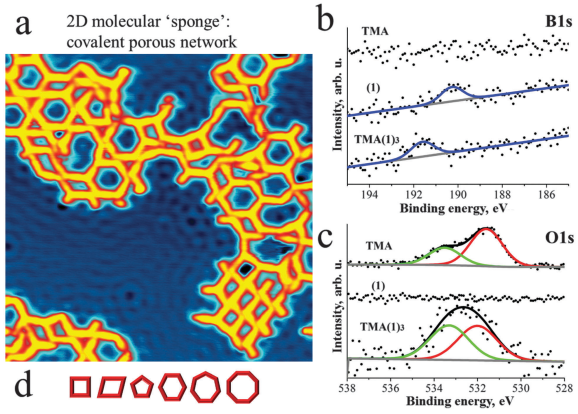

Fig. 2 Deposition of **TMA** and **1** on Cu(111) at RT and subsequent annealing to 120 °C leads to the formation of an aperiodic covalent molecular network {**TMA(1)$_3$**}. (a) STM micrograph taken at 5 K depicts pores of different size and shape (30 × 30 nm^2). Scattering of surface state electrons leads to standing wave patterns on the substrate. (b) The XP spectra of **TMA**, **1** and **TMA(1)$_3$** reveal a significant shift (+1.35 eV) of the B1s peak towards higher binding energy and (c) the change of the ratio between O1s peaks upon the thermally activated formation of the covalent network. These observations strongly support the formation of a covalent O–B bond in the on-surface polymer, as sketched in Fig. 1. (d) Schematic representation of the various pore sizes and shapes.

The 2D network acts as a system of different quantum wells interacting with the surface state electrons. Scattering at the ad-polymer can be clearly observed by the standing wave patterns in the STM data shown in Fig. 2a. For a further in-depth analysis of the quantum confinement effects we used scanning tunnelling spectroscopy (STS) at 5 K to probe the local (electronic) density of states (LDOS). The dI/dV spectrum, taken in the center of a certain pore, reveals a confined electronic surface state characterized by a peak energy dependent on the pore dimension (Fig. 3). Note that occupied and unoccupied states are probed at negative and positive sample bias voltage, respectively. The Cu(111) surface state is detected at −450 mV[12] with respect to the Fermi level (E_F) (red curve in Fig. 3a). The following peak values were measured by STS for the different sized and shaped pores: square −90 mV, parallelogram −180 mV, pentagon −265 mV, hexagon −336 mV, heptagon −360 mV and octagon −382 mV (Fig. 3a).

The pore confines the surface state electrons which are free in 2D on the extended Cu(111) substrate. In the following the energies E of the different confined states are referred to the onset of the native surface state E_0. These energies $E' = E - E_0$ are known to scale linearly with the inverse area ($1/A$) as $E' = C/A$ with $C = \alpha_1 \hbar^2\pi/(2m^*)$[13] Here $m^* = 0.38\ m_e$[12] is the effective electron mass (note, exact value of m^* slightly deviates in literature, 0.41 m_e[14]) and α_1 is a shape-dependent parameter for the first confined state. Thus, we plot E' *vs.* $1/A$ (Fig. 3b). Since the shape-dependence for the first confined state is rather small (~9% between square and circle), we employ here for a first approximation the value of a circular pore ($\alpha_1 = 5.783$).[13] This yields a calculated slope $C_{calc} = 1.82$ eV nm^2 (Fig. 3b, dashed blue line) which does not

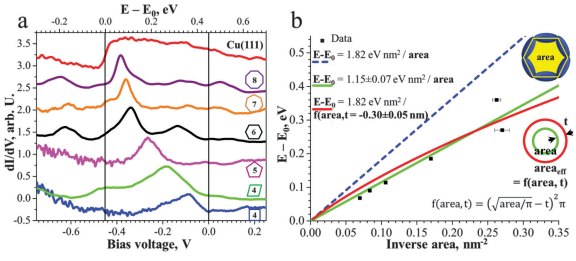

Fig. 3 The porous molecular network on Cu(111) locally confines the surface state and leads to quantum well states with their characteristics depending on the size and shape of the pore. (a) The dI/dV plot of the spectroscopy data reflects the shift of the surface state towards the Fermi level with decreasing pore size. (b) The plot of the energy *versus* the inverse area reflects a linear characteristic for the quantum well state in the confinement. The error bars reflect the average error during defining of the area from the STM image.

agree well with the experimental data or its fitted slope C_{fit} = 1.15 eV nm^2 (Fig. 3b, solid green line). Indeed, the effective area occupied by the confined surface state may deviate from the measured (from the center of the molecular backbones) area, as in case of surface states confined by monoatomic steps.[9c] Thus, we fit the data with an effective area which may be smaller or greater by a perimeter t (indicated in Fig. 3b). We find that if the slope C is kept fixed to the value of C_{calc} this yields t = −0.30 nm, *i.e.* that the effective area extends by 0.3 nm beyond the molecular backbone. This result indicates that the barrier height is small enough to allow for a considerable penetration of the surface-state even beyond the center of the molecular backbone as observed earlier for a different porous network.[10c]

The ''imperfections'' of the pore structures in the 2D polymer sponge also allowed us to study the behaviour of the surface state electrons inside a partial confinement, *i.e.* inside ''pores'' with missing borders. In fact we observed significant electron confinement inside the hexagonal pores even if barriers are missing (Fig. 4). To the best of our knowledge such results have not been reported previously. Comparison of the STS peak-positions recorded in the centre of the closed hexagonal pore as well as in the centre of the pore with 1 and 2 missing barriers reveals the same position (∼−340 mV). By opening the barriers, however, a broadening of the STS peak (Fig. 4b) is evident, which we attribute to interference between partially confined and free 2D electrons. These findings suggest that the size of the pore plays an important role in defining the electronic characteristics of the quantum well state.

We have shown that the flexible covalent linkage formed upon coupling of **DIBOTAP** and **TMA** (liberating H_2) allows for the formation of a nanoporous sponge-like 2D-network. The C–O–B bond formation, which gives rise to this surface network, was previously also found to occur in solution.[8] The network forms pores of different architecture, in particular size, shape and symmetry which provides an interesting model system for the investigation of the confinement of Shockley type surface state electrons in a wide range of porous confinements. As expected, decreasing the surface area of the polygon shifts the confined state towards the Fermi level. Interestingly, this work provides further evidence that the confinement by polymer networks is not perfect. Furthermore, we analysed the confinement effects in open hexagonal pores with a varying number of absent side-walls or barriers. Notably, as shown here for the first time, the confined state energy remains identical to the intact pore. The removal of barriers leads to a broadening of the observed electronic quantum well state. Future work aims at employing modified building blocks to restrict the flexibility of the linker and thus to gain greater control of the porous on-surface architecture.

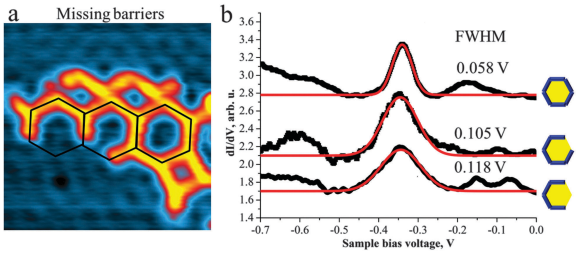

Fig. 4 The dimensions of the **TMA(1)$_3$** pore determine the energy of the surface state confined inside: (a) hexagonal **TMA(1)$_3$** pores with missing barriers (STM image: 12 × 12 nm^2) confine the surface state in considerable similarity to a full hexagon. (b) The d*I*/d*V* curves for closed pores and for open pores with 1-, 2-barriers missing reveal the same peak position (∼0.340 eV). The peak width is increasing with increasing number of absent barriers.

This work was supported by University of Heidelberg, the Doctoral College ''Molekulare Sonden'', the National Centre of Competence in Research, ''Nanoscience'' (NCCR-Nano), Swiss Nanoscience Institute (SNI), Swiss National Science Foundation (grants No. 200020-137917, 206021-113149, 206021-121461), Foundation for Fundamental Research on Matter (FOM), part of the Netherlands Organisation for Scientific Research (NWO), NWO (Chemical Sciences, VIDI-grant No. 700.10.424) and the European Research Council (ERC-2012-StG 307760-SURFPRO).

Notes and references

1 (*a*) T. Lin, X. S. Shang, J. Adisoejoso, P. N. Liu and N. Lin, *J. Am. Chem. Soc.*, 2013, **135**, 3576–3582; (*b*) M. El Garah, J. M. MacLeod and F. Rosei, *Surf. Sci.*, 2013, **613**, 6–14; (*c*) Y.-Q. Zhang, N. Kepčija, M. Kleinschrodt, K. Diller, S. Fischer, A. C. Papageorgiou, F. Allegretti, J. Björk, S. Klyatskaya, F. Klappenberger, M. Ruben and J. V. Barth, *Nat. Commun.*, 2012, **3**, 1286; (*d*) S. Schlögl, W. M. Heckl and M. Lackinger, *Surf. Sci.*, 2012, **606**, 999–1004; (*e*) L. Lafferentz, V. Eberhardt, C. Dri, C. Africh, G. Comelli, F. Esch, S. Hecht and L. Grill, *Nat. Chem.*, 2012, **4**, 215–220; (*f*) M. Bieri, M.-T. Nguyen, O. Gröning, J. Cai, M. Treier, K. Aït-Mansour, P. Ruffieux, C. A. Pignedoli, D. Passerone, M. Kastler, K. Müllen and R. Fasel, *J. Am. Chem. Soc.*, 2010, **132**, 16669–16676; (*g*) D. F. Perepichka and F. Rosei, *Science*, 2009, **323**, 216–217; (*h*) M. Matena, T. Riehm, M. Stöhr, T. A. Jung and L. H. Gade, *Angew. Chem., Int. Ed.*, 2008, **47**, 2414–2417; (*i*) A. Gourdon, *Angew. Chem., Int. Ed.*, 2008, **47**, 6950–6953.
2 L. Grill, M. Dyer, L. Lafferentz, M. Persson, M. V. Peters and S. Hecht, *Nat. Nanotechnol.*, 2007, **2**, 687–691.
3 L. Xu, X. Zhou, Y. Yu, W. Q. Tian, J. Ma and S. Lei, *ACS Nano*, 2013, **7**, 8066–8073.
4 H.-Y. Gao, H. Wagner, D. Zhong, J.-H. Franke, A. Studer and H. Fuchs, *Angew. Chem., Int. Ed.*, 2013, **52**, 4024–4028.
5 (*a*) P. Fesser, C. Iacovita, C. Wäckerlin, S. Vijayaraghavan, N. Ballav, K. Howes, J.-P. Gisselbrecht, M. Crobu, C. Boudon, M. Stöhr, T. A. Jung and F. Diederich, *Chem. – Eur. J.*, 2011, **17**, 5246–5250; (*b*) F. Bebensee, C. Bombis, S.-R. Vadapoo, J. R. Cramer, F. Besenbacher, K. V. Gothelf and T. R. Linderoth, *J. Am. Chem. Soc.*, 2013, **135**, 2136–2139; (*c*) O. Díaz Arado, H. Mönig, H. Wagner, J.-H. Franke, G. Langewisch, P. A. Held, A. Studer and H. Fuchs, *ACS Nano*, 2013, **7**, 8509–8515.
6 A. C. Marele, R. Mas-Ballesté, L. Terracciano, J. Rodríguez-Fernández, I. Berlanga, S. S. Alexandre, R. Otero, J. M. Gallego, F. Zamora and J. M. Gómez-Rodríguez, *Chem. Commun.*, 2012, **48**, 6779–6781.
7 (*a*) N. A. A. Zwaneveld, R. Pawlak, M. Abel, D. Catalin, D. Gigmes, D. Bertin and L. Porte, *J. Am. Chem. Soc.*, 2008, **130**, 6678–6679; (*b*) T. Faury, F. Dumur, S. Clair, M. Abel, L. Porte and D. Gigmes, *CrystEngComm*, 2013, **15**, 2067–2075.
8 T. Riehm, G. De Paoli, H. Wadepohl, L. De Cola and L. H. Gade, *Chem. Commun.*, 2008, 5348–5350.
9 (*a*) M. F. Crommie, C. P. Lutz and D. M. Eigler, *Science*, 1993, **262**, 218–220; (*b*) K.-F. Braun and K.-H. Rieder, *Phys. Rev. Lett.*, 2002, **88**, 096801; (*c*) J. Li, W.-D. Schneider, R. Berndt and S. Crampin, *Phys. Rev. Lett.*, 1998, **80**, 3332–3335.
10 (*a*) P. Han and P. S. Weiss, *Surf. Sci. Rep.*, 2012, **67**, 19–81; (*b*) L. Gross, F. Moresco, L. Savio, A. Gourdon, C. Joachim and K.-H. Rieder, *Phys. Rev. Lett.*, 2004, **93**, 056103; (*c*) J. Lobo-Checa, M. Matena, K. Müller, J. H. Dil, F. Meier, L. H. Gade, T. A. Jung and M. Stöhr, *Science*, 2009, **325**, 300–303; (*d*) F. Klappenberger,

D. Kühne, W. Krenner, I. Silanes, A. Arnau, F. J. García de Abajo, S. Klyatskaya, M. Ruben and J. V. Barth, *Nano Lett.*, 2009, **9**, 3509–3514; (*e*) F. Klappenberger, D. Kühne, W. Krenner, I. Silanes, A. Arnau, F. J. García de Abajo, S. Klyatskaya, M. Ruben and J. V. Barth, *Phys. Rev. Lett.*, 2011, **106**, 026802; (*f*) R. Stiufiuc, L. M. A. Perdigão, B. Grandidier, D. Deresmes, G. Allan, C. Delerue, D. Stiévenard, P. H. Beton, S. C. Erwin, M. Sassi, V. Oison and J.-M. Debierre, *Phys. Rev. B*, 2010, **81**, 045421; (*g*) S. Wang, W. Wang, L. Z. Tan, X. G. Li, Z. Shi, G. Kuang, P. N. Liu, S. G. Louie and N. Lin, *Phys. Rev. B*, 2013, **88**, 245430.

11 (*a*) S. Stepanow, T. Strunskus, M. Lingenfelder, A. Dmitriev, H. Spillmann, N. Lin, J. V. Barth, C. Wöll and K. Kern, *J. Phys. Chem. B*, 2004, **108**, 19392–19397; (*b*) J. V. Barth, J. Weckesser, N. Lin, A. Dmitriev and K. Kern, *Appl. Phys. A: Mater. Sci. Process.*, 2003, **76**, 645–652.
12 M. F. Crommie, C. P. Lutz and D. M. Eigler, *Nature*, 1993, **363**, 524–527.
13 E. Lijnen, L. Chibotaru and A. Ceulemans, *Phys. Rev. E*, 2008, **77**, 016702.
14 F. Reinert, G. Nicolay, S. Schmidt, D. Ehm and S. Hüfner, *Phys. Rev. B*, 2001, **63**, 115415.

Supporting information:

Covalent assembly of a two-dimensional molecular "sponge" on a Cu(111) surface: Confined electronic surface states in open and closed pores

Aneliia Shchyrba,[a] Susanne C. Martens,[a,b] Christian Wäckerlin,[c,&] Manfred Matena,[a] Toni Ivas,[a] Hubert Wadepohl,[b] Meike Stöhr, [d] Thomas A. Jung,[c,*] and Lutz H. Gade[b,*]

[a] *Department of Physics, University of Basel, Klingelbergstrasse 82, 4056 Basel, Switzerland.*
[b] *Anorganisch-Chemisches Institut, Universität Heidelberg, Im Neuenheimer Feld 270, 69120 Heidelberg, Germany.*
[c] *Laboratory for Micro- and Nanotechnology, Paul Scherrer Institute, 5232 Villigen PSI, Switzerland.*
[d] *Zernike Institute for Advanced Materials, University of Groningen, Nijenborgh 4, 9747 AG Groningen, The Netherlands.*

Present address: [&] Institute of Condensed Matter Physics, Ecole Polytechnique Fédérale de Lausanne, 1015 Lausanne, Switzerland

Content:

1. Molecular structure of *N*,*N*';*N*'',*N*'''-diborylene-3,4,9,10-tetraaminoperylene (1).

The molecular structure of (1) by X-ray diffraction was characterized by X-ray diffraction (Figure S1). As has been described in the main text, the dimensions of the molecule are as follows: **H**B – B**H** 13.7 Å; B-B 11.4 Å and in width: H3-H9 6.6 Å; H2A-H8 6.6 Å.

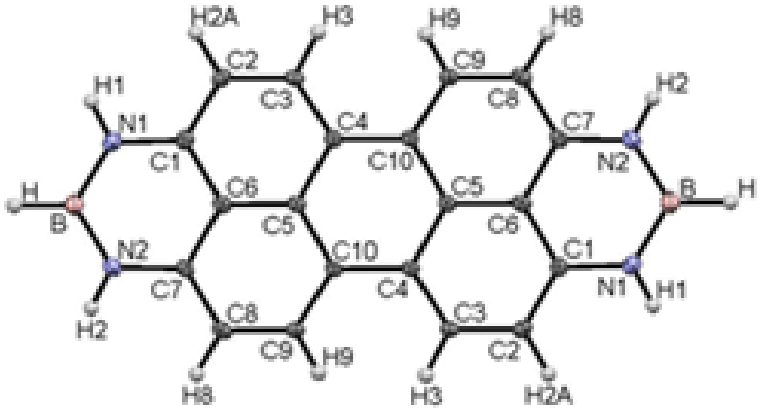

Fig. S1 Molecular structure of *N*,*N*';*N*'',*N*'''-diborylene-3,4,9,10-tetraaminoperylene (**1**).

Crystal data: $C_{20}H_{14}B_2N_4 \cdot 2(C_4H_8O)$, monoclinic, space group $P2_1/c$, a = 11.8021(4), b = 11.1964(3), c = 10.1080(3) Å, β = 115.025(4) °, V = 1210.30(8) Å^3, Z = 2, μ = 0.082 mm^{-1}, F_{000} = 504. T = 110(1) K, θ range 3.6 to 28.9 °. Index ranges h, k, l: -15 ... 15, -15 ... 15, -13 ... 13. Reflections measd.: 23170, indep.: 3021 [R_{int} = 0.027], obsvd. [$I > 2\sigma(I)$]: 2453. Final R indices [$F_o > 4\sigma(F_o)$]: $R(F)$ = 0.0513, $wR(F^2)$ = 0.1426, $GooF$ = 1.09.

Data collection: Agilent Technologies Supernova-E CCD diffractometer, Mo-K_α radiation, microfocus X-Ray tube, multilayer mirror optics, λ = 0.7107 Å. Lorentz, polarization and semi-empirical absorption correction.[1] Structure solution: charge flip.[2] Refinement: full-matrix least squares methods based on F^2;[3] all non-hydrogen atoms anisotropic, hydrogen atoms taken from difference fourier maps and refined.

CCDC 988044 contains the supplementary crystallographic data for this paper. These data can be obtained free of charge from The Cambridge Crystallographic Data Centre via www.ccdc.cam.ac.uk/data_request/cif.

2. Details of the experimental methods

Preparation procedures for all samples were carried in ultra-high vacuum with a base pressure $5*10^{-10}$ mbar. The Cu(111) substrate was prepared by repeated cycles of sputtering with Ar+ ions (at energy ~ 2000 eV, ion current ~ 10 μA) and annealing to ca. 450°C in order to achieve atomically flat and clean surfaces with extended terraces. The purity of the substrate was verified by X-Ray Photoelectron Spectroscopy (XPS) and Scanning Tunneling Microscopy (STM). The molecules were deposited by thermal evaporation from a commercial evaporator (Kentax). The deposition rates were tracked by a quartz-crystal microbalance.

The STM measurements were performed at helium temperatures (~5 K) on the Omicron LT-STM. The bias voltage is with respect to the sample, i.e. negative voltage corresponds to the occupied states of the sample. The STM micrographs were recorded in the constant current mode.

The Scanning Tunneling Spectroscopy (STS) measurements were acquired with a lock-in amplifier frequency of 512 Hz and modulation amplitude of 8 mV (zero-to-peak value). The initial tip settings were: 35 pA; 77.5 mV. The condition of the tip was verified before and after acquisition of the STS spectrum by recording dI/dV spectra on the bare Cu(111) surface.

XPS measurements were performed at room temperature (RT) with a monochromatic Al-K_α X-Ray source. The resolution reaches a value ~ 1 eV of full width at half maximum (FWHM). The calibration of the energies was performed via reference measurements on a clean Au crystal (Au $4f_{7/2}$ ≡ 84.0 eV).

3. Identification of the reaction product between (1) and TMA on Cu(111)

Deposition of borylene functionalized molecule **1** and trimesic acid (TMA) onto room temperature Cu(111) substrate and annealing to 120°C results in the formation of aperiodic molecular network, observed by means of STM (Fig. S2c). In order to investigate the nature of the resulting polymer, we probed the chemical environment of C, B, N (present in **1**) and C, O (present in TMA) before and after annealing by measuring XPS of C1s, B1s and O1s core levels. The B1s and O1s spectra are presented in the main text, C1s and N1s spectra are shown in Figure S2.

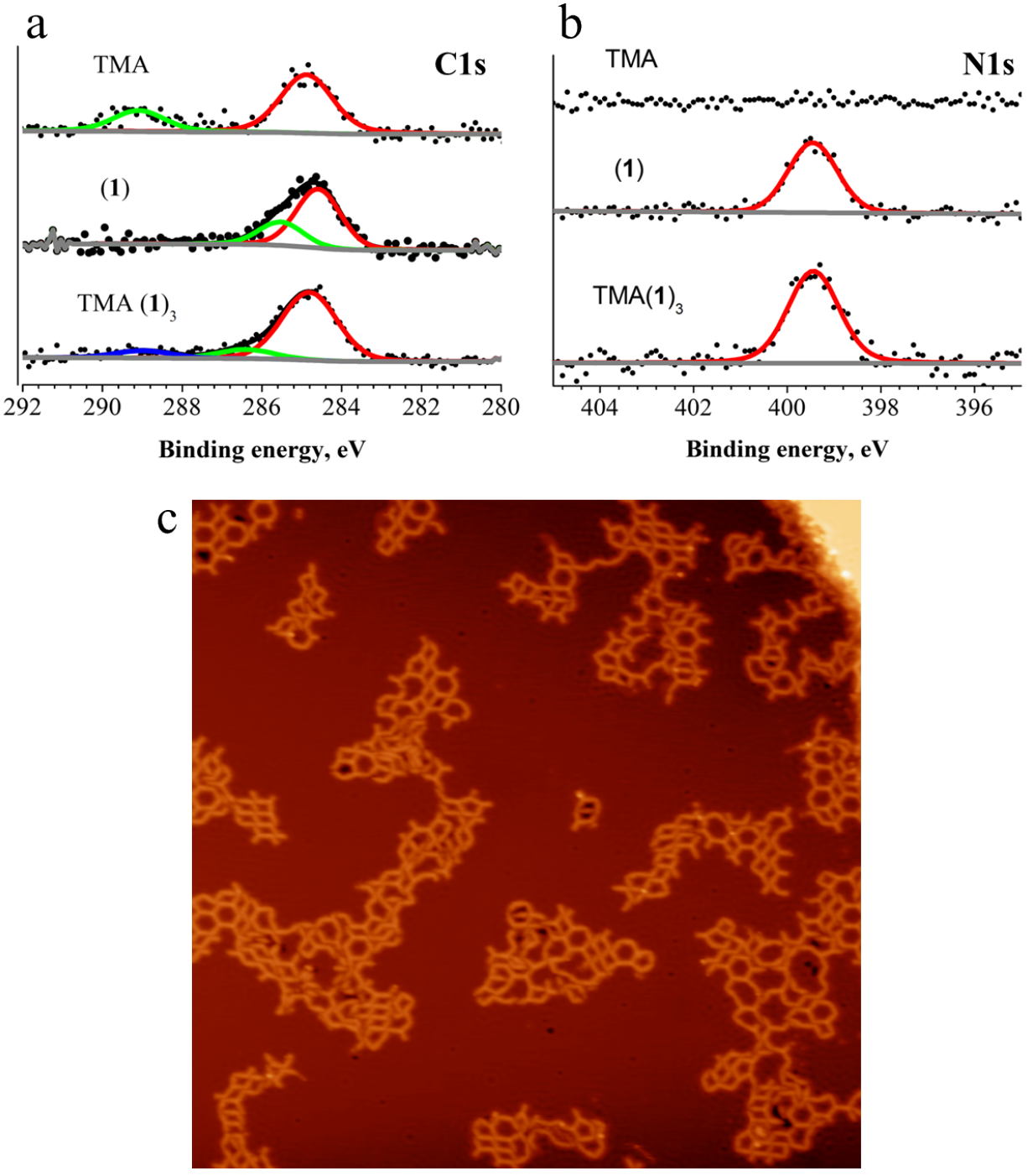

Fig. S2 The XPS data of each reactant (TMA and **1**) deposited onto Cu(111) at RT and the resulting reaction product (TMA(**1**)$_3$) are presented under each other for comparison: (a) C1s spectra and (b) N1s spectra. (c) The STM overview (at 5K, 100x100 nm^2) of the aperiodic molecular network formed at Cu(111) after annealing to 120°C.

First, we sublimed sub-monolayer of TMA on Cu(111). The resulting amount of C is 4.3 % and O1s - 3.4 % with respect to the Cu surface. The experimental ratio C:O can be estimated to 9:7.1, which reflects well the stoichiometry of TMA (C_9O_6). B1s, N1s were not detected. The two peaks in C1s correspond to C*-C and C*=O.

The next step was an investigation of sub-monolayer of (**1**) on Cu(111). The XP spectra of C1s, N1s and B1s reveal 3.34 % of carbon, 0.61% of nitrogen and 0.19% of boron with respective ratio C:N:B equals 20:3.65:1.19, reflecting well the stoichiometry of the molecule ($C_{20}N_4B_2$). Oxygen was not observeable in O1s spectra. XPS reveals one peak in the N1s spectra, corresponding to the BH-group, and two peaks in C1s, corresponding to C*-C and C*-N.

Finally, to the previous sample of 1 on Cu(111) a sub-monolayer amount of TMA was added and the sample was annealed (to ca 120°C). The resulting sample contained: 5.48% C1s; 0.83% O1s; 0.57% N1s and 0.21% B1s. The B1s binding energy (BE) of the resulting product (presented in the main text) differs significantly 191.6 eV in comparison to B1s of unreacted 1 (190.25 eV) on Cu(111). The N1s BE is not modified upon reaction.

The summary of N1s, O1s, B1s binding energies for all 3 samples (TMA, **1**, TMA(**1**)$_3$) are presented in a Table S1.

Molecule	**N1s BE, eV**	**O1s BE, eV**	**B1s BE, eV**
TMA	-	531.6: 533.5	-
1	399.4	-	190.25
TMA(**1**)$_3$	399.4	532.0; 533.3	191.6

Table S1. Binding energies of the N1s, O1s and B1s for TMA, **1** and TMA(**1**)$_3$ on Cu(111) support a covalent reaction between TMA and **1** after annealing to 120°C with the formation of TMA(**1**)$_3$, as a resulting product.

4. STM overviews of unreacted (1) on Cu(111)

We have investigated the behaviour of borylene-functionalized molecule **1** on Cu(111) surface upon deposition at RT. The STM micrographs reveal no long-range order and randomly distributed molecular conglomerates (Fig. S3a). Among the conglomerates, can be distinguished two types of trimers, which are pro-chiral (Fig. S3 b,c). Possible model for these types of nodes are reflected on the schemes (Fig. S3 d-e).

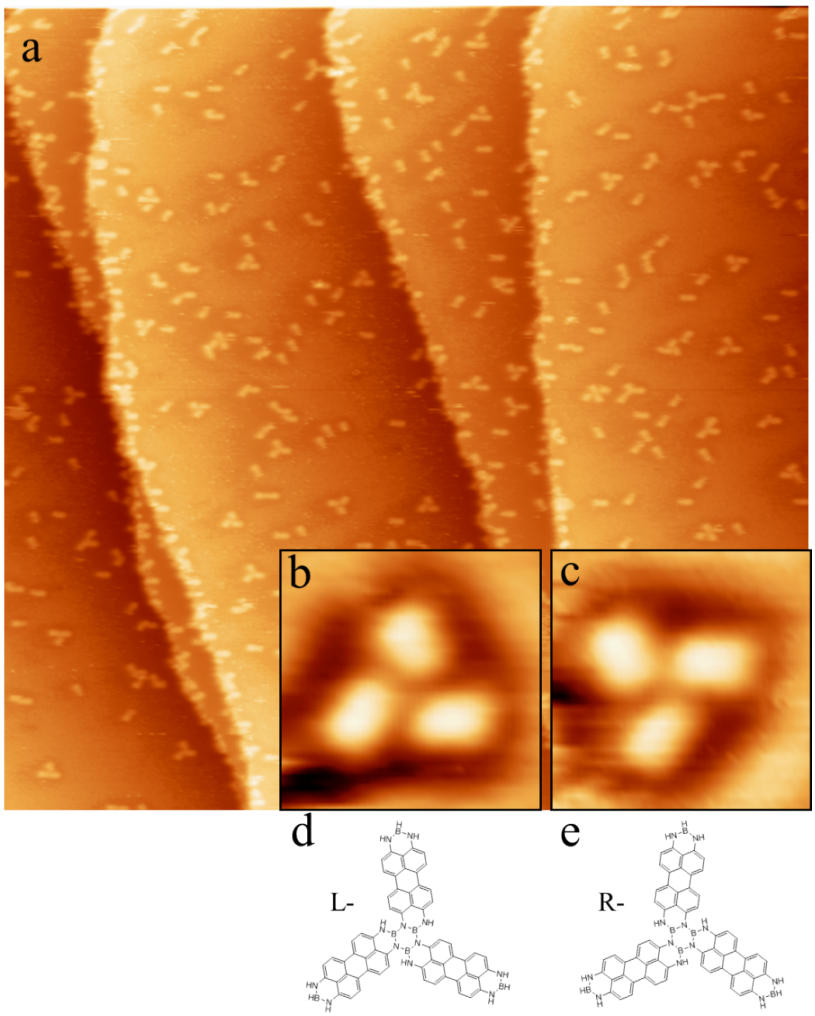

Fig. S3 Deposition of **1** onto Cu(111) at RT results in the formation of H-bonded molecular islands, as reflected on the (a) STM image (-1.5 V, 50 pA; 100x100 nm^2 at 5K). The assemblies are randomly distributed over the surface showing the local repulsion character. The frequently met pattern is characterized by the trimetric shape: (b), (c) pro-chiral L- and R- structures (-1.5V, 60 pA; 4x4nm^2 at 5K). (d),(e) The corresponding chemical schemes reflect possible types of intermolecular connection for L- and R- nodes, respectively.

5. Various shapes of the pores

Deposition of **1** and TMA results in the covalent molecular 'sponge'-like network after annealing to 120°C (see chapter 3 and main text of the manuscript). The flexibility of the covalent connection between **1** and TMA allows for the formation of differently shaped pores (Fig. 1 of the main text). Typically 4-8 polygons can be identified from the STM images (Fig. S4).

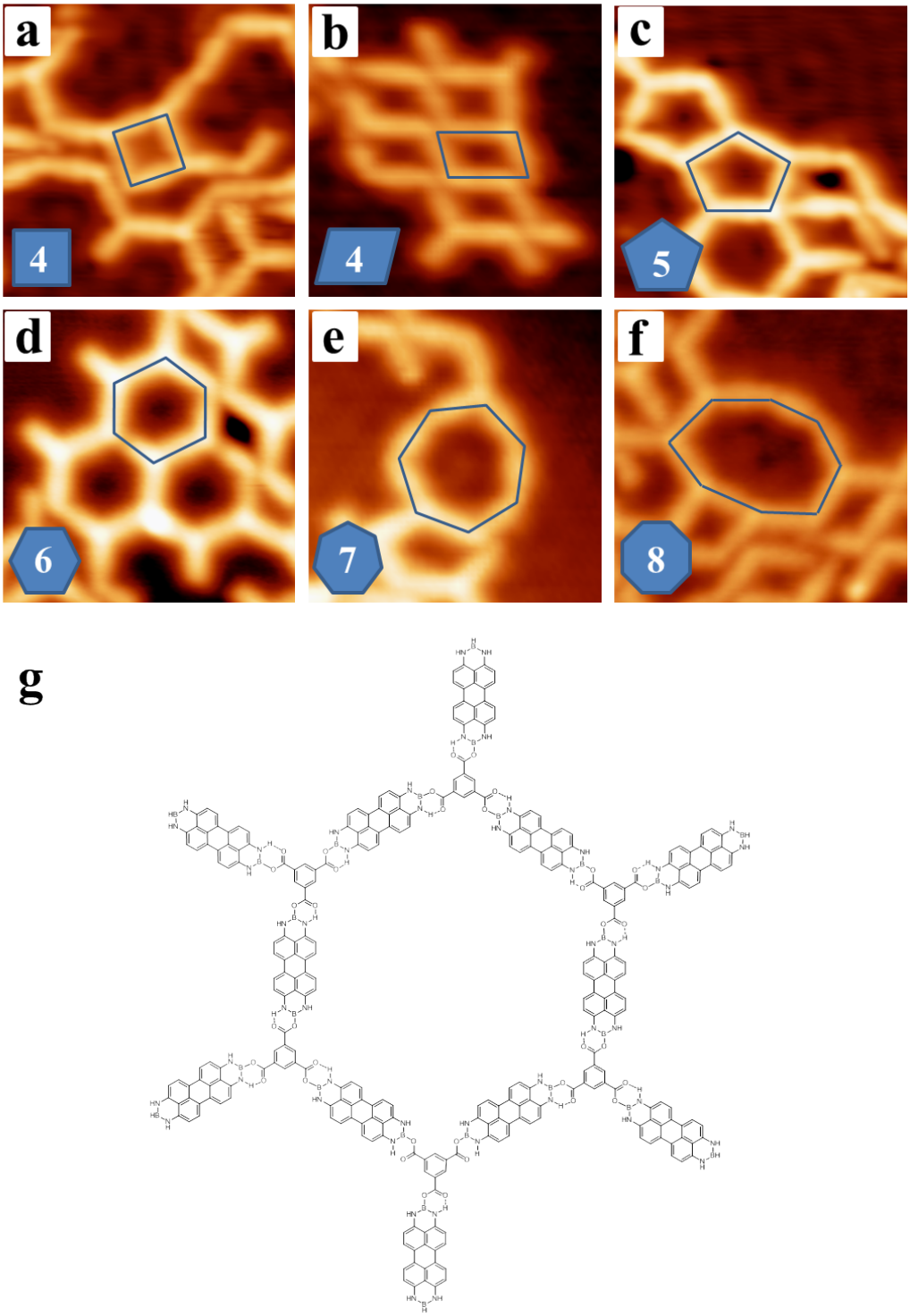

Fig. S4 Deposition of **1** and TMA on Cu(111) at RT and subsequent annealing to 120°C results in the formation of covalent networks. (a - f) The STM micrographs (10 x 10 nm^2) reflect typical pores of various shape, containing 4 - 8 borylene-functionalized molecules. (g) Chemical scheme serves as one of the possible models for the hexagonally shaped pore.

6. Network formation on Ag(111)

We have shown in chapter 4 the occurrence of the on-surface reaction between **1** and TMA after annealing on Cu(111) with resulting covalent networks. In order to verify the influence of the substrate, the same preparation procedure has been performed on the less reactive Ag(111) substrate. Deposition of 1 and TMA on Ag(111) and annealing to 120°C results in similar polymer architectures as on Cu(111) (Fig. S5). The pores have different size and shape (Fig. S5 b,c). Excess of one of the pre-cursors can lead to the trapping of molecule inside of the formed pores. This fact indicate that pores can serve as a host system for molecular adsorbates (Fig. S5d).

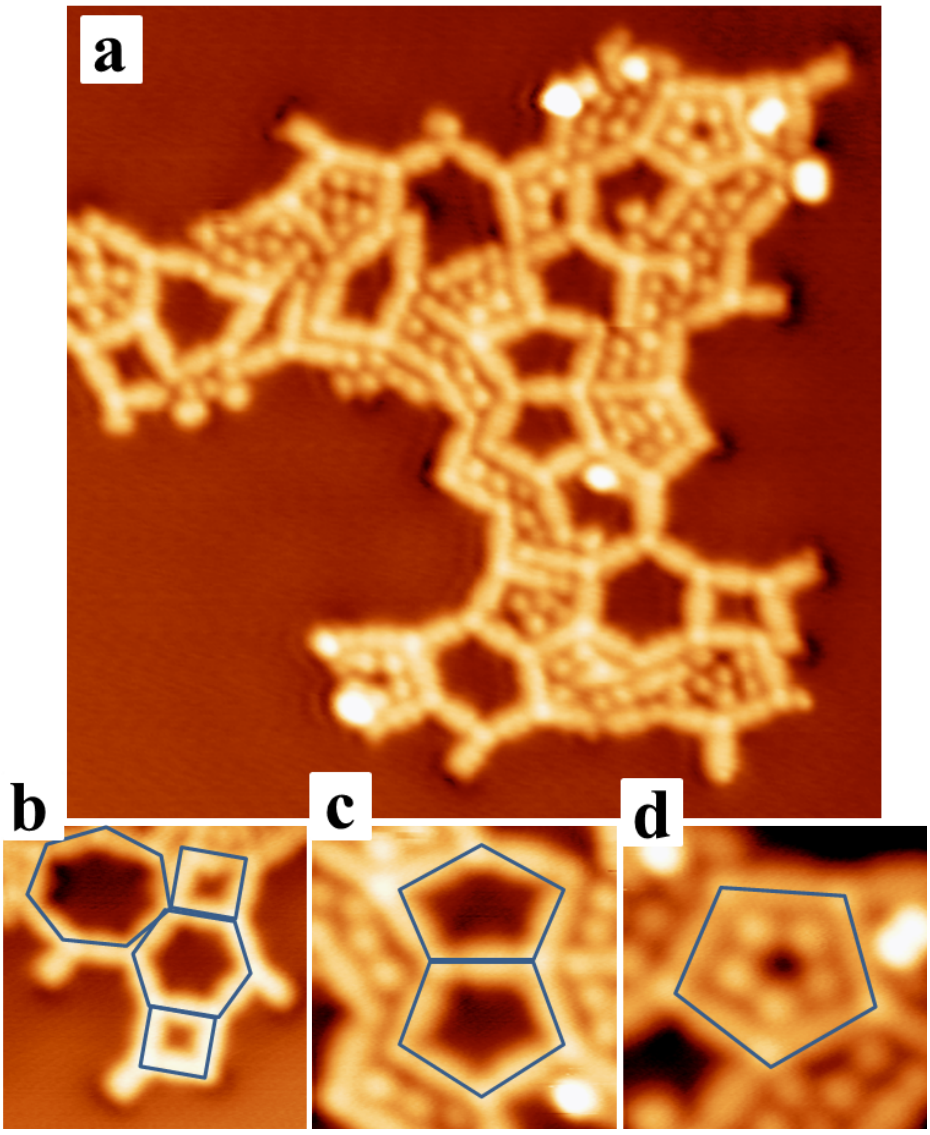

Fig. S5 (a) Deposition of **1** and TMA on Ag(111) at RT and subsequent annealing to 120°C results in the formation of networks similar to the ones observed on Cu(111). The STM micrograph reveal pores containing trapped in inside precursors, which were in excess (25 x 25 nm^2). (b, c) Pores have different size and shape (10 x 10 nm^2 and 6 x 6 nm^2, respectively). (d) Each pore can serve as a host for the smaller adsorbates: STM image of the pentagonal pore and 5 TMA molecules inside (5 x 5 nm).

7. Pore area value and the energy of the confined surface state in the TMA(1)$_3$ polygons

n	Area, nm^2	Energy with respect to E_F, meV
4 - square	3.65	90
4 - parallelogram	3.72	180
5	6.01	265
6	9.26	336
7	11.9	360
8	14.46	382

Table S2. The values of the area, extracted from the STM images, and energy of the confined state measured in the center of the pore.

References:

1. R. H. Blessing, *Acta Cryst.* 1995, **A51**, 33; *SCALE3 ABSPACK, CrysAlisPro*, Agilent Technologies UK Ltd., Oxford 2011.
2. (a) L. Palatinus, *SUPERFLIP*, EPF Lausanne, Switzerland, 2007; (b) L. Palatinus, G. Chapuis, *J. Appl. Cryst.* 2007, **40**, 786.
3. (a) G. M. Sheldrick, *SHELXL-2014*, University of Göttingen and Bruker AXS, Karlsruhe 2014; (b) G. M. Sheldrick, *Acta Cryst.* 2008, **A64**, 112.

Molecule-specific energy level alignment inducing opposite charge transfer dipoles and formation of a self-sorted bimolecular chessboard on Bi reconstructed Cu(100)

Summary:

A new mechanism for the electronic intermolecular recognition by surface dipoles created by selective charge transfer is demonstrated, which leads to the sorting of molecules in an alternating chessboard like fashion. The Bismuth 2D interface (Bi/Cu(100)) here serves as a substrate mediating the sorting of this bi-molecular system (CuPc and MnPc) by its specific electronic properties. We investigate single component molecular layers as well as the resulting co-assembled array on the bismuth reconstructed substrate by means of scanning tunnelling microscopy (STM) and spectroscopy (STS). We find that by adsorption of pure CuPc/MnPc molecules on Bi the relative local work function is increased/decreased respectively. The modification of the work-function evidences the charge transfer (CT) occurring on the molecule/surface interface. Due to their different electronic properties, the molecule/substrate CT systems exhibit different dipole moments: MnPc becomes more positively charged and CuPc more negatively, therefore the surface dipole moments point downward for CuPc and upward for MnPc molecules, respectively. Another important factor is provided by the Bismuth substrate which exhibits a significantly higher Debye length in comparison to bare metal substrates. Therefore, the charge/dipole moment is less screened in comparison to other metallic substrate. By the formation of the assembly our STM/STS data supports that the molecular properties are strongly modified in comparison to the single component system. For example, the local work functions undergo a significant change and a realignment of the corresponding LUMO/HOMO levels for both CuPc and MnPc after the molecules have become sorted. MnPc/CuPc dipoles are strengthened by this effect. The strengthening of the charge transfer evidences that nearest neighbour interactions between the electron-rich CuPc by the electron-deficient MnPc come into play, which is most probably but not necessarily mediated by the substrate. Our work presents an unique example of supramolecular sorting by a purely electrostatic mechanism.

Manuscript [[4]] is in preparation.

Contribution of Aneliia Shchyrba: carried out the experimental investigation (STM, STS), analysed the data, wrote the manuscript.

Molecule-specific energy level alignment inducing opposite charge transfer dipoles and formation of a self-sorted bimolecular chess-board on Bi reconstructed Cu(100)

A. Shchyrba, S. Fatayer, C. Wäckerlin, T. Nijs, S. Nowakowska, T. A. Jung

Understanding the physics and chemistry of interactions between ad-molecules at surfaces is crucial from a fundamental point of view. Such interactions also depend on the distribution of energy levels in organic molecules before and after their adsorption on a specific substrate. The proximity of the surface to the ad-molecule induces energy level realignment and promotes or inhibits charge transfer.[1,2] The relative position of the energy levels of the molecule and the substrate affects the degree and the direction of the energy alignment and thereby also the charge transfer. Depending on the charge transfer and the resulting local surface dipoles an adsorbate interaction arises. If two different ad-molecules are in a qualitatively different state of charge transfer with the substrate, their proximity may induce a charge redistribution by polarization as well as by the degree of energy level realignment.[3] Few studies on molecular self-assembly have been undertaken considering charged molecules and/or surface dipoles as the cause of the ordering phenomenon.[4] Substrates exhibiting a pattern of surface dipoles were shown to selectively trap molecules.[5,6] In particular no report is available of a multi-component self-sorted and self-assembled molecular array created by the interaction of different charge transfer dipoles in ad-molecules.

Here we present a molecule-specific energy alignment within a bi-component molecular system with the substrate, which drives a self-sorting of the components by purely electronic interactions. We use a Bi reconstructed Cu(100) substrate (Bi/Cu(100), which serves as a partner for the molecule-specific vertical charge transfer for the two molecular components: the more electron affine CuPc and the less electron affine MnPc[7]. Reported examples for the sorting of on-surface multi-component ordered arrays are based on a distinctively different mechanism, i.e. on the basis of hydrogen bonds[8–11]. Another mechanism, which has been demonstrated, involves the trapping of an ad-molecule inside of pre-prepared molecular templates[10].

We explore the ordering of ad-molecules on a Bi-reconstructed Cu(100) substrate by Scanning Tunneling Microscopy and Spectroscopy (STM/STS), i.e. dI/dV spectroscopy as well as current-distance I(z) spectroscopy. The results reveal a significant change in the local density of states (LDOS) and the local work function (Wf) of the two different ad-molecules. We find that the difference in the energy level alignment of the CuPc and MnPc with the Bi substrate leads to a different vertical charge transfer rendering opposite dipole moments. Upon mixing of the two molecules, the charge transfer is significantly enhanced, a phenomenon which is attributed to lateral electronic interactions.

The Bi-reconstructed substrate was prepared by deposition of a sub-monolayer amount of Bi onto Cu(100) and by subsequent annealing to ~200°C. This procedure has been well established in earlier studies.[12–14] At a Bi coverage close to a monolayer, the Bi layer contains regular dislocation arrays along the <100> directions of the substrate and superimposes a rectangular but not strictly periodic porous superlattice (Figure 1a, pore dimension: ~1.6 x 1.8 nm²). The dislocation arrays appear in the STM image data with a different contrast and can be classified by three regions: pore, wall and cross (A, B and C on Figure 1a). For each region we have probed the LDOS by recording the differential conductivity (dI/dV) and the relative work-function (extracted from I(z)). Each region exhibits only a slight intensity difference in the differential conductivity (Figure 1b), which is also reflected in a slight difference in the work-function values. The relative work function on the wall and on the cross is slightly higher than in the pore (by 70±20, 80±20 meV resp.). Note that the absolute Wf value averaged over the Bi reconstruction amounts to 4.33 eV, as measured by HR-ARUPS.[14] The deposition of both the more electron affine CuPc and the less electron affine MnPc on Bi-reconstructed substrate leads to formation of a highly ordered bimolecular array, which is sorted in a 1:1 chessboard-like fashion (Figure 1c). The sorting is expected to be initiated only by intermolecular electronic interactions, as no dependence of the supramolecular pattern on the variably sized Bi pores has been observed.

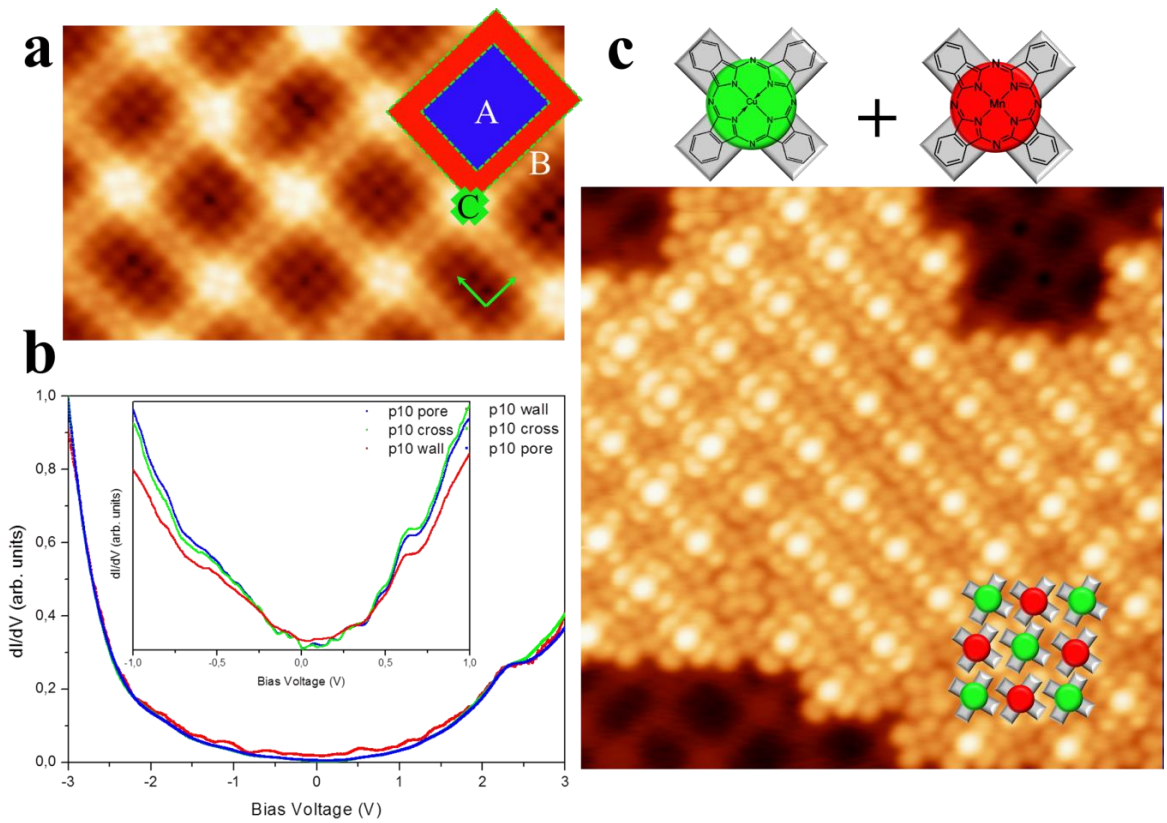

Figure 1 Bismuth reconstructed Cu(100) substrate mediates the sorting of a bi-molecular mixture of CuPc and MnPc into a chess-board array. (a) Bi reconstructed Cu(100) is atomically resolved by STM (8x5 nm², 5 mV, 400 pA). The reconstruction appears as square porous network and can be characterized into three regions: A –Pore (blue), B – Wall (red), C – Cross (green). (b) The local density of states of each reconstruction region exhibits virtually no variation. The dI/dV spectra, recorded over each region (pore - blue, wall - red, cross – green curves, correspondingly), reveal a very slight variation in the intensity of the Bi induced features. (c) Irrespective of the deposition sequence, in the same sorted 1:1 molecular chess-board is formed, as shown in the STM image (16x16 nm^2, 5mV, 5pA). The more electron affine CuPc is marked by green color and the less electron affine MnPc by red color.

In order to get further insight into the sorting mechanism, we have investigated the adsorption of only CuPc, only MnPc and of mixed CuPc+MnPc arrays on Bi/Cu(100). Each of the molecules can be easily distinguished by their appearance in the STM images: CuPc with the dark center, MnPc with the bright center. Deposition of CuPc in a sub-monolayer coverage onto bismuth reconstructed Cu(100) leads to the formation of well-formed supramolecular islands (Figure 2a), which is not observed on bare Cu(100). Notably, molecules appear in two types of orientation (marked with normal and out-lined green crosses), which results in different STM contrast. The fact that supramolecular islands are formed on bismuth indicates that the diffusion is facilitated which is the consequence of the lower interaction with the Bi (compared to Cu) surface. As the next step, we investigated pure MnPc islands. Surprisingly, we found a different assembly behavior. The MnPc islands are smaller in comparison to CuPc islands, typically only 3x3 molecules in size. The bigger islands are constructed from smaller 3x3 grains and exhibit numerous phase shift domain boundaries and defects between the small 3x3 2D grains. Each segregate contains molecules of the same orientation. Overall at least 2 of the most often appearing orientations are observed (marked with normal and out-lined red crosses, Figure 2b). Correspondingly, differently oriented MnPc 3x3 grains exhibit a different brightness: the MnPc which is co-aligned with the Bi reconstruction (white arrows) appears brighter than the MnPc which is rotated ~45°. Adding CuPc molecules to a sub-monolayer coverage of MnPc at Bi/Cu(100) results into highly ordered bi-molecular arrays (Figure 2c). Moreover, the bi-molecular mixture is perfectly sorted into alternating MnPc-CuPc patterns with 1:1 ratio. Molecules appear with an enhanced contrast: MnPc – bright, CuPc –dark. Excess of one

molecular component results in the substitution of the minority-component by the majority-component, while still maintaining the formation of the chess-board array. Surprisingly, the sorted bimolecular array exhibits only 1 molecular orientation for each component (CuPc – green outlined, MnPc – red outlined). It is this selection which is responsible for the enhanced contrast between 'dark' CuPc and 'bright' MnPc.

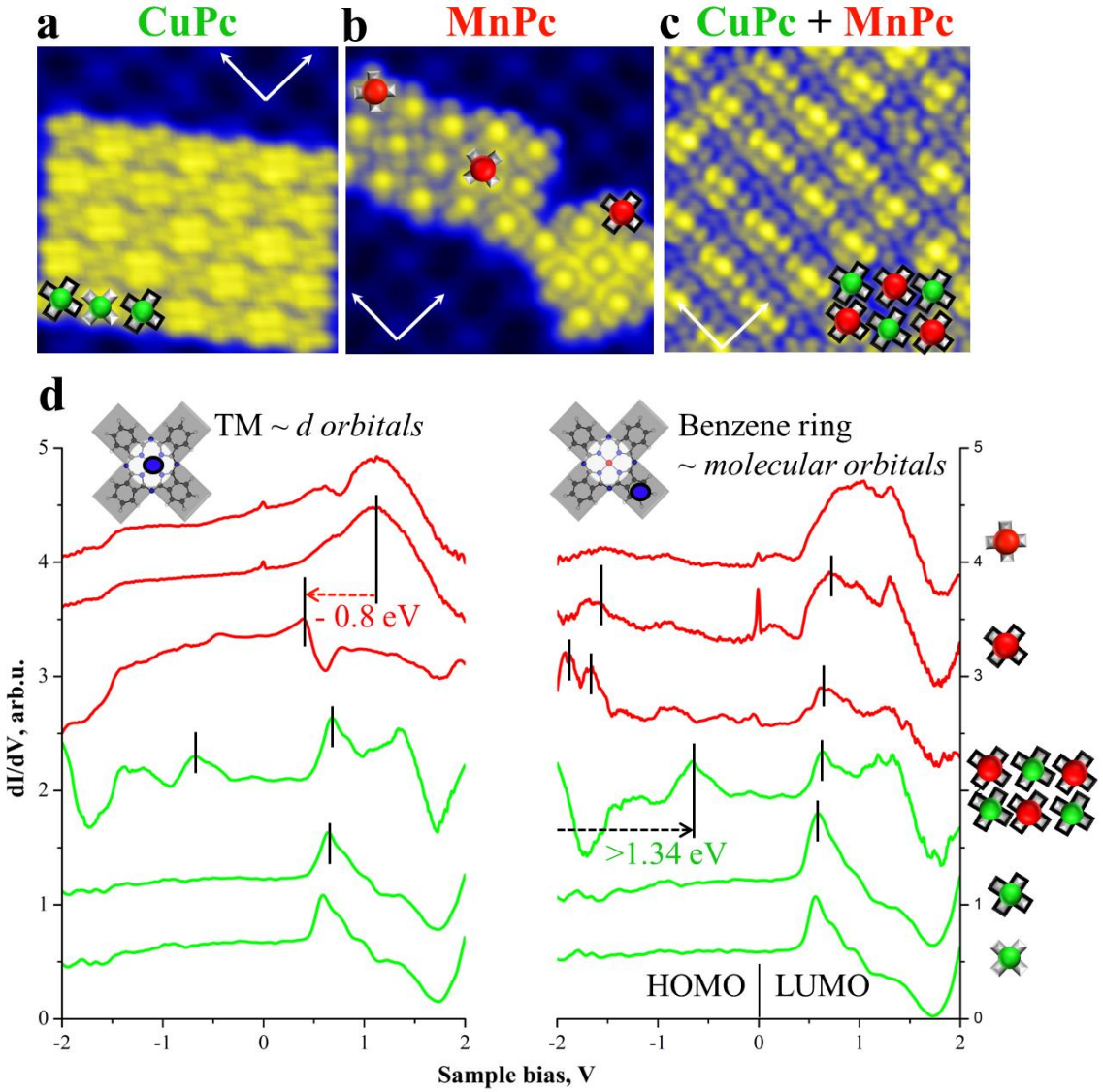

Figure 2 Modification of the electronic structure of the CuPc and the MnPc before and after mixing on the Bi reconstructed Cu(100). (a) STM images (10x10 nm^2) of CuPc, MnPc and the self-sorted bi-molecular array. The CuPc island exhibits a pronounced Moiré pattern appearing from two types of molecular orientations (one orientation marked by a green cross and the other by an out-lined green cross). (b) The assembly of only MnPc exhibits a different character: islands are small and contain more defects. Two types of molecular orientations with respect to the substrate result in two types of islands with different STM-contrast: molecules, which are co-aligned with the Bi reconstruction, appear brighter. (c) Deposition of both MnPc and CuPc results in the formation of a chess-board bimolecular array where molecules are sorted 1:1 independently on the ratio of components. In order to reveal a sorting mechanism, the electronic structure of each component was probed by STS on the transition metal core and on the benzene ring of phtalocyanine (red curves – for MnPc, green curves – for CuPc). The electronic structure of both components is significantly modified by interaction with its neighbours in the co-assembled array.

In order to investigate the local electronic structure of each molecule in pure and mixed islands, we probed the LDOS on the transition metal (TM) center and the phtalocyanine (Pc) benzene

ring by recording dI/dV spectra (Figure 2d). dI/dV provides an insight into the charge transfer and into the doping mechanisms for the transition metal containing Pc at surfaces.[3,6,15–17] The LDOS of the *d*-orbitals can be obtained by spectroscopy on the TM ion. Information about molecular orbitals can be extracted from spectroscopy on the Pc ring, as was shown by Mugarza et al.[18] On the Figure 2d we present STS, which were recorded on the TM and on the Pc ring for each case: pure CuPc, pure MnPc and the mixed chess-board islands (MnPc – red, CuPc – green curves, correspondingly). All STS were acquired with a lock-in amplifier (8 mV; 513 Hz) at the constant height (initially set point: 300pA at 2V). In order to magnify the molecular features and to simplify the comparison, all spectra were normalized after subtraction of the bismuth background. The spectroscopic features of each molecular component are virtually the same for the two different on-surface orientations (marked by out-lined or not out-lined crosses in each case). Mixing CuPc and MnPc components results in the significant modification of the in-plane and out-of-plane molecular orbitals, which is reflected by a completely different shape of the DOS features visible in the differential conductivity spectra (STS) which we attribute to the modified charge state[16] of the molecule. The peak positions of LUMO/HOMO for CuPc can be attributed to a neutral CuPc before mixing and to a more negative charge state after mixing.[19] The change in the HOMO-LUMO gap reflects a modified Coulomb repulsion between molecular orbitals and impacts the nearby located MnPc. Thus our data evidences a long-range electrostatic interaction.[15] The MnPc on the Bi surface before mixing is expected to be in close to a Mn(2+) state.[20] After mixing the modified electronic structure state can not be assigned in a straight forward way. Thereby we additionally employ relative work-function measurements (*vide infra*). The sharp feature observed in STS near the Fermi level is attributed to a Kondo resonance[21] and will be discussed elsewhere.

We probe a local charge modification on each molecule by measuring current-distance I(z) spectra before and after mixing of phtalocyanines. Each I(z) spectra of the exponentially decaying tunneling current varies with the different work function or the tunneling barrier height.[22] The Wf can be extracted from the fit of the I(z) curves. Since I(z) spectroscopy is reliable only as a relative measure, we discuss the relative work-function ΔWf, i.e. we set ΔWf = 0 meV on Bi. Thus, recording a 2D array of I(z) spectra across the surface/molecule gives an estimate of the relative local Wf. The resulting Wf map corresponds to the two-dimensional potential landscape at the surface.[23] We find that adsorption on Bi leads to a decreased Wf for both orientations of MnPc (ΔWf = -430/-140 meV) evidencing a negative vertical charge transfer from the molecule into the substrate. Thereby the molecule becomes *more positively charged* (Table 1). Contrary, adsorption of CuPc on Bi leads to an increased Wf in both orientations (ΔWf = 350/540 meV) suggesting removal of negative charge from the substrate and rendering the molecule *more negatively charged*. The adsorption geometry (orientation with respect to the substrate) also influences the resulting Wf value for both molecules (Table 2). Note that the resulting dipole moment, which is formed on the molecule-surface interface, is expected to be higher on Bi reconstructed Cu(100) in comparison to the bare Cu surface due to the lower screening described by a higher Debye length (in bulk: Bi ~ 3 Å, while for Cu ~ 0.5 Å).[24]

The sorted bimolecular chess-board array, which is formed upon deposition of both CuPc and MnPc, has a significantly modified work function on each molecule (see scheme in Figure 3a). Within the mixed islands, where MnPc becomes surrounded by CuPc, MnPc exhibits a significantly reduced Wf (ΔWf = -1600 meV) and becomes significantly more positively charged. The work-function of CuPc in the bi-molecular islands is ΔWf = 80 meV after it has been surrounded by MnPc. Remarkably, this value is significantly lower than for the pure CuPc layers on Bi/Cu(100).

The dependence of an adsorbate's charge state on the modified environment in the bimolecular array reflects a lateral electronic interaction and *charge transfer* which asks for further analysis to separate the role of the surface – molecular and the intermolecular interaction.

Table 1: Vertical charge transfer. Comparison of Wf values for the substrate before and after molecular adsorption. The values of Wf in bulk CuPc/MnPc are shown for the reference as well.

Sample	Wf, eV	Sample	Wf, eV
Bi/Cu(100)	4.33[14]	Bi/Cu(100)	4.33[14]
CuPc layer@Bi, average	4.77	MnPc layer@Bi, average	4.09
CuPc bulk (UPS)	3.85[25]	MnPc bulk (UPS)	4.3[25]

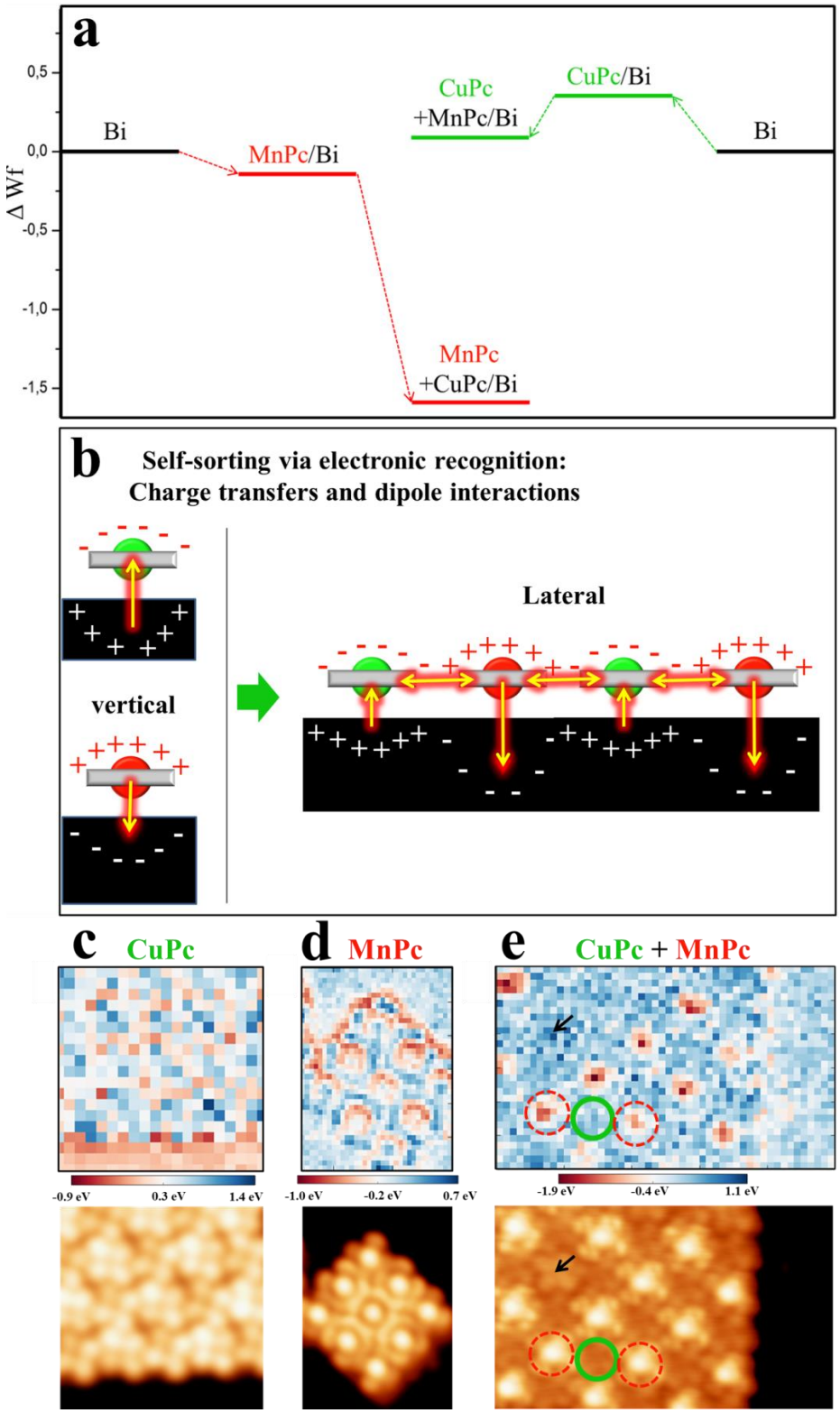

Figure 3 Modification of the local relative work-function on CuPc and MnPc after forming a bi-molecular chess-board array evidences intermolecular interactions and suggest an electronic interaction between nearest neighbours acting as a sorting mechanism. (a) Comparison of the relative work-function before and after sorting. (b) Possible model of the surface-molecule and molecule-molecule interactions. Work-function maps for pure (c) CuPc (13x13 nm²) and (d) MnPc (5x6 nm²) islands, as well as for (c) sorted bi-molecular arrays (10x6 nm²). The bi-molecular chessboard exhibits a periodically modulated pattern of alternating low/high Wf values reflecting a charge transfer as a sorting mechanism.

Table 2: Lateral charge transfer. Comparison of Wf values on each type of molecule before and after sorting into mixed bi-molecular array. The values are additionally illustrated on Figure 3a.

Molecule	Pure islands, ΔWf		Co-assembled, ΔWf
	First orientation ("dark")	Second orientation ("bright")	
MnPc	-0.43±0.13 eV	-0.14±0.12eV	-1.60±0.04 eV
CuPc	+0.35±0.06 eV	+0.54±0.06 eV	+0.08±0.04 eV,

On the basis of the local relative work functions, measured by I(z) spectroscopy, we propose a schematic model to describe the charge interactions occurring at the molecule/surface interface (Figure 3b). The first part of the scheme reflects the surface-molecular interaction upon molecular adsorption and depicts the opposite charge transfer for CuPc and MnPc at Bi/Cu(100). The second part of the scheme depicts the resulting bi-molecular chess-board arrangement with an enhanced positive charge on MnPc and a negative charge on CuPc. The Wf maps measured on pure CuPc island (Figure 3c) and of the pure MnPc island (Figure 3d) reveal rather homogeneous charge-distribution pattern within the molecules. This is very different after mixing (Figure 3e). The potential landscape of the bi-molecular chess-board exhibits the enhanced alternating contrast, i.e. a positive charge state of the MnPc and a negative charge state of the CuPc (red and blue protrusions on Figure 3e, respectively). The perfectly sorted alternating opposite charges evidence the maximization of Coulomb interactions acting as a driving mechanism for an electronic molecular recognition and the resulting self-sorting. The modification of charge on each component upon sorting is expected to be induced by the re-alignment of the molecule-surface and molecule-molecule energy levels after two components mix.

Conclusions

A novel sorting mechanism for ad-molecules has been identified. A different direction of charge transfer is observed for the two Pcs, which differ in their electron affinity due to the difference in the energy level alignment with the substrate. Self-assembly occurs due to the maximization of Coulomb interaction between the opposite charges and due to the increased diffusion on the Bi/Cu(100) substrate. Additionally, we identify a strong modification of the charge transfer by the nearest-neighbour molecular components. Remarkably, the behavior is affected by the interaction of electronic states of the adsorbate and the substrate, but also by the restricted screening of the dipolar fields in the Bi/Cu being facilitated by the longer Debye length of Bi (compared to a metal substrate). Thereby a new effect causing supramolecular self- assembly has been described.

We presented a system, which serves as a unique example of the information propagation on the single molecular level, which leads to the electronic molecular recognition and makes a significant step towards a high level of control in the molecular arrays.

References:

(1) Braun, S.; Salaneck, W. R.; Fahlman, M. *Adv. Mater.* **2009**, *21*, 1450.
(2) Flores, F.; Ortega, J.; Vázquez, H. *Phys. Chem. Chem. Phys.* **2009**, *11*, 8658.
(3) Zhong, J.-Q.; Qin, X.; Zhang, J.-L.; Kera, S.; Ueno, N.; Wee, A. T. S.; Yang, J.; Chen, W. *ACS Nano* **2014**, 140116123939006.
(4) De Wild, M.; Berner, S.; Suzuki, H.; Yanagi, H.; Schlettwein, D.; Ivan, S.; Baratoff, A.; Guentherodt, H.-J.; Jung, T. A. *ChemPhysChem* **2002**, *3*, 881.
(5) Dil, H.; Lobo-Checa, J.; Laskowski, R.; Blaha, P.; Berner, S.; Osterwalder, J.; Greber, T. *Science* **2008**, *319*, 1824.
(6) Joshi, S.; Bischoff, F.; Koitz, R.; Ecija, D.; Seufert, K.; Seitsonen, A. P.; Hutter, J.; Diller, K.; Urgel, J. I.; Sachdev, H.; Barth, J. V.; Auwärter, W. *ACS Nano* **2013**, 131211132833009.
(7) Mazur, U.; Hipps, K. W. *J. Phys. Chem. B* **1999**, *103*, 9721.

(8) Hipps, K. W.; Scudiero, L.; Barlow, D. E.; Cooke, M. P. *J. Am. Chem. Soc*. **2002**, *124*, 2126.
(9) Goiri, E.; Matena, M.; El-Sayed, A.; Lobo-Checa, J.; Borghetti, P.; Rogero, C.; Detlefs, B.; Duvernay, J.; Ortega, J. E.; de Oteyza, D. G. *Phys. Rev. Lett.* **2014**, *112*.
(10) Zhang, J. L.; Niu, T. C.; Wee, A. T. S.; Chen, W. *Phys. Chem. Chem. Phys.* **2013**, *15*, 12414.
(11) Wäckerlin, C.; Nowakowski, J.; Liu, S.-X.; Jaggi, M.; Siewert, D.; Girovsky, J.; Shchyrba, A.; Hählen, T.; Kleibert, A.; Oppeneer, P. M.; Nolting, F.; Decurtins, S.; Jung, T. A.; Ballav, N. *Adv. Mater.* **2013**, 2404.
(12) H.L Meyerheim. *Surf. Sci.* **1998**, *418*, 295.
(13) Paul Wynblatt. *Surf. Sci.* **2007**, *601*, 1623.
(14) Gargiani, P.; Izzo, M. G.; Bussolotti, F.; Betti, M. G.; Achilli, S.; Trioni, M. I. *J. Chem. Phys.* **2010**, *132*, 174706.
(15) Krull, C.; Robles, R.; Mugarza, A.; Gambardella, P. *Nat. Mater.* **2013**, *12*, 337.
(16) Schulz, F.; Drost, R.; Hämäläinen, S. K.; Liljeroth, P. *ACS Nano* **2013**, 131025155453006.
(17) Järvinen, P.; Hämäläinen, S. K.; Banerjee, K.; Häkkinen, P.; Ijäs, M.; Harju, A.; Liljeroth, P. *Nano Lett.* **2013**, *13*, 3199.
(18) Mugarza, A.; Robles, R.; Krull, C.; Korytár, R.; Lorente, N.; Gambardella, P. *Phys. Rev. B* **2012**, *85*.
(19) Swart, I.; Sonnleitner, T.; Repp, J. *Nano Lett.* **2011**, *11*, 1580.
(20) Stróżecka, A.; Soriano, M.; Pascual, J. I.; Palacios, J. J. *Phys. Rev. Lett.* **2012**, *109*.
(21) Franke, K. J.; Schulze, G.; Pascual, J. I. *Science* **2011**, *332*, 940.
(22) Chen, C. J. *Introduction to scanning tunneling microscopy*; Oxford University Press: New York, 1993.
(23) Ruffieux, P.; Aït-Mansour, K.; Bendounan, A.; Fasel, R.; Patthey, L.; Gröning, P.; Gröning, O. *Phys. Rev. Lett.* **2009**, *102*.
(24) Kittel, C. *Introduction to solid state physics*; 8th ed.; Wiley: Hoboken, NJ, 2005.
(25) Haidu, F.; Fechner, A.; Salvan, G.; Gordan, O. D.; Fronk, M.; Lehmann, D.; Mahns, B.; Knupfer, M.; Zahn, D. R. T. *AIP Adv.* **2013**, *3*, 062124.

Conclusion

The work presented in this thesis addresses the following questions: i) how a reduced dimension – the surface, can influence the chemistry and lead to novel effects, ii) how physics and chemistry can be used to control on-surface molecular architectures with atomic precision.

This thesis demonstrates a tunable molecular 1D self-assembly, built-up from an inherently chiral helicene molecule on the basis of H-bonding and metal-coordination. This system serves as a model for the investigation of chirality propagation in linear coordination polymers. We show how the interplay of molecular flexibility and strength of the bonding motif can affect chirality transfer. The calculations performed by our partners provide insight into the energetics of the on-surface metal coordination, chain architectures and the electrostatic interactions driving the parallel arrangement of the chains. Moreover, we address the temperature dependent availability of metal adatoms as well as repulsive on-surface interactions, as factors leading to control of the bonding motif and long-range order.

In the scope of this thesis, we also present a new on-surface reaction which is promoted to a different degree depending on the type of metal used to initiate the coordination. The amino-functionalized perylene precursor can undergo different levels of dehydrogenation depending on the type of the transition metal used. Specifically, Co, Ni, Fe adatoms are inducing the conversion of the molecular precursor into an imino-ligand while Cu adatoms induce conversion into an azo-ligand. Both ligands are interlinked in the corresponding coordination complexes after initial dehydrogenation. Moreover, we show that the combination of the right ligand with the right type of the surface can be used to control the dimensionality of the on-surface coordination polymers.

Furthermore, in this thesis we show a new bi-component on-surface reaction, which is based on bolylene and results in a polymer linked by covalent bonds. The availability of various pore-sizes and shapes allowed us to investigate the electronic confinement effects, remaining within the barriers of the same covalent molecular skeleton, which has been not reported in the literature before. We show shifting of the confined state towards the Fermi level with decreasing area of the pore, which acts as a confining quantum well. We proposed a theoretical model for the analysis of the confined state and its effective size. Furthermore, we have shown a confinement effect inside of the pores with missing barriers.

The last chapter of presented results of this thesis, reports on a new molecular recognition mechanism in bi-molecular systems on surface which drives self-sorting of molecules into 1:1 chess-board array and which occurs without any chemical bond but purely by electronic interactions. The investigated system is based on a molecular mixture of CuPc and MnPc at a bismuth reconstruction on Cu(100). We analysed the electronic characteristics of molecules in pure and mixed islands.

The supramolecular architectures, explored and presented here, serve as model systems to investigate physical and chemical effects at reduced dimensions, which have not been addressed in the scientific literature before. We are convinced that with our results we also have

contributed to supramolecular, on-surface coordination and covalent chemistry. Moreover, we have addressed different ways of molecular recognition in the scope of chirality propagation, as well as in the scope of molecular sorting. We have shown that the broad range of experimental techniques applied here, i.e. STM, STS, XPS, NEXAFS together with complementary DFT calculations can give deep insight into the properties of on-surface supramolecular systems. We anticipate that the supramolecular properties, discovered here, contribute to increase of the molecular control on the nanoscale which is of both fundamental and applied interest, e.g. for future sensors and devices.

Bibliography

[1] J. D. Halley and D. A. Winkler, Complexity **14**, 10 (2008).
[2] L. Bartels, Nat. Chem. **2**, 87 (2010).
[3] X. Zhang, Q. Zeng, and C. Wang, Nanoscale **5**, 8269 (2013).
[4] M. E. Cañas-Ventura, W. Xiao, D. Wasserfallen, K. Müllen, H. Brune, J. V. Barth, and R. Fasel, Angew. Chem. Int. Ed. **46**, 1814 (2007).
[5] S. Clair, S. Pons, A. P. Seitsonen, H. Brune, K. Kern, and J. V. Barth, J. Phys. Chem. B **108**, 14585 (2004).
[6] W. Krenner, F. Klappenberger, N. Kepčija, E. Arras, Y. Makoudi, D. Kühne, S. Klyatskaya, M. Ruben, and J. V. Barth, J. Phys. Chem. C **116**, 16421 (2012).
[7] S. Clair, S. Bedwani, S. Fabris, S. Baroni, H. Brune, K. Kern, and J. V. Barth, J. Phys. Chem. B **110**, 5627 (2006).
[8] S. Stepanow, N. Lin, and J. V. Barth, J. Phys. Condens. Matter **20**, 184002 (2008).
[9] S. Stepanow, R. Ohmann, F. Leroy, N. Lin, T. Strunskus, C. Wöll, and K. Kern, ACS Nano **4**, 1813 (2010).
[10] U. Schlickum, R. Decker, F. Klappenberger, G. Zoppellaro, S. Klyatskaya, M. Ruben, I. Silanes, A. Arnau, K. Kern, H. Brune, and J. V. Barth, Nano Lett. **7**, 3813 (2007).
[11] S. Weigelt, C. Busse, C. Bombis, M. M. Knudsen, K. V. Gothelf, E. Lægsgaard, F. Besenbacher, and T. R. Linderoth, Angew. Chem. Int. Ed. **47**, 4406 (2008).
[12] M. Bieri, M.-T. Nguyen, O. Gröning, J. Cai, M. Treier, K. Aït-Mansour, P. Ruffieux, C. A. Pignedoli, D. Passerone, M. Kastler, K. Müllen, and R. Fasel, J. Am. Chem. Soc. **132**, 16669 (2010).
[13] T. Lin, X. S. Shang, J. Adisoejoso, P. N. Liu, and N. Lin, J. Am. Chem. Soc. **135**, 3576 (2013).
[14] L. Lafferentz, V. Eberhardt, C. Dri, C. Africh, G. Comelli, F. Esch, S. Hecht, and L. Grill, Nat. Chem. **4**, 215 (2012).
[15] D. G. Blackmond, Cold Spring Harb. Perspect. Biol. **2**, a002147 (2010).
[16] J. McConathy and M. J. Owens, Prim Care Companion J. Clin. Psychiatry **5(2)**, 70 (2003).
[17] M. Nunez, M. Garcia-Rubino, A. Conejo-Garcia, O. Cruz-Lopez, M. Kimatrai, M. Gallo, A. Espinosa, and J. Campos, Curr. Med. Chem. **16**, 2064 (2009).
[18] D. Heim, D. Écija, K. Seufert, W. Auwärter, C. Aurisicchio, C. Fabbro, D. Bonifazi, and J. V. Barth, J. Am. Chem. Soc. **132**, 6783 (2010).
[19] G. Pawin, K. L. Wong, D. Kim, D. Sun, L. Bartels, S. Hong, T. S. Rahman, R. Carp, and M. Marsella, Angew. Chem. Int. Ed. **47**, 8442 (2008).
[20] J. Björk, Theory and Modelling of Organic Molecules on Surfaces, University of Liverpool.
[21] F. Richard Keene, Coord. Chem. Rev. **187**, 121 (1999).
[22] T. Riehm, G. De Paoli, H. Wadepohl, L. De Cola, and L. H. Gade, Chem. Commun. 5348 (2008).
[23] P. Gargiani, M. G. Izzo, F. Bussolotti, M. G. Betti, S. Achilli, and M. I. Trioni, J. Chem. Phys. **132**, 174706 (2010).
[24] P. Gargiani, S. Lisi, M. G. Betti, A. T. Ibrahimi, F. Bertran, P. Le Fèvre, and L. Chiodo, J. Chem. Phys. **139**, 184707 (2013).
[25] G. Thayer, J. Sadowski, F. Meyer zu Heringdorf, T. Sakurai, and R. Tromp, Phys. Rev. Lett. **95**, (2005).
[26] U. Mazur and K. W. Hipps, J. Phys. Chem. B **103**, 9721 (1999).

[27] S. Stepanow, A. Lodi Rizzini, C. Krull, J. Kavich, J. C. Cezar, F. Yakhou-Harris, P. M. Sheverdyaeva, P. Moras, C. Carbone, G. Ceballos, A. Mugarza, and P. Gambardella, J. Am. Chem. Soc. **136**, 5451 (2014).
[28] M. F. Craciun, S. Rogge, and A. F. Morpurgo, J. Am. Chem. Soc. **127**, 12210 (2005).
[29] M. F. Craciun, S. Rogge, M.-J. L. den Boer, S. Margadonna, K. Prassides, Y. Iwasa, and A. F. Morpurgo, Adv. Mater. **18**, 320 (2006).
[30] C. J. Chen, *Introduction to Scanning Tunneling Microscopy* (Oxford University Press, New York, 1993).
[31] P. Ruffieux, K. Aït-Mansour, A. Bendounan, R. Fasel, L. Patthey, P. Gröning, and O. Gröning, Phys. Rev. Lett. **102**, (2009).
[32] J. C. Vickerman, I. S. Gilmore, and Wiley InterScience (Online service), *Surface Analysis the Principal Techniques* (John Wiley & Sons, Hoboken, NJ, 2009).
[33] J. Stöhr, *NEXAFS Spectroscopy* (Springer-Verlag, Berlin; New York, 1992).
[34] R. Wiesendanger, *Scanning Probe Microscopy and Spectroscopy Methods and Applications* (Cambridge University Press, Cambridge, 1994).

Acknowledgements

Here I would like to express my gratefulness to all people, who have helped and supported me during my doctoral study.

First of all, I would like to acknowledge my PhD supervisor Thomas Jung for his supervision, being always open to discussions, giving freedom for the creativity, creating possibilities for our scientific growth and giving a great support during writing the manuscripts. I sincerely acknowledge Christian Wäckerlin, who being a senior PhD student in our PSI team, was teaching with a lot of patience and sharing all his experience in the Laboratories, in data analysis and experiments' design with all our Nanolab group.

I want especially to thank all our members of Nanolab group. Many thanks to Sylwia Nowakowska, Thomas Nijs, Susanne Martens, Toni Ivas for their great support during the experiments, discussions and developing the scientific strategies. Separate acknowledgement goes to Marco Martina, who being our technician, kindly provided a lot of support during our significant reconstructions of the Laboratory.

Many grateful acknowledgements go to my Master student Shadi Fatayer and my Block-course student Henrik Peters. They were excellent students, learning fast and helping a lot during the experiments.

I sincerely thank our all PSI team: Jan Nowakowski, Jan Girovsky, Dorota Siewert, Milos Baljozovic, Harald Rossmann for their always very good support during the spectroscopy experiments performed in PSI Lab as well on the SLS synchrotron. Separate acknowledgements to Nirmalya Ballav for his help and support during beam-time experiments. Especially a lot of thanks goes to Rolf Schelldorfer, who being technician at PSI, was ready to help and support PSI as well as Nanolab team. Whenever we had to fix the equipment during our very intensive measurements and very tight time frames, he was always ready to help in solving any technical problems.

All the group was a fantastic team - helping, discussing, supporting each other during days and nights spent in the Lab and at the synchrotron.

I sincerely thank to our collaborators from chemistry side for the synthesis of investigated in this thesis molecules, as well as for their teaching and support during writing the manuscripts: Jesse Roose, Carlo Thilgen, François Diederich, Susanne Martens and Lutz Gade. I would like separately to acknowledge a great support and significant contribution from the computational side shown in this thesis: Jonas Björk, Daniele Passerone, Carlo Pignedoli and Manh-Thuong Nguyen.

Curriculum vitae

Aneliia Wäckerlin (Shchyrba)

Contact Address:
Madretschstrasse 43
CH-2503 Biel/Bienne
Switzerland

E-mail: aneliia@waeckerlin.com
Date of birth: 4th February 1989
Nationality: Ukrainian

EDUCATION

2011 – now **PhD student in Nanoscience**, University of Basel, Switzerland
My research is focused on the design and characterization of molecular thin films and self-assembled nanoarchitectures at surfaces, defining their chemical, electronic and magnetic properties. The following directions were addressed:

- development of new on-surface reactions as a tool to control polymers dimensionality (0D, 1D, 2D),
- investigation of the chirality transfer mechanisms in 1D,
- creation of new approaches for the self-sorting of bi-molecular mixtures,
- study of on-surface quantum confinement effects created by porous molecular templates,
- exploring new ways to probe/assign the charge on the nanoscale.

The investigations were performed via broad tool-kit of the Laboratory- and Synchrotron-based experimental techniques at University of Basel, Laboratory for Micro- and Nanotechnology at Paul Scherrer Institut and at the Swiss Light Source**.**

2009 – 2011 **Master of Science**, Engineer-Researcher, Assistant, Lecturer
Nanophysics and Nanoelectronics Department, National Taras Shevchenko University of Kyiv, Ukraine.
Master thesis: *STM-investigation of the Bi nanostructures on the Ge(111) surface*.

2005 – 2009 **Bachelor of Science** in Applied Physics
Cryogenic and Microelectronics Department, National Taras Shevchenko University of Kyiv, Ukraine.
Bachelor thesis: *Statistical properties of surface micro-relief in air-clad optical fibers*.

WORK EXPERIENCE

2014 - now PostDoc, Physics Department, Basel University, Switzerland
2011 – 2014 PhD in Nanoscience, Physics Department, Basel University, Switzerland
2009 – 2011 Lecturer at Kiev natural-scientific lyceum No. 145, Kiev, Ukraine

RESEARCH TECHNIQUES

- Scanning Tunneling Microscopy and Spectroscopy (STM/STS),
- Non-contact Atomic Force Microscopy (nc-AFM),
- Auger Electron Spectroscopy (AES),
- X-ray Photoelectron Spectroscopy (XPS),
- X-ray Magnetic Circular Dichroism (XMCD) Spectroscopy,
- Near edge X-ray absorption fine structure (NEXAFS) Spectroscopy.

Languages: English (fluent), German (intermediate), French (beginner), Russian (fluent), Ukrainian (native).

The following professors have contributed to my education:

Thomas A. Jung, Lutz H. Gade, François Diederich, Carlo Thilgen, Nirmalya Ballav, Meike Stöhr, Edwin Constable, Catherine Housecroft, Ernst Meyer.

LIST OF PUBLICATIONS AND MANUSCRIPTS

1. ***Kondo effect in a molecular system at the Bismuth reconstructed Cu(100)***, A. Wäckerlin, C. Wäckerlin, S. Fatayer, T. Nijs, S. Nowakowska, T.A. Jung, manuscript in preparation;

2. ***Molecule-specific energy level alignment inducing different charge transfer dipoles and formation of a self-sorted bimolecular chess-board on Bi reconstructed Cu(100)***, A. Wäckerlin, S. Fatayer, C. Wäckerlin, T. Nijs, S. Nowakowska, T.A. Jung, manuscript in preparation;

3. ***Controlling the dimensionality of on-surface coordination polymers via endo- or exo-ligation***, A. Shchyrba, C. Wäckerlin, J. Nowakowski, S. Nowakowska, J. Björk, S. Fatayer, J. Girovsky, T. Nijs, S. Martens, A. Kleibert, M. Stöhr, N. Ballav, T. A. Jung, L. Gade, *J. Am. Chem. Soc.*, 2014, 136 (26), 9355–9363;

4. ***Covalent assembly of a two-dimensional molecular "sponge" on a Cu(111) surface: Confined electronic surface states in open and closed pores***, A. Shchyrba, S. C. Martens, C. Wäckerlin, M. Matena, T. Ivas, H. Wadepohl, M. Stöhr, T. A. Jung and L. H. Gade, *Chem. Commun.*, 2014, 50, 7628-7631;

5. ***Chirality Transfer in 1D Self-Assemblies: Influence of H-Bonding vs Metal Coordination between Dicyano[7]helicene Enantiomers***, A. Shchyrba, M.-T. Nguyen, C. Wäckerlin, S. Martens, S. Nowakowska, T. Ivas, J. Roose, T. Nijs, S. Boz, M. Schär, M. Stöhr, C. Pignedoli, C. Thilgen, F. Diederich, D. Passerone and T. A. Jung, *J. Am. Chem. Soc.*, 2013, 135 (41), 15270–15273;

6. ***Interplay of weak interactions in the atom-by-atom condensation of xenon within quantum boxes,*** S. Nowakowska, A. Wäckerlin, S. Kawai, T. Ivas, J. Nowakowski, S. Fatayer, C. Wäckerlin, T.Nijs, E. Meyer, J. Björk, M. Stöhr, L. H. Gade, T. A. Jung, submitted manuscript;

7. ***Quantum confinement playground***, S. Nowakowska, A. Shchyrba, S. Kawai, J. Nowakowski, C. Wäckerlin, S. Fatayer, T. Nijs, M. Stöhr, L. Gade, T. A. Jung, manuscript in preparation;

8. ***Probing the spatial and momentum distribution of confined surface states in a metal coordination network,*** J. Zhang, A. Shchyrba, S. Nowakowska, E. Meyer, T. A. Jung and M. Muntwiler, *Chem. Commun.*, 2014, 50, 12289-12292;

9. ***Substrate-molecule distance dependence on magneto-chemical coupling strength,*** J. Nowakowski, J. Girovsky, M. Baljozovic, C. Wackerlin, A. Shchyrba , H. Rossmann, T. Nijs, A. Kleibert, P. M. Oppeneer, N. Ballav, T. A. Jung, manuscript in preparation;

10. ***Unexpected antiferromagnetic coupling of a Cr-porphyrin to bare cobalt substrate***, J. Girovsky, K.Tarafder, C. Wäckerlin, J. Nowakowski, D. Siewert, T. Hählen, A. Shchyrba, A. Kleibert, N. Ballav, T. A. Jung, and P. M. Oppeneer, manuscript under review;

11. ***Magnetic exchange coupling of metallo-porphyrins on nitrogen and chlorine terminated ferromagnetic substrates***, J.Girovsky, K.Tarafder, C. Wäckerlin, J. Nowakowski, D. Siewert, T. Hählen, A. Shchyrba, A. Kleibert, N. Ballav, T. A. Jung, and P. M. Oppeneer, manuscript in preparation.

12. ***Magnetic exchange coupling of a synthetic Co(II)-complex to a ferromagnetic Ni substrate***, C. Wäckerlin, P. Maldonado, L. Arnold, A. Shchyrba, J. Girovsky, J. Nowakowski, Md. E. Ali, T. Hählen, M. Baljozovic, D. Siewert, A. Kleibert, K. Müllen, P. M. Oppeneer, T. A. Jung and N. Ballav, *Chem. Commun.*, 2013, 49, 10736;

13. ***Ammonia Coordination Introducing a Magnetic Moment in On-Surface Low-Spin Porphyrin***, C. Wäckerlin, K. Tarafder, J. Girovsky, J. Nowakowski, T. Hählen, A. Shchyrba, D. Siewert, A. Kleibert, F. Nolting, P. M. Oppeneer, T. A. Jung and N. Ballav, *Angew. Chem. Int. Ed.* 2013, 52, 1 – 5;

14. ***Two-dimensional supramolecular electron spin arrays***, C. Wäckerlin, J. Nowakowski, S.-X. Liu, M. Jaggi, D. Siewert, J. Girovsky, A. Shchyrba, T. Hählen, A. Kleibert, P. M. Oppeneer, F. Nolting, S. Decurtins, T. A. Jung, N. Ballav, *Adv. Mat.*, 2013, 25 (17), 2404–2408;

15. ***Initial stages of Bi/Ge(111) interface formation: a detailed STM study***, A. Goriachko, P.V. Melnik, A. Shchyrba, S.P. Kulyk, M.G. Nakhodkin, *Surf. Sci.* 605 (2011) 1771–1777;

16. ***Experimental investigations of Bi nanostructures on the Ge-surface via scanning tunneling microscopy,*** A. Shchyrba, A. Goriachko, P. Melnik, M. Nakhodkin, Bulletin of the University of Kiev, Series: Radiophysics & Electronics, 14 (2011);

17. ***Experimental investigations of intrinsic roughness at the surface of air-clad optical fibers***, A. Goriachko, A. Kovalenko, V. Kurashov, A. Shchyrba, Bulletin of the University of Kiev, Series: Radiophysics & Electronics, 13 (2010).